Evaluation of the Altered Pathophysiological Mechanism of the Human Arg302Gln-PRKAG2 Mutation-Induced Metabolic Cardiomyopathy: Studying the Glucose Metabolism Pathway in a Transgenic Mouse Model

by

Stephanie Thorn

Thesis submitted to the

Faculty of Graduate and Posdoctoral Studies

in partial fulfillment of the requirements

for a doctoral degree in Cellular and Molecular Medicine.

Department of Cellular and Molecular Medicine

Faculty of Medicine

University of Ottawa

ABSTRACT

Characterized by excessive myocardial glycogen deposition, cardiac hypertrophy, frequent cardiac arrhythmias and progressive conduction system disease, the PRKAG2 cardiac syndrome stems from a genetic mutation in the γ2-subunit of AMP-activated protein kinase (AMPK). Although functionally diverse, the main role of AMPK is to modulate cardiac metabolism in response to depleted ATP levels. A comprehensive study of the dysfunctional regulation of AMPK activity involved in the progression of the human PRKAG2 cardiac syndrome is hindered by the limitations of in vitro techniques. Positron emission tomography (PET) imaging with the glucose analogue, FDG, offers a quantitative assessment of myocardial glucose uptake non-invasively. The aim of this thesis was to determine the ability of FDG to detect changes in glucose uptake, storage and metabolism in the heart in relation to AMPK activity and provide insights into the mechanism of PRKAG2 cardiac hypertrophy. To achieve this aim, a transgenic AMPK γ2-subunit Arg302Gln mouse model was evaluated with small animal FDG PET with correlation to biochemical assays of cardiac AMPK activity and the glycogen metabolism pathway. Using the vena cava blood input function, FDG myocardial glucose uptake was reliably assessed in mice for the first time with Patlak modeling. Reduced FDG uptake in the Arg302Gln PRKAG2 mouse model suggested a feedback pathway reducing exogenous glucose uptake due to excessive intracellular glycogen stores. Despite an increase in FDG uptake in the skeletal muscle of the PRKAG2 mutant mice following insulin stimulation, there was no change in cardiac uptake, signifying myocardial insulin resistance. Increased reliance on glucose oxidation by TMZ inhibition of fatty acid oxidation reduced glycogen stores, restored cardiac function and eliminated ventricular preexcitation. The observed reduction in mouse myocardial FDG

uptake mirrors the reduction previously observed in the human PRKAG2 patients. The potential now exists to evaluate both progression and therapeutic interventions for the PRKAG2 cardiac syndrome with the transgenic mouse model with translation to the affected patients using FDG cardiac imaging.

ACKNOWLEDGMENTS

I would like to thank my supervisors, Dr Jean DaSilva and Dr Michael Gollob for their encouragement, guidance, and mentoring which have been instrumental in my pursuit and achievement of my PhD. I would also like to thank Dr Rob Beanlands, Dr Rob deKemp and Dr Mary-Ellen Harper for all their work on my committee and mentoring me as well through these years. Thanks to OGS, the Heart and Stroke Foundation, and the University of Ottawa for scholarship support.

Over the years I have had the privilege of working with so many wonderful people. To all of you, too numerous to mention, thank you. ACVS, I will always be grateful for the assistance you gave me and all the laughter and friendship. PET Radiochemistry, thank you for your effort and dedication.

There are a few people I would like to especially thank. Cynthia- AMPK, geography and cells- all while having a dance party in the lab. Sam and Ran, you have both supported me for so many years, and I'm so grateful to be a part of your lives, here's to many more backyard campfires and fondue nights (thanks to the Swiss as well!). Miran, you were a constant support for me, and still are- thanks for all the sanity checks, laughter and friendship- I wouldn't have gotten this far without you. And Jules, there are no words. Hard to believe that we've only known each other for four years- seems like we've been friends for much longer. Can't wait to see what gong shows we come up with next.

Finally, I dedicate this thesis to my family: my brother, and my best friends and sisters, Lis and Col for always giving me a place to come home to and supporting me unconditionally, and my parents who have never stopped supporting me, loving me, and are everything to me. I would never have gotten this far without you, I love you.

TABLE OF CONTENTS

LIST OF TABLES

LIST OF FIGURES

LIST OF ABBREVIATIONS

^{11}C	carbon-11
^{18}F	fluorine-18
^{13}N	nitrogen-13
%ID	percentage of total injected dose
ACC	acetyl-coA carboxylase
ACC-P	acetyl-coA carboxylase- phosphatase
ADP	adenosine diphosphate
AMP	adenosine monophosphate
AMPK	adenosine monophosphate kinase
ANOVA	analysis of variance
AS	acetyl-CoA synthetase
ATP	adenosine triphosphate
AVC	average vena cava
Bq	becquerel
BW	body weight
CAT	carnitine-acylcarnitine translocase
CBS	cystathionine beta synthase
COV	coefficient of variance
CPT-1	carnitine palmitoyltransferase-1
CPT-2	carnitine palmitoyltransferase-2
CR	coefficient of repeatability
Cr	creatine
DM	diabetes mellitus
DNA	deoxyribonucleic acid
DPET	dedicated positron emission tomography
ECG	electrocardiogram
ETC	electron transport chain
FBP	filtered backprojection
FDG	[^{18}F]fluorodeoxyglucose
FA	fatty acid
FFA	free fatty acids
FOV	field of view
FS	fractional shortening
FTHA	[^{18}F]fluoro-4-thia-palmitate
FWHM	full width half max
GAA	acid alpha-glucosidease
GAPDH	glyceraldehydes 3-phosphate dehydrogenase
GLUT	glucose transporter
GP	glycogen phosphorylase
GS	glycogen synthase
GSK-3	glycogen synthase kinase-3
GYS1	glycogen synthase 1
GYS2	glycogen synthase 2
HLA	horizontal long axis

IAW	Inveon analysis workstation
IDIF	image derived input function
ip	intraperitoneal
iv	intravenous
3-KAT	3-ketoacyl-coenzyme A thiolase
Ki	influx rate constant
Km	Michaelis constant
LAD	left anterior descending
LV	left ventricle
LVDV	left ventricle diastolic volume
MAP	maximum a posterior
MCD	malonyl carboxylase dehydrogenase
mCi	milicuries
MHC	myosin heavy chain
MIM	mitochondria inner membrane
MOM	mitochondria outer membrane
N488I	Asparagine 400 isoleucine
NH_3	[^{13}N]ammonia
NYHA	New York heart association
OSEM(3D)	ordered-subsets expectation maximization(3 dimensional)
P	phosphate
PCr	phosphocreatine
PCR	polymerase chain reaction
PET	positron emission tomography
PI3K	phosphatidylinositol 3-kinase
PIP3	phosphatidylinositol (3,4,5)-triphosphate
po	per os
PRKAG2	protein kinase AMPK gamma 2
PSF	point spread function
R302Q	arginine 302 Glutamine
R531G	arginine 531 glycine
rMGU	myocardial glucose uptake rate
RC	recovery coefficient
RNA	ribonucleic acid
ROI	region of interest
SA	short axis
STZ	streptozotocin
SUV	standard uptake value
T1DM	type 1 diabetes mellitus
T2DM	type 2 diabetes mellitus
T400N	threonine 400 asparagine
TAC	time activity curve
TCA	tricarboxylic acid cycle
TGmut	transgenic mutant
TGwt	transgenic wildtype
TMZ	trimetazidine

VC_{50}	50% of the maximal threshold vena cava activity
VLA	vertical long axis
WPW	Wolf-Parkinson White

CHAPTER 1: INTRODUCTION

1.0 Introduction

In 2001, the PRKAG2 cardiac syndrome was clinically observed in clusters of families in the Ottawa region (Gollob, 2003; Gollob et al., 2001a; Gollob et al., 2002; Gollob and Roberts, 2002; Gollob et al., 2001b), though detection of the syndrome has now been noted worldwide. Similar to other glycogen storage diseases of the heart, these affected patients progressively develop cardiomyopathy, arrhythmias and conduction system disease. At the Ottawa Heart Institute, we continue to follow about 20 patients with this genetic disease with about 70% of our patients needing the assistance of cardiac devices, including pacemakers and defibrillators. The morbidity of these patients is considerable with a high mortality due to heart failure.

Our group identified the gene causative for this condition to be *PRKAG2* (Gollob et al., 2001a; Gollob et al., 2001b). The *PRKAG2* gene codes for the gamma-2 regulatory subunit of the heterotrimeric AMP-activated protein kinase (AMPK) (Gollob et al., 2001a). The physiologic functions of AMPK on cardiac metabolism are diverse; AMPK is recognized to play a vital role in muscle cell glucose metabolism, regulating enzymes involved in glucose utilization, glycogen synthesis and glycogen degradation (Carling, 2004; Dolinsky and Dyck, 2006b; Hardie, 2003; Kahn et al., 2005; Kemp et al., 2003; Woods et al., 2000).

The generation of a mouse line by cardiac restricted transfection of the human Arg302Gln gene (Sidhu et al., 2005) has permitted intensive investigation of the underlying biochemistry. Positron emission tomography (PET) provides a translational tool to evaluate cardiac metabolism in both the affected patients and the PRKAG2 transgenic animal model. The utility of this tool is the ability to investigate the molecular mechanisms and biochemistry in the tissue of the mouse PRKAG2 model, work that we are unable to

complete in the human patients. With an improved understanding of the underlying pathology from the mouse model, this knowledge can be translated to the clinical setting with PET for diagnosis and therapeutic evaluation.

1.1 Substrate Metabolism

1.1.1 Cardiac Substrate Metabolism for ATP synthesis

The contractile process of the heart requires a large turnover in ATP regeneration to maintain energy levels. The heart has a relatively low ATP content (~5 μmol/g wet wt) compared with an extremely high rate of ATP hydrolysis at rest (~0.5 μmol/g wet wt·s), calculating to a complete hydrolysis of myocardial ATP content in approximately 10s (Ingwall, 2001; Opie, 1991). The majority of ATP (60-70%) is hydrolysed for contractile shortening with the remaining utilized for diverse other processes (Gibbs, 1978; Suga, 1990). The requirements for ATP by the heart, and consistent rate of turnover even at resting levels, require a constant generation of ATP. Regeneration of ATP occurs primarily through three substrate pathways: glycolysis, oxidative phosphorylation, and creatine kinase reactions (Sahlin et al., 1990). In the normal heart, less than 10% of ATP is produced by glycolysis with 10-40% of the ATP generated by pyruvate oxidation (Dyck and Lopaschuk, 2006; Stanley et al., 2005). The remaining 60-90% of ATP synthesis generated by free fatty acid (FFA) oxidation (Figure 1.1) (Dyck and Lopaschuk, 2006; Stanley et al., 2005). In times of starvation, protein will be broken down by the body and ketone levels in the blood will increase (Bertrand et al., 2008). The heart can use ketone bodies as a substrate, primarily during chronic heart failure or uncontrolled diabetes (Stanley et al., 2005). The metabolism of ketones will inhibit other substrate oxidation by metabolism through pyruvate dehydrogenase via acetyl-CoA production (Stanley et al., 2005).

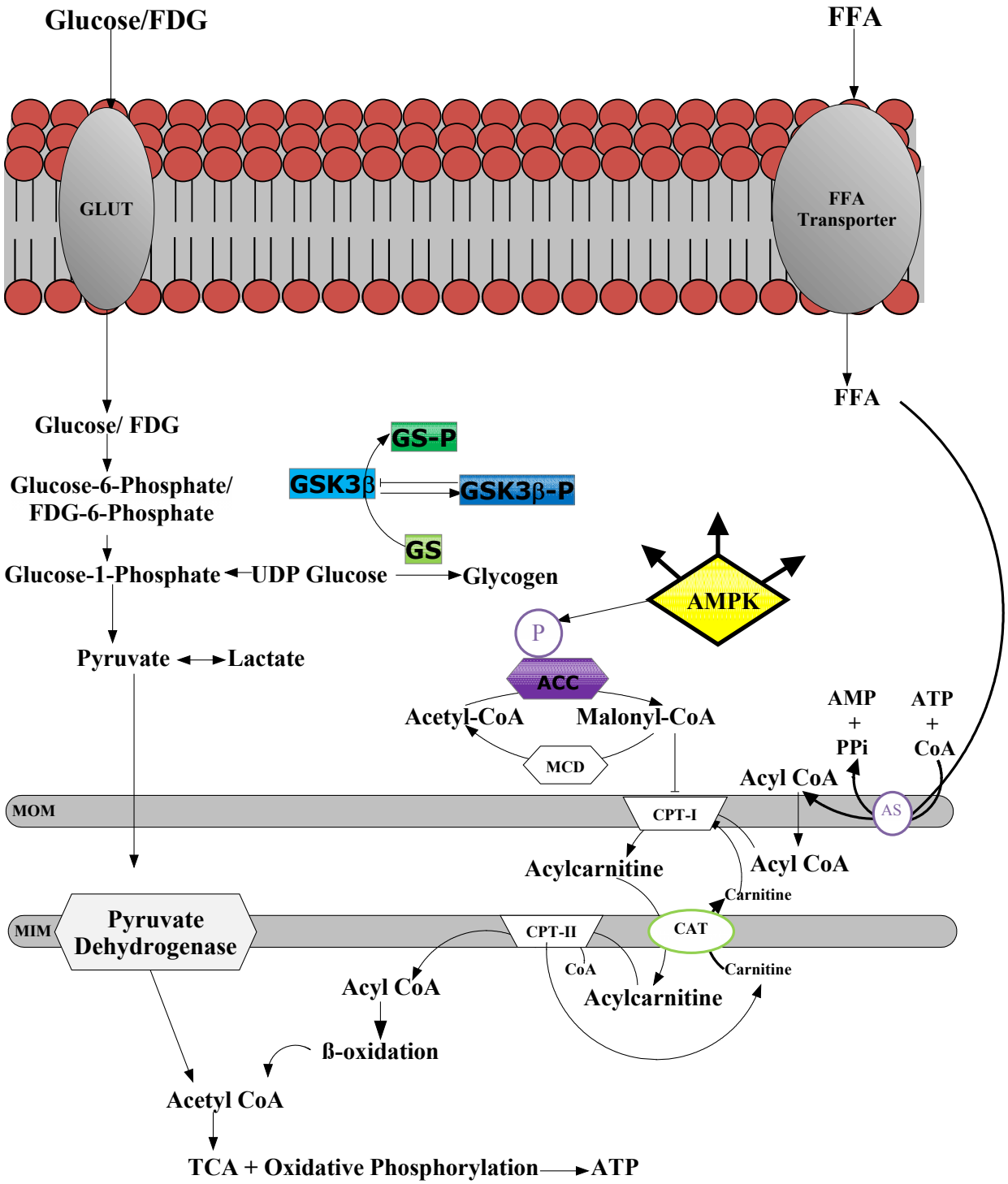

Figure 1.1: Schematic of cardiac substrate metabolism.

1.1.2 Fetal Cardiac Metabolism

In pathologic cardiac conditions, including ischemia, type 2 diabetes and cardiac hypertrophy, there is an adaptation in cardiac metabolism to a fetal metabolic state. Fetal metabolism infers a preference for carbohydrates over FFA due to the relative anaerobic environment of the fetal heart (Taegtmeyer et al., 2010). Within 24 hours (humans) to 3 days (mice) after birth, metabolism shifts towards the aerobic state found in a normal adult hearts. The consequence of fetal metabolism is the greater efficiency of ATP production per mole of oxygen consumed via carbohydrates (Goodwin et al., 1998). Secondly, during metabolic stress, there is a rapid mobilization of carbohydrate energy stores (Goodwin et al., 1998).

1.1.3 Skeletal Muscle Metabolic Substrates

In all mammals, glucose, along with FFA and protein, used by skeletal muscle as an energy resource in the production of ATP. The preferential use of substrates is substantially dependent upon the energy requirements of the muscle fibre. FFA are preferentially metabolized during times of increased intensity of exercise, whereas glucose is preferred with an increase in duration during low to moderate exercise (Spriet and Watt, 2003). As well, the skeletal muscle will increase the oxidation of glucose due to an increase in endogenous or exogenous glucose levels or increase the utilization of FFA due to an increase in exogenous FFA levels (Spriet and Watt, 2003). Endurance exercise training decreases the dependence of muscle on glucose metabolism, favouring an increase in lipid oxidation as an energy resource (Coggan et al., 1990; Coggan et al., 1993; Hargreaves, 2000). Protein oxidation is rarely utilized by skeletal muscle as excess protein metabolism can cause cell apoptosis, and generally contributes less than 5-10% of substrate energy (Lemon, 1987;

Tirone and Brunicardi, 2001). Muscle glycogen is the preferential carbohydrate fuel during moderate intensity exercise (Felig and Wahren, 1975; Lewis and Haller, 1990) as it produces less protons and more ATP than glycolysis with exogenous glucose (Robergs et al., 2004). As well, muscle glycogen is primarily employed during the initial stages of exercise as an energy source due the unavailability of FFA (Coakley et al., 1992). Depending on the duration and intensity of exercise, muscle glycogen levels are decreased by approximately 50-60% in the maintenance of skeletal muscle energy homeostasis and the production of ATP via glycogenolysis (Spriet et al., 1987).

1.2 Cardiac Glucose Metabolism

1.2.1 Glucose Transporters

The facilitated glucose transporters (GLUT) are the rate-limiting step in exogenous cellular glucose uptake. Primarily due to capacity of hexokinase activity, the membrane gradient supports an influx of glucose into the cell via the GLUTs (Montessuit and Lerch, 2012). There are currently 14 known glucose transporters in mammalian cells classified in three GLUT transporter classes (Class I, Class II, and Class III) (Thorens and Mueckler, ; Wood and Trayhurn, 2003), differing by substrate specificity, transport kinetics, and tissue distribution. GLUT 1, 4, 8, 10 and 12 have been identified in the normal myocardium (Abel, 2004; Aerni-Flessner et al., 2012; Doege et al., 2000; Grover-McKay et al., 1999). Among these, GLUT 1 and 4 are the most widely studied GLUT transporters. GLUT1 is identified as the "basal" transporter in the adult human heart, found primarily in the sarcolemma. In fetal cardiac metabolism, GLUT 1 is the primary transporter and found in abundance throughout the heart (Smoak and Branch, 2000). However, post-switch to adult metabolism, the insulin-responsive GLUT4 is the most abundant transporter found in the heart. GLUT4,

unlike GLUT1, is primarily located in an intracellular vesicular compartment. The binding of insulin to the insulin receptor stimulates a cascade of phosphorylation and upregulation of kinases that promote the translocation of GLUT4 to the plasma membrane. GLUT4 has a higher affinity for glucose (Km= 4-7 mM) than GLUT1 (Km= 20-26mM) (Nishimura et al., 1993; Palfreyman et al., 1992).

Recently, a study identified the GLUT involved in the basal and diseased state mouse myocardium (Aerni-Flessner et al., 2012). Using a model of dilated, hypertrophic myocardium (via aortic constriction), this study assess the relative RNA content of each of the cardiac GLUT isoforms (Aerni-Flessner et al., 2012). They found that in the normal heart, GLUT 4, 1 and 8 were the most profuse by order of expression. However, in the disease state, there was an increased expression of GLUT1 (Aerni-Flessner et al., 2012). These data match that previously seen in other cardiac disease state (Rosenblatt-Velin et al., 2001; Tardy-Cantalupi et al., 1999; Tian et al., 2001) whereby GLUT 1 is the predominate isoform.

1.2.2 Insulin Signaling

Glucose substrate utilization in the heart is primarily dependent on insulin stimulation of GLUT4 transporters (see Figure 1.2). Insulin produced by the pancreas binds to the insulin receptor, a terameric enzyme comprising of two extracellular α-subunits and two transmembrane β-subunits (Ottensmeyer et al., 2000). The binding of insulin to the receptor induces autophosphorylation of receptors on the β-subunits via activation of tyrosine kinase (Bertrand et al., 2008; Montessuit and Lerch, 2012). The activation and phosphorylation of the receptor results in further phosphorylation of tyrosine residues. This phosphorylation leads to activation of phosphatidylinositol 3-kinase (PI3K) which phosphorylates PI

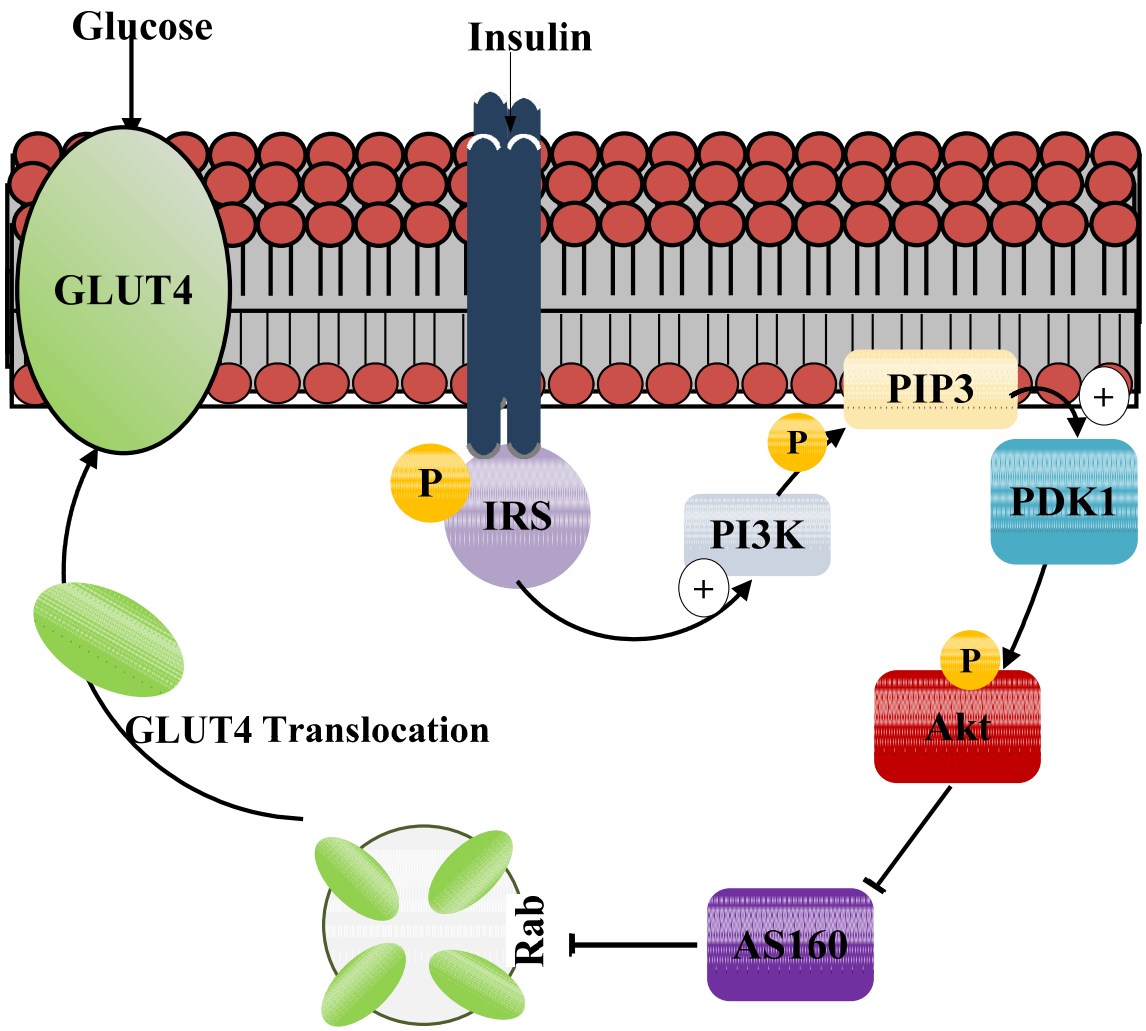

Figure 1.2: Schematic representation of GLU4 translocation to the cell membrane from intracellular vesicles in response to insulin binding.

phosphates and produces phosphatidylinositol (3,4,5)-triphosphate (PIP3) (Bertrand et al., 2008; Montessuit and Lerch, 2012). PIP3 activates phosphoinositide-dependent protein kinase 1 (PDK1) leading to the phosphorylation of the protein kinase Akt. Phosphorylation of Akt leads to inhibition of AS160, preventing Rab GAP function and subsequently allows for the translocation of GLUT4 to the plasma membrane (Bertrand et al., 2008; Montessuit and Lerch, 2012).

1.3 Glycogen

As a branched polymer of glucose, glycogen is a cellular store of carbohydrates in all mammals. Glycogen stores are located in liver, brain, kidney, fat, skeletal muscle and heart (Roach et al., 2012), and are utilized as energy stores in times of metabolic need. Not surprisingly, the major glycogen stores are located in the liver and skeletal muscle. Glycogen reserves in skeletal muscle serve as an isolated resource of glucose, as skeletal muscle lacks glucose-6-phosphatase and cannot, unlike liver glycogenolysis, release glucose into plasma for circulation (Tirone and Brunicardi, 2001). Glycogen synthesis and breakdown is believed necessary for the formation of a normal heart (Pederson et al., 2004). In the fetal heart, glycogen occupies more than 30% of the myocyte (Navaratnam, 1987). However, in the adult cardiomyocyte glycogen will only occupy about 2% (Navaratnam, 1987). Glycogen stores are associated with increased cardiomyocyte survival due to several mechanisms (Taegtmeyer, 2004). One may be that by shuttling glucose into glycogen deposition, the cell prevents augmented glucose concentrations and subsequent glucotoxicity (Taegtmeyer et al., 2010). Glycolysis has additionally been linked as the fuel source for the ATP dependent ion pumps (Taegtmeyer et al., 2010). In times of metabolic stress, the ability to increase ATP production from glycolysis may either maintain or increase the

efficiency of these transporters, preventing or reducing the progression of cardiac dysfunction. Glycogen stores, can therefore, be utilized in these times of stress to maintain cardiac function.

1.3.1 Glycogen Synthesis

The protein glycogen synthase (GS) modulates glycogen synthesis in response to glucose-6-phosphate levels (Roach et al., 2012). Two GS genes have been identified in mammals and listed by the common abbreviation GYS1 and GYS2. GYS1 is present in all tissues that metabolize glycogen while GYS2 is restricted to liver (Browner et al., 1989; Nuttall et al., 1994). Glycogen synthase kinase (GSK-3) was originally recognized for its role in phosphorylating GS and inhibiting its activity (Embi et al., 1980) (Figure 1.3). GSK-3 is a highly conserved serine/threonine protein kinase present in two isoforms in mammalian tissue: GSK-3α and GSK-3β (Haq et al., 2000), though the specific isoform roles are still under investigation. GSK-3 is an unusual protein kinase as it is active in the non-stimulated cell becoming inactive on stimulation (Haq et al., 2000). For example, insulin phosphorylates GSK-3 inhibiting its action on GS thereby promoting glycogen accumulation (Cohen, 2006). Additional to GSK's primary role in glycogen metabolism, GSK has been linked to cardiac hypertrophy due to its modulation of downstream targets of cardiac hypertrophy such as the calcium-calcineurin pathway, a potent inducer of myocardial hypertrophy (Molkentin et al., 1998).

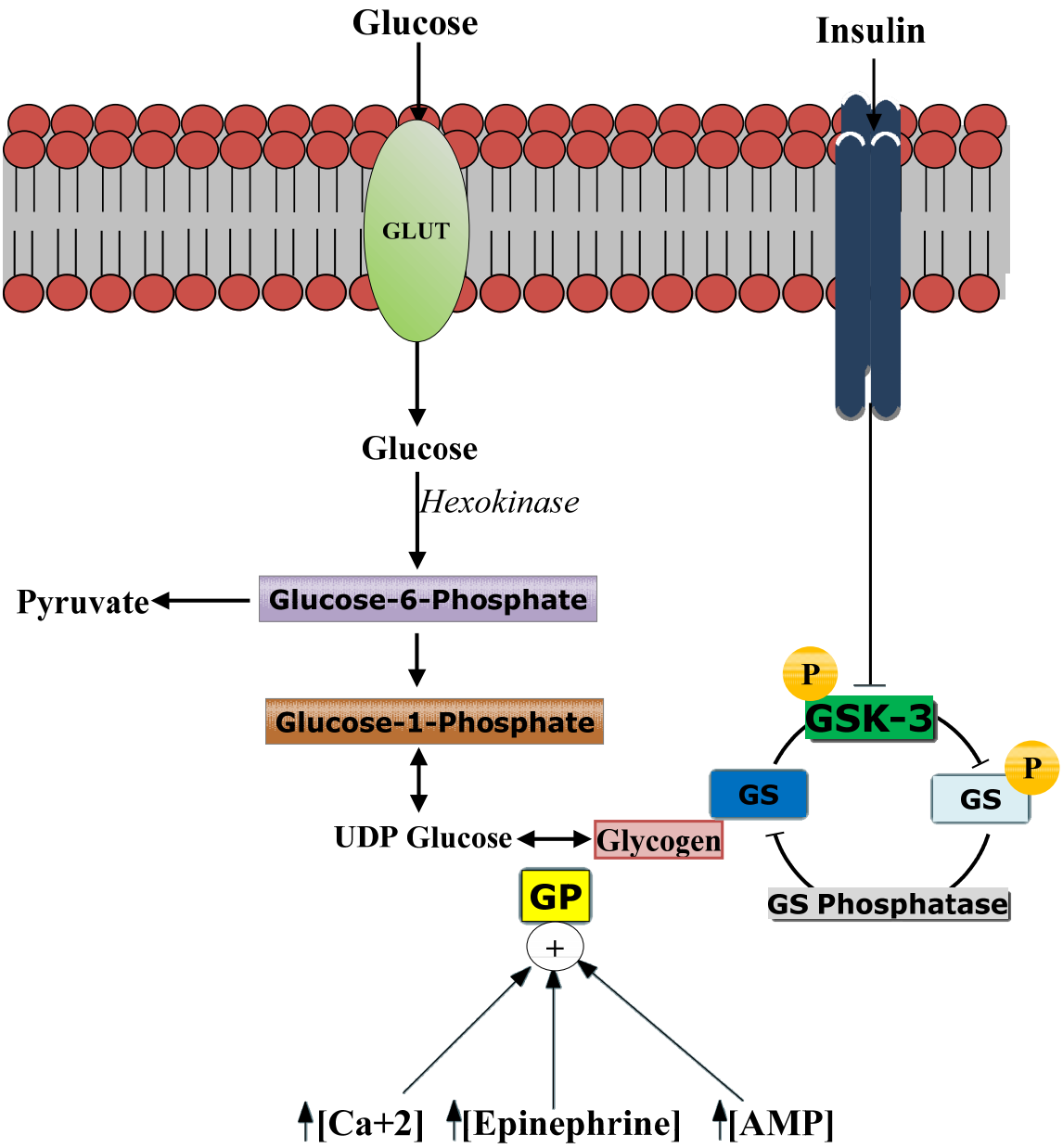

Figure 1.3: Glycogen synthesis and phosphorylation is modified by insulin, and cellular energy level indicators.

1.3.2 Glycogenolysis

While GS is the primary enzyme responsible for conversion of glucose residues into glycogen, glycogen phosphorylase (GP) hydrolyzes the α-1,4-glycosidic bonds of glycogen in the metabolic pathway of glycogenolysis producing glucose-1-phosphate (Tarnopolsky, 2006). As such, glucose-1-phophate can be metabolized for either aerobic or anaerobic glycolysis. GP exists as two forms, the less active *b* form and the active *a* form (Blomstrand and Saltin, 1999). GP*b* is transformed to the active form *a* in response to three stimuli: an increase in sarcoplasmic calcium concentration with muscle contractions, epinephrine stimulation during exercise, and increases in the concentrations of AMP, inosine monophosphate and inorganic phosphate (Hargreaves, 2000; Johnson, 1992; Richter et al., 1982). Glycogen itself can bind to GP and has been found to be a potent enhancer of GP activity (Shearer et al., 2001).

Glycogen metabolism is modulated by factors such as dietary intake, muscle temperature, and exercise. An increased dietary intake of carbohydrates amplifies the storage of glycogen in skeletal muscle thereby increasing the amount of glycogen available for glycogenolysis which in turn increases the reliance of muscle energy metabolism on glycogenolysis (Hargreaves et al., 1995). Temperature increases in working muscle have been found to increase glycogenolysis via an exercise-induced increase in plasma epinephrine (Hargreaves, 2000) which, as stated previously, is a known modulator of GP to its more active form.

1.3.3 Cardiac Glycogen Storage Diseases

Glycogen storage diseases are inherited metabolic diseases characterisized by excessive glycogen accumulation (storage) in various tissues (Shin, 2006). At least 15 genetic forms

of this disease have been described, with at least half known to affect the heart leading to a progressive cardiomyopathy, arrhythmia, and early death in the majority of cases (Shin, 2006). The genetic defects leading to glycogen storage disease share a common feature with all forms of glycogen storage disease due to gene mutations coding for enzymes involved in regulating the equilibrium between glycogen synthesis and glycogen degradation, representing a common pathway in the pathogenesis.

Clinical care for these conditions is primarily supportive, although in two forms of glycogen storage disease with severe cardiac consequences, enzyme replacement therapy has been utilized for treatment.

1.4 AMP-activated Protein Kinase (AMPK)

AMPK is a heterotrimeric serine-threonine kinase that serves to regulate cellular metabolism, ion channels and gene expression (Hallows et al., 2003; Hardie, 2003; Kahn et al., 2005; Kemp et al., 2003; Woods et al., 2000). AMPK behaves as a metabolic sensor for the cells, activated in times of metabolic stress, increasing ATP producing pathways and decreasing ATP consumption pathways (Carling, 2004). In the heart, ATP producing pathways are upregulated with increased FFA oxidation (Carling, 2004; Kudo et al., 1995; Luiken et al., 2003), and accelerated glucose uptake (Russell et al., 1999) stimulating glycolysis (Marsin et al., 2000). Genetic defects in the regulatory γ2 subunit of AMPK have been identified in the development of a metabolic cardiomyopathy, suggesting a dysregulation in the metabolic sensor function of AMPK.

1.4.1 Structure of AMPK

The heterotrimeric structure of AMPK contains both a catalytic subunit (α) and regulatory subunits (β and γ). Studies have found homologous subunits for each subunit of AMPK in

every eukaryate species (Carling, 2005), indicating the elemental necessecity of these subunits for the structure and function of AMPK. Additionaly Dyck *et al*., found that expression of the α, β, and γ subunits together resulted in a 50-100 fold increase in the AMPK activity compared to the expression of the α-subunit alone (Dyck et al., 1996). Each subunit of AMPK is encoded by distinctive genes and is differentially expressed in tissue regions (Hardie, 2003).

1.4.2 AMPK α Subunit

The α subunit of AMPK contains both an N- and C-terminus domain. The 63kDa α subunit (Dolinsky and Dyck, 2006a) contains two isoforms: α1 is widely expressed and encodes a 548 amino acid protein (Stapleton et al., 1996), while α2 is the predominate form found in the heart and skeletal muscle (Musi and Goodyear, 2003) and encodes a 552 amino acid protein (Stapleton et al., 1996). The α1 and α2 isoforms are 90% identical on the N-terminus and 60% identical on the C-terminus (Dolinsky and Dyck, 2006a). The N-terminus of the α-subunit is the kinase domain and contains the serine-threonine protein kinase domain (Carling, 2005; Dolinsky and Dyck, 2006a; Woods et al., 2003). The C-terminus contains a 150 amino acid residue domain at the extreme end, which is required for the interaction of the β and γ subunits (Carling, 2005; Crute et al., 1998). The C-terminus of the α subunit also contains the Thr 172 unit. Phosphorylation of Thr 172 is essential for the activation of AMPK activity (Crute et al., 1998; Stein et al., 2000) and is catalyzed by upstream kinases such as AMPKK and LKB1 (Carling, 2005).

In the heart, α2 activity has been reported to predominate over α1 activity (Li et al., 2006; Sakamoto et al., 2006). α2 is activated during exercise in both skeletal muscle and the heart (Coven et al., 2003; Fujii et al., 2000). It has been postulated from this that the α2 subunit

may then have an increased sensitivity to changes in the AMP concentration (Salt et al., 1998), and has been hypothesized to be important in glucose transport in both skeletal muscle and heart (Jorgensen et al., 2004; Young et al., 2005). This hypothesis has been studied in α2 knockout mice (Viollet et al., 2003b). These mice under a hyperinsulemic-euglycemic clamp were glucose intolerant, displayed low plasma insulin levels, decreased skeletal muscle glycogen synthesis, and increased excretion of catecholamines in the urine, suggesting an increase in sympathetic tone (Viollet et al., 2003b). However, this increase in sympathetic tone was not consistently exhibited, but found only during glucose challenges and under the hyperinsulinemic-euglycemic clamp (Viollet et al., 2003b).

1.4.3 AMPK β Subunit

The β subunit of AMPK has been long considered to be the scafolding protein of the heterotrimer structure of AMPK (Woods et al., 2000). β subunits contain a C-terminus ASC domain which is required for the interaction of the α and γ subunits (Iseli et al., 2005; Thornton et al., 1998). However, recent studies have found that the amino acid region 72-151 in the rat β subunit is analogous with the N-isoamylase domain (Hudson et al., 2003; Polekhina et al., 2003), traditionaly found in enzymes that metabolize the α-1-6 branch points in the α1-4 glucans such as glycogen and starch (Carling, 2005). This becomes very important in the role of AMPK in sensing ATP depletion, as glycogen levels can serve as a predetermination of ATP levels (Carling, 2005).

The two isoforms of the 43kDa β subunit (Dolinsky and Dyck, 2006a), β1 and β2 share a 71% amino acid identity and contain similar domains, including the glycogen binding domains (Hudson et al., 2003). The β1 isoform is found everywhere, while the β2 isoform is

highly expressed in the heart and skeletal muscle with a lower expression in the lung and kidney (Chen et al., 1999; Thornton et al., 1998).

1.4.4 AMPK γ Subunit

The γ subunit of AMPK contains four cystathionine-β-synthase domains (CBS), which have been reported previously in a wide variety of proteins in tandem pairs (Scott et al., 2004). The CBS proteins in the γ subunit bind either of the nucleotides AMP or ATP (Cheung et al., 2000; Scott et al., 2004). The four CBS domains bind either 2 molecules of ATP or AMP together, thereby increasing the sensitivity of the AMPK system to small changes in the nucleotide system (Hardie and Sakamoto, 2006). Binding of AMP to the CBS proteins serves to activate AMPK, while the binding of ATP inhibits the activation of AMPK (Hardie and Sakamoto, 2006), thereby making the AMP:ATP ratio the best predictor of AMPK activity (Corton et al., 1994) and a key energetic sensor for the heart (Young et al., 2005). Point mutations in the CBS domains of the γ subunit have been reported to alter AMPK activity (Daniel and Carling, 2002; Scott et al., 2004).

The 38kDa γ subunit (Dolinsky and Dyck, 2006a) is expressed as three isoforms; γ1 is ubiquitously distributed, γ2 is expressed mostly in the heart, while γ3 is specific to skeletal muscle (Cheung et al., 2000; Viollet et al., 2003a; Yu et al., 2004). Additionally, there are three transcripts of the γ2 isoform: γ2a (3.8Kb) which is expressed in brain, kidney, pancreas and liver but not found in the heart (Dolinsky and Dyck, 2006a), γ2a (3.0Kb) is highly expressed in the heart with low levels in the muscle, kidney, spleen and testis (Cheung et al., 2000) and γ2b (2.4Kb) which is found in the heart, testis and placenta (Lang et al., 2000) .

1.4.5 Activation of AMPK

AMPK is activated by the binding of AMP to the two CBS domains on the γ subunit (Jorgensen et al., 2006). This activation of AMPK by AMP occurs by two mechanisms: directly by allosteric activation, and indirectly by enhancing AMPK as a substrate for upstream kinases (Jorgensen et al., 2006) (Figure 1.4) . This allows for phosphorylation of Thr 172 on the α subunit, and activation of AMPK (Adams et al., 2004; Baron et al., 2005; Hawley et al., 1996; Hawley et al., 1995; Kahn et al., 2005; Scott et al., 2004). The binding of AMP to AMPK also inhibits dephosphorylation of AMPK by protein phosphatases (Davies et al., 1995). The adenylate charge hypothesis (Atkinson, 1970) therorizes that the small changes in the concentration of AMP would indicate changes in the cellular energy balance, and would regulate AMPK activity to maintain ATP concentration (Ponticos et al., 1998), therefore with only minor changes in ATP concentration, there are major changes in the AMP concentration causing an activation of AMPK (Dolinsky and Dyck, 2006a). This activation by AMP results in five-fold increase in AMPK activity (Adams et al., 2004; Cheung et al., 2000; Scott et al., 2004).

AMPK has also been reported to be activated by a decrease in the phosphocreatine (PCr): creatine (Cr) ratio, which would serve as precursor to a decrease in ATP levels as phosphocreatine is depleated to maintain ATP levels in the Lohmann reaction ($PCr + ADP + H^+ \rightarrow ATP + Cr$) (Ponticos et al., 1998). AMPK is also believed to be directly activated by other compounds such as leptin (Minokoshi et al., 2002), adiponectin (Yamauchi et al., 2002), and FFA (Clark et al., 2004; Folmes et al., 2006; Watt et al., 2006).

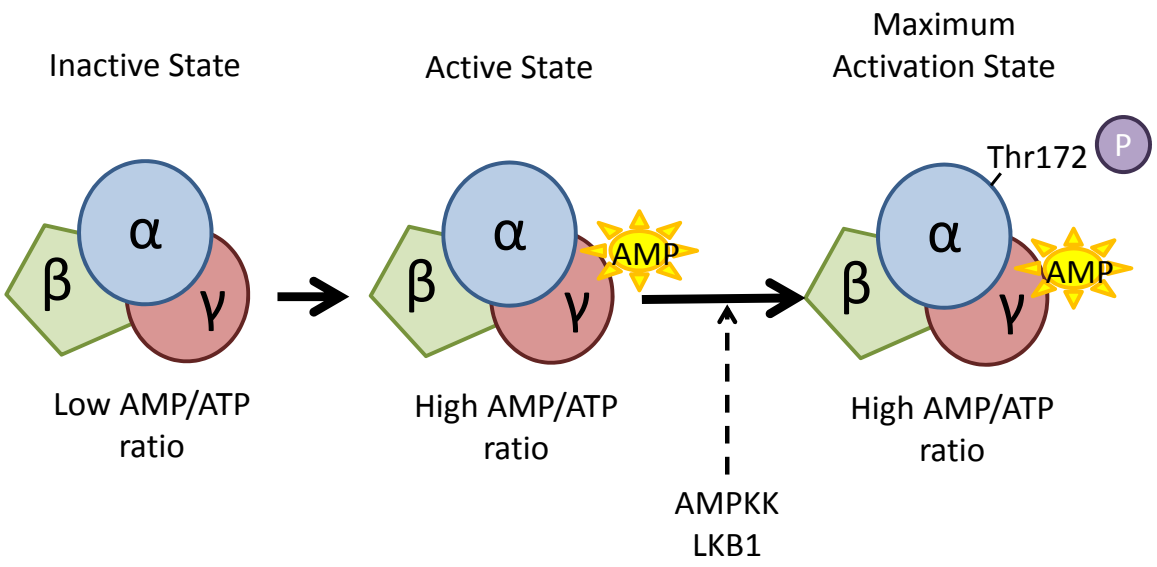

Figure 1.4: AMPK activation states through an increase in the AMP/ATP ratio with phosphorylation by upstream kinases of the Thr-172 unit on the α-subunit.

Exercise activates AMPK in both the skeletal muscle and heart (Coven et al., 2003; Winder and Hardie, 1996). The heart increases its metabolism of both FFA and glucose during exercise to meet the increase in energy demands and therefore, supply of ATP (Kudo et al., 1995; Marsin et al., 2000; Russell et al., 1999). Indicative of this is that AMPK activity has been reported to increase in proportionality to both exercise intensity (Coven et al., 2003) and workload (Beauloye et al., 2002), most likely due to an increase in AMP levels (Musi et al., 2005).

1.4.6 Alterations in AMPK isoform expression

A recent study investigated the isoform expression of AMPK in mouse myocardial tissue during cardiac development and following induction of heart failure (Kim et al., 2012). The findings were also compared to cardiac tissue harvested from human heart failure patients during the implantation of an LV assist device with control tissue harvested from donor hearts that were deemed unsuitable for transplantation (not due to cardiac disease). Expression levels of α1 and γ2 isoforms are increased appproximately three-fold in the mouse fetal heart compared to post-birth levels (Kim et al., 2012). In the heart failure model, the protein expression and mRNA levels of α2, β2 and γ2 isoforms were all augmented. Interesting, it was the α1, β1 and γ2 isoforms that displayed increased protein expression in the human failing heart, though no change in mRNA expression was found (Kim et al., 2012). These authors do however stipulate, that differences in harvesting of cardiac tissue from mice and human subjects, as well as the influence of disease state, therapies and genetic factors in human subjects, may be a limitation to this data (Kim et al., 2012).

1.5 AMPK and glucose metabolism

1.5.1 AMPK regulation of glucose metabolism

AMPK stimulates glucose uptake by promoting the translocation of GLUT 4 to the sarcolemma independent of insulin (Bertrand et al., 2006; Russell et al., 1999; Yang and Holman, 2006; Young et al., 2005). However, the exact mechanism by which AMPK stimulates GLUT4 is unknown. The increase in GLUT 4 transporters expressed on the plasma membrane (Dolinsky and Dyck, 2006b) would cause an increase in glucose uptake and stimulate an increase in glycolysis, thereby producing ATP (Merrill et al., 1997).

AMPK has also been reported to increase phosphofructokinase-2 (Marsin et al., 2000), producing fructose 2-6-biphosphate which stimulates glycolysis (Depre et al., 1998). Together, these results provide a pathway for AMPK to increase glucose uptake and glycolysis, and glucose mediated ATP production. Excess glucose however, would be stored in the form of glycogen, the proportion of which is controlled by the activity of GS. Glycogen levels in the heart are relatively maintained by GS despite rapid catabolism (Henning et al., 1996).

1.5.2 AMPK regulation of Glycogen Synthase

GS activity is regulated by glycogen levels and by both glucose-6 phosphate activity and insulin, due to their activation and involvement in increased glucose uptake (see section 1.3). Recently, research has indicated a role for AMPK in regulation of GS. *In vitro* studies have shown an inhibitory effect of AMPK on GS (Carling and Hardie, 1989; Wojtaszewski et al., 2002) with acute activation of AMPK *in vivo* displaying increased glycogenolysis (Longnus et al., 2003; Polekhina et al., 2003). However, *in vivo* data from transgenic mouse models with mutations in AMPK do not appear to support this relationship in the heart (Arad et al.,

2003; Beyer et al., 2000; Longnus et al., 2003). The activation of AMPK and effect on the GLUT4 transporters to the sarcolemma effectively increases glucose uptake despite high glycogen levels (Nielsen et al., 2002). An increase in glucose uptake has also been linked to a decrease in glucose-6-phosphate inhibition of hexokinase due to the decrease in glycogenolysis (Richter and Galbo, 1986). These conflicting data have left the exact mechanism by which AMPK regulates glycogen storage and metabolism unknown.

1.6 AMPK in Pathological Cardiac Metabolism

1.6.1 Ischemia-Reperfusion Injury

When flow is reduced to the myocardium there is a disruption in myocardial metabolism due to reduced substrate availability (glucose, FFA) and a reduction in ATP resynthesis (Bak and Ingwall, 1998; Stanley, 2004). The decrease in ATP resynthesis activates anaerobic glycolysis, which increases lactate formation, decrease cellular pH resulting in alterations in ion kinetics (Stanley, 2004). It has also been demonstrated that ATP produced by glycolysis is used for cellular ion homeostasis, and the maintenance of this homeostasis will be to the detriment of contractile function (Dennis et al., 1991; Kloner and Jennings, 2001; Liu et al., 2002; Oliver and Opie, 1994; Opie, 1990). Sufficiently prolonged ischemia (more than 20-30 minutes) can result in an infarction where irreversible cell injury and death leads to scar formation. Once cell death occurs, the tissue region is no longer viable and will not recover even if adequately revascularized. However, metabolic derangements in the myocyte after short bouts of ischemia may result in more prolonged reductions in contractile function that can eventually recover (Bolli, 1992; Braunwald and Kloner, 1982). Reperfusion prior to cell death may salvage cellular viability, commonly seen in cases of hibernating myocardium. The hallmark of hibernating myocardium is an increase in glucose uptake in a hypoperfused

tissue region indicating cell viability (Beanlands et al., 2008). The restoration of blood flow is critical in restoring cardiac function (Beanlands et al., 2008). In all cases, following reperfusion, it appears that FA oxidation recovers faster than glucose oxidation, thus maintaining the uncoupling from glycolysis (Lopaschuk et al., 1988; Lopaschuk et al., 1993; Neely and Morgan, 1974; Saddik and Lopaschuk, 1994). Thus, as in ischemia, the uncoupling between glycolysis and glucose oxidation continues to push lactate production, and subsequent proton accumulation with a decrease in cellular pH (Liu et al., 1996; Lopaschuk, 1997; Lopaschuk et al., 1993).

The activation of AMPK during ischemia attempts to restore ATP levels through its role in upregulation of metabolic substrate utilization. What is currently disputed is if the increase in FA oxidation is through both an increase in lipoprotein lipase activity (Pulinilkunnil et al., 2010)and increased translocation of CD36 to the cell membrane (Habets et al., 2007; Luiken et al., 2003), or simply by the phosphorylation of ACC inhibiting malonyl-CoA activity resulting in an increase in FA oxidation (Kim et al., 1989; Kudo et al., 1996). Although this increase in FA oxidation by AMPK may appear to be detrimental by uncoupling glycolysis from glucose oxidation, the metabolism of FFAs may in itself prevent cellular accumulation and lessen the potential of developing lipotoxicity (Cao et al., ; Li et al., 2010; Minokoshi et al., 2002).

1.6.2 Metabolic Syndrome

The metabolic syndrome is defined by a cohort of risk factors including high blood pressure, elevated triglycerides with low high density lipoprotein cholesterol, abdominal obesity and the presence of insulin resistance (Hardie, 2008). Insulin resistance in itself, results from a failure to compensate to increased endogenous pancreatic insulin secretion. The liver fails to

respond to the inhibition of insulin with a continuation of gluconeogenesis and hepatic glucose production (Hardie, 2008). Tissue fails to respond to insulin signaling resulting in decreased insulin-mediated glucose uptake defining insulin resistance. The failure in this progression leads to the development of a chronic hyperglycemic state otherwise termed type 2 diabetes mellitus (T2DM) (Hardie, 2008).

1.6.3 Type 2 Diabetes

The cardiovascular consequences of T2DM are diverse, with structural changes resulting in LV hypertrophy, systolic and diastolic dysfunction, lipotoxicity with increased triglyceride storage, and the above mentioned insulin resistance (Hardie, 2008).

The interplay of insulin signaling and AMPK appears to be through the Akt and AS160 proteins. The activation of Akt by insulin has been demonstrated to inhibit AMPK via the phosphorylation of the AMPK α-subunits on Ser485 or Ser491(α-1 and α-2 respectively) (Horman et al., 2006) subsequently blocking phosphorylation of Thr^{172} by upstream kinases. Conversely, AMPK has been shown to phosphorylate and thereby inhibit AS160 independently of insulin, which in turn prevents Rab GAP function and thus increases translocation of GLUT4 (Treebak et al., 2006) (see Figure 1.2). The strongest evidence for interplay between AMPK and insulin resistance comes from the use of metformin in T2DM. The biguanide class drug has been employed as treatment for T2DM for over 50 years. Metformin is currently not thought to be a direct activator of the AMPK complex in itself, instead it has been proposed to an inhibitor of the mitochondrial ETC complex 1 resulting in an increase in the AMP/ATP ratio and subsequent activation of AMPK (Owen et al., 2000). The activation of AMPK and contribution of T2DM morbidity is conflicting. While the activation of AMPK inhibiting FFA synthesis and increases FFA oxidation may reduce the

cardiac lipotoxicity well documented in T2DM, the "Randle" cycle effect on glucose oxidation incurs the same repercussions as outlined in the ischemic model. Thus whether AMPK activation in metabolic syndrome, and more specifically T2DM, is beneficial or detrimental has yet to be determined.

1.6.4 Type 1 Diabetes

Often termed juvenille diabetes, type 1 diabetes mellitus (T1DM) occurs due to a genetic autoimmune destruction of pancreatic β-cells, thereby initiating a reliance on insulin for the duration of the patient's lifespan. Although exogenous insulin provides an effective treatment, the fluctuations in blood glucose levels are known to cause alterations in myocardial metabolism. Interestingly, in type 1 diabetic patients, high circulating plasma FFA levels have been linked to increased myocardial FFA uptake and reduced glucose uptake despite physiological stimulation with insulin (Herrero et al., 2006). These alterations in cardiac metabolism have also been noted in experimental mouse models (An and Rodrigues, 2006). Streptozotocin (STZ) induced type 1 diabetes, is one of the most commonly used diabetic animal models. STZ is an alkylating agent that is similar to glucose in structure, and is preferentially transported into pancreatic β-cells by GLUT2 transporters (Szkudelski, 2001). In rats, STZ induced diabetes is produced by a singular iv injection of 45-65 mg/kg (Ganguly et al., 1987; Ganguly et al., 1986; Tesch and Allen, 2007), while mouse models are produced via 5 days of ip injections at a dose range of 50-55 mg/kg (Rabbani et al., 2011; Tesch and Allen, 2007). The STZ model provides a physiological platform for the analysis of the effect of severe hyperglycemia (when left untreated), whereby there is a report of a loss of LV function in chronic state (Aneja et al., 2008), indicating that dysregulation of cardiac glucose metabolism is linked to cardiac function.

1.6.5 PRKAG2

Mutations in the γ2 subunit of AMPK have been identified in humans as an autosomal dominant disease found in selected families worldwide, collectively termed PRKAG2 (protein kinase, AMP-activated, γ2 non-catalytic subunit). The hallmark of this disease is the excessive deposition of glycogen in cardiac muscle (Figure 1.5) with the development of a clinical phenotype consisting of ventricular pre-excitation (Wolf-Parkinson-White syndrome (WPW)), atrial fibrillation, progressive conduction system disease and cardiac hypertrophy. PRKAG2 is a progressive disease, with symptoms of WPW found in children progressing to pacemaker implantation by the patients' fourth decade of life and in some cases the need for a heart transplantation with the risk for early cardiac death (Gollob, 2003; Gollob et al., 2002; Gollob and Roberts, 2002). Although this is not a sex-linked disease, hormonal differences between males and females have been previously reported to affect the progression and development of cardiac disease, necessitating the need to investigate both sexes (Du, 2004). Cardiac hypertrophy resulting from the excess glycogen is currently being defined as a distinct form of hypertrophic cardiomyopathy. Hypertrophic cardiomyopathy is classically described as a "disease of the cardiac sarcomere" (Oliveira et al., 2003), with histopathology that includes myocyte enlargement, myocyte disarray and increased interstitual enlargement (Arad et al., 2002). Histopathology of PRKAG2 tissues presents similar enlarged myocytes as well as vacuoles containing glycogen derivatives
which are not specific to hypertrophic cardiomyopathy (Arad et al., 2002). Contradictory to hypertrophic cardiomyopathy is an absence of myocyte disarray and minimal interstitial fibrosis in PRKAG2 tissues (Arad et al., 2002). In the PRKAG2 hearts, the resultant increase in cardiac mass appears to result from the increased glycogen storage and water in

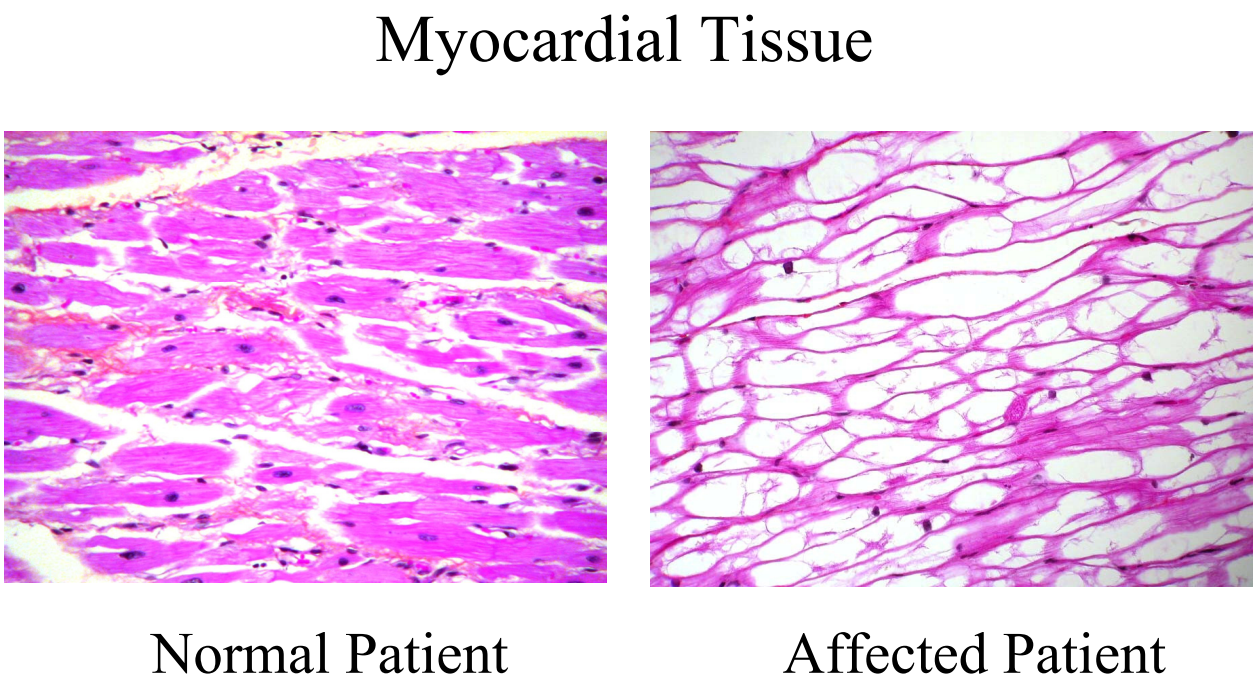

Figure 1.5: Periodic acid Schiff (PAS) histopathology of myocardial tissue taken from a control subject (left) and from an affected PRKAG2 patient (right). Note the large vacuoles in the affected patient due to glycogen deposition (unpublished data, UOHI).

the cardiomyocytes (Verloes et al., 1997).

The electrophysiological abnormalites present in the PRKAG2 patients could be due to a direct effect of AMPK on ion channels, or due to the increase in glycogen interfering with the ion channels (Arad et al., 2002; Dyck and Lopaschuk, 2006). This dysfuction in electrophysiology has been noted in other glycogen storage diseases such as Pompe's and Danon's disease (Bulkley and Hutchins, 1978; Danon et al., 1981; Francesconi and Auff, 1982; Verloes et al., 1997).

1.6.6 PRKAG2 Mouse Model

The altered mechanisms of the PRKAG2 cardiac syndrome are currently being investigated at the University of Ottawa Heart Institute in a transgenic (TG) mouse line with the AMPK γ2 subunit R302Q mutation; the same mutation found in the Ottawa region PRKAG2 human patients (Folmes et al., 2009; Sidhu et al., 2005). The Arg302Gln (or R302Q) PRKAG2 mutant mouse (TGmut) displays very similar phenotypes to the human PRKAG2 disease with progressive development of WPW, electrophysiological dysfunction, increased glycogen content and cardiac hypertrophy (Sidhu et al., 2005). There are currently six different AMPK γ2 subunit amino acid sequence mutations that develop the human PRKAG2 phenotype including WPW (Zaha and Young, 2012), with four of these mutations currently under investigation in transgenic mouse models (R302Q, T400N, N488I, R531G). However, despite these mice developing similar cardiac phenotype, the data regarding AMPK activity have been conflicting. The N488I mouse model reports increased AMPK activitity compared to wild-type litermates (Arad et al., 2003). The R531G displays a differential progression with no detectible PRKAG2 phenotype and similar AMPK activity levels to their nontransgenic litermates at one week of age (Davies et al., 2006). However, at

4 weeks of age, mice develop cardiac hypertophy, electrophysiological dysfunction and increased glycogen accumulation along with reduced AMPK activity (Davies et al., 2006). These authors proposed that the decrease in AMPK activity may be a result of negative feedback due to increased glycogen levels, as the change in AMPK activity seems to be correlated to changes in the glycogen levels (Davies et al., 2006). The apparent discrepancy in AMPK activity may be due to biphasic expression. In the Thr400N mutant mouse model, AMPK activity was found to change dramatically over the age of the animals (Banerjee et al., 2007) with AMPK increased from 2 days to 2 weeks of age, and reduced from 4 to 12 weeks of age. Indeed, in our R302Q model, AMPK activity is observed to be increased at 7 days of age and then reduced at 2-5 months of age (Folmes et al., 2009; Sidhu et al., 2005). Additionally, GS activity was decreased with a reduction of AMPK activity at 2-5 months of age (Folmes et al., 2009).

An increase in AMPK activity could cause an increase in GLUT4 translocation and subsequent increase in glucose transport and storage. While a decrease in AMPK activity may be a result of negative feedback by either glucose-6-phosphate or glycogen levels.

Interestingly, in both the transgenic wildtype N4881 and R531G mice, there was increase in glycogen deposition noted in cardiac muscle at higher levels than found in the non-transgenic littermates, but at lower levels than the mutant PRKAG2 transgenic mice (Davies et al., 2006; Sidhu et al., 2005). These results suggest an effect of the increased PRKAG2 expression alone on glycogen storage.

These studies provide a conflicting theory on how AMPK may regulate glucose uptake and storage and the mechanism by which dysfunction of AMPK activity in PRKAG2 contributes to glycogen storage disease. The clear understanding of the mechansim by which this disease

develops is relevant to the development of an appropriate therapy for the affected individuals which does not currently exist.

1.6.7 PRKAG3

Analagous to the human Arg302Gln-PRKAG2 mutation (Gollob et al., 2001a; Gollob et al., 2001b; Sidhu et al., 2005) is a naturally occuring R225Q γ3 subunit mutation (PRKAG3) found in pigs (Arad et al., 2002; Milan et al., 2000; Yu et al., 2006). The PRKAG3 mutant pig was found to have an increase in skeletal muscle glycogen content, hypothesized to be the prevelant means for acidic tissue pH via lactic acidosis (Arad et al., 2002; Milan et al., 2000; Yu et al., 2006). Interestingly, a homogolous mutation in humans, the R225W, results in increased AMPK activity, glycose uptake and glycogen content (Costford et al., 2007). In opposition to the detrimental effects of the AMPK mutation on cardiac morbidity and mortality, in skeletal muscle, the PRKAG3 is a gain of function mutation, modifiying metabolism for resistance of muscle fatigue, enhancing exercise capacity (Crawford et al., 2010).

1.7 Metabolic Modulators

1.7.1 Inhibition of fatty acid uptake

Targeting fatty acid (FA) oxidation in cardiac disease is attractive, theoretically preventing the uncoupling of glycolysis and lactate formation from glucose oxidation. Carnitine palmitate transferase-1 (CPT-1) is the rate limiting step for incorporation of FA into the mitochondria and subsequent FA oxidation. Two inhibitors of CPT-1, Etomoxir (Reaven et al., 1988) and Perhexiline (Lee et al., 2005) have shown promise for their anti-ischemic effects and treatment of heart failure. Another target of pharmacological inhibition is

malonyl-CoA decarboxylase. The inhibition of the activity of this enzyme, has been shown to increase glucose oxidation and insulin sensitivity in rodent models of heart failure (Hardie, 1989).

1.7.2 Targeting FA oxidation

Trimetazidine (TMZ) is an anti-ischemic agent that has shown no hemodynamic effects. TMZ is clinically approved in over 80 countries, but has not yet been approved in the USA or Canada due to the requirement of demonstrating its effect on the QT interval of the electrocardiogram. TMZ selectively inhibits the activity of long chain 3-ketoacyl-coenzyme A thiolase (3-KAT), the final enzyme of the FA β-oxidation pathway (Figure 1.6). This leads to a partial inhibition of FA β-oxidation with a concurrent increase in glucose oxidation (Kantor et al., 2000).

Previous studies have reported an increase in glucose utilization with TMZ treatment. Mody et al (Mody et al., 1998) treated canines with a "low-dose" (1 mg/kg) or "moderate-dose" (5 mg/kg) of TMZ prior to LAD ligation surgery to induce ischemia. Each animal underwent PET scanning with [^{13}N]ammonia (a flow tracer to delineate the ischemic zone), [^{11}C]acetate (as a measurement of total oxidative metabolism), and 2-[^{18}F]fluoro-2-deoxyglucose (myocardial glucose uptake) 30 min post-ligation surgery. An increase in myocardial glucose uptake was observed in the high-dose TMZ group in both the ischemic and non-ischemic zone with no significance difference of total oxidative metabolism between either TMZ group or controls (Mody et al., 1998). These authors concluded that the increase in glucose utilization was either due to an increase in glycolysis or a shift in myocardial metabolism towards increased glucose oxidation equal to the decrease in FA

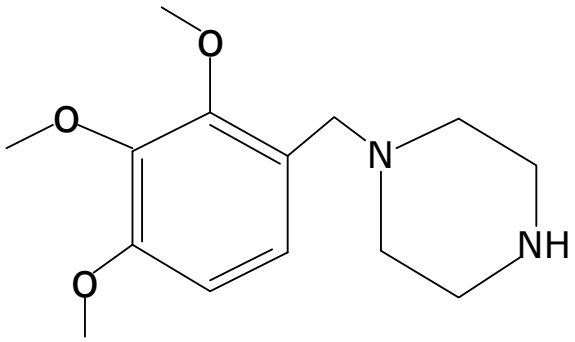

Figure 1.6: Molecular structure of 1-(2,3,4-trimethoxybenzyl)piperazine (Trimetazidine or TMZ)

oxidation thereby presenting as no net change in total oxidative metabolism (Mody et al., 1998). An additional study by Szkilnik et al (Szkilnik et al., 2005) investigated the use of 5.0 mg/kg ip TMZ for 14 days in rats and found a significant increase in [^{3}H]glucose uptake in the right ventricle. More recently, Di Napoli et al (Di Napoli et al., 2007) showed that chronic (18 months) TMZ treatment significantly improved cardiac function in New York Health Association (NYHA) class II and III patients with ischemic cardiomyopathy. Li et al (Li et al., 2010) have recently aimed to investigate the metabolic modulation effect of TMZ on diabetic cardiomyopathy in db/db mice. This study gavaged animals with a TMZ dose of 10 or 30 mg/kg/day for 8 weeks. There was a significant difference between the TMZ treated and control db/db mice in their measurements of lipotoxicity, oxidation status of the heart, or improvement in cardiac function (Li et al., 2010). Additionally, there was no difference between the TMZ doses of 10 and 30 mg/kg with both showing equal efficacy.

1.8 PET

PET is a non-invasive nuclear imaging modality used to assess biological processes *in vivo* serially in the same subject reducing intersubject variability. PET utilizes spatiotemperal imaging to quantify in absolute units, the distribution of radiolabeled probes (Wahl, 2002). PET radiotracers are produced via a cyclotron and include carbon-11, nitrogen-13, oxygen-15 and fluorine-18 isotopes. The advantage of these PET isotopes is that they can be substituted for C, N, O or OH ions in multiple biological compound maintaining the biological and pharmacodynamics of the parent compound. PET isotopes are 'unstable' containing a higher number of protons than neutrons (Figure 1.7). The proton decays to a neutron, emitting a positron that travels a short distance (mm) before annihilation with the

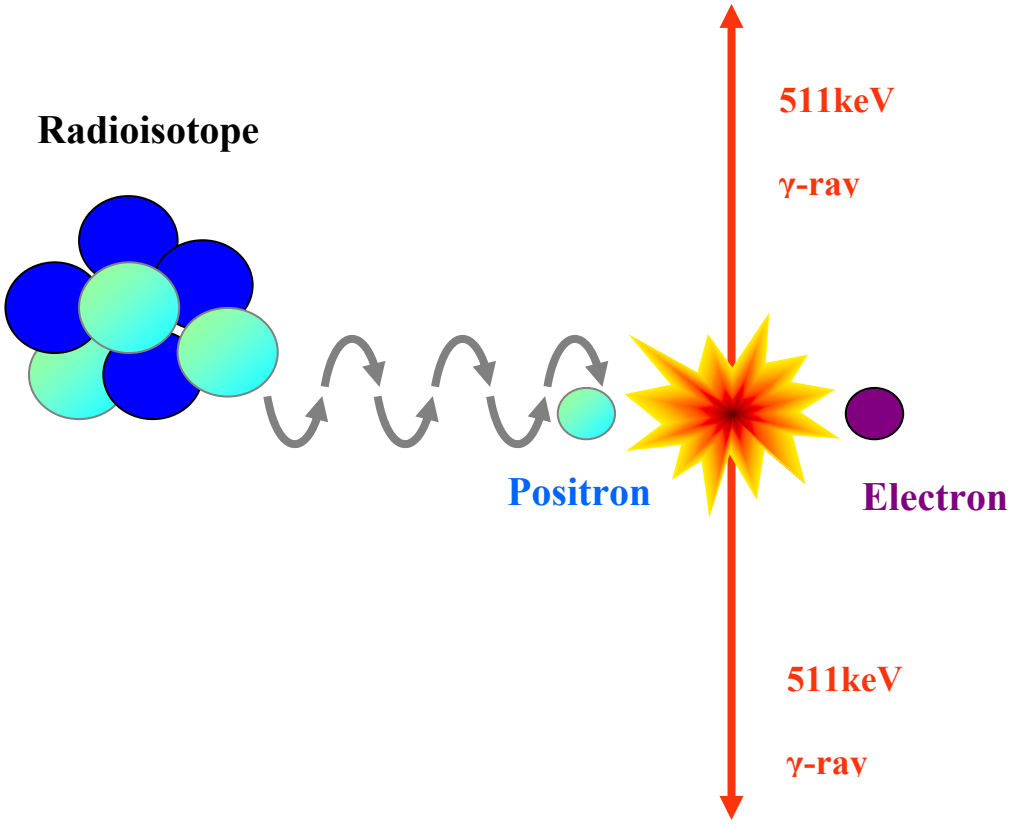

Figure 1.7: Molecular basis for PET. Detection of positrons occurs following annihilation of the positron for unstable isotope nucleus. Scintillation crystals in detector rings detect the 511 keV gamma rays to produce a three dimensional PET image.

valence electrons and emitting two 180° photons of 511 keV (gamma rays). The photons are registered by high-density crystal detectors in the rings of PET cameras. The registration of coincidence events, produces an electronic signalling. This signal is subsequently amplified, and corrected for decay, scatter and attenuation producing a three-dimensional PET image of the radioactive concentration within the living organism. PET has high sensitivity typically in the picomolar to fentomolar range. Cardiac imaging has become integral in the investigation, diagnosis and development of therapies. Myocardial metabolism is primarily investigated with PET due to its capacity for radiolabeling metabolic substrates (Table 1.1). Quantitative metabolic imaging can be obtained with dynamic scans, accurate blood sampling, and kinetic modeling. In the clinical investigation of adult PRKAG2 patients, we measured a 45% reduction in myocardial glucose uptake in affected patients versus control subjects (Ha et al., 2009).

1.8.1 MicroPET Imaging

Small animal PET cameras were developed to increase the image resolution and sensitivity from human cameras; alterations needed to image small animal regions of interest. This was achieved by utilizing smaller crystals with a smaller detector ring diameter, and longer axial coverage.

The Siemens Inveon™ camera was developed to increase the spatial resolution for small animal imaging. This camera uses lutetium oxyorthosilicate crystals (1.51 x 1.51 x 10 mm) with 400 crystals in an array and 64 detector blocks. The camera has an axial field of view (FOV) of 12.7 cm and transaxial FOV of 10.0 cm. The longer axial FOV allows the whole mouse to be positioned within the image (Figure 1.8).

Table 1.1: PET cardiac metabolism tracers

Tracer	**Function**
[^{11}C]Acetate	Oxidative metabolism
[^{11}C]Glucose	Glucose uptake, glycolysis, glycogen storage, glucose oxidation
2-[^{18}F]Fluoro-2-deoxyglucose (FDG)	Glucose uptake (GLUT, Hexokinase activity)
L-3-[^{11}C]Lactate	Lactate uptake and oxidation
[^{11}C]Palmitate	FFA uptake and oxidative metabolism
[^{18}F]fluoro-4-thia-palmitate (FTHA)	FFA uptake and oxidative metabolism
14(*R,S*)-[^{18}F]fluoro-6-thia-heptadecanoic acid	FFA uptake and oxidative metabolism

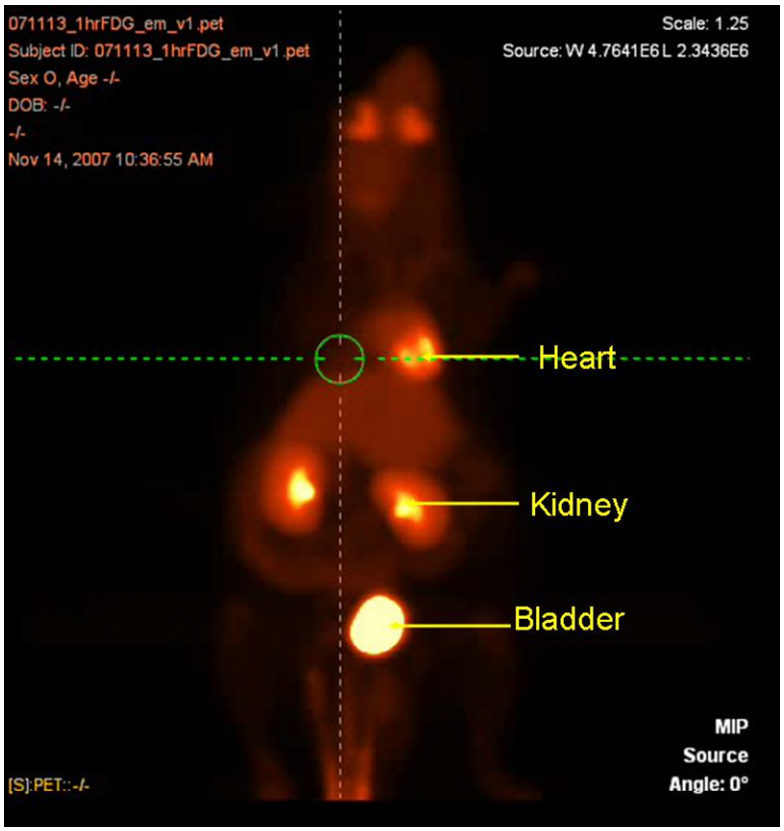

Figure 1.8: Whole body mouse FDG image acquired with the Inveon DPET system.

Despite these advances in camera engineering and increases in spatial resolution, mouse myocardial imaging is challenging. Blood input function in PET imaging is traditionally sampled from the LV cavity. In mice, the LV cavity is on the spatial resolution of the current systems. The inaccuracy of the LV cavity blood pool image derived input function (IDIF) is a major hinderance for reliable kinetic measurements (Fang and Muzic, 2008; Ferl et al., 2007; Locke et al., 2011). As a result, investigators have used blood sampling to determine the input function (Convert et al., 2007; Fang and Muzic, 2008; Ferl et al., 2007; Kreissl et al., ; Tantawy and Peterson, 2010). While manual blood sampling can provide accuracy, it incorporates invasive procedures, reducing the serial imaging capabilities. Other studies have suggested using gated iterative reconstruction (12 subset OSEM 2D 2 iterations, 18 MAP iterations) to measure an accurate IDIF with the LV cavity (Locke et al., 2011). This methodology presents practical issues due to long reconstruction times (~34 hr per mouse) and a reliance on a stable ECG for the duration of the scan, which may be difficult in models of ischemia or in the PRKAG2 mouse model.

1.9 PET Tracers

1.9.1 FDG

2-[^{18}F]fluoro-2-deoxyglucose (FDG) (Figure 1.9) is a glucose analogue, routinely produced by $^{18}F^-$ nucleophilic substitution of the triflate group, to assess cardiac glucose uptake and cell viability with PET (Yoshinaga et al., 2005) (Figure 1.10). FDG enters the cell via GLUT transporters (K1 and k2 rate constants) and is phosphorylated by hexokinase to [^{18}F]FDG-6-phosphate (k3 rate constant). The chemical structure of [^{18}F]FDG-6-phosphate traps the radiolabeled product within the cell. The FDG uptake rate constant, K_i =

A

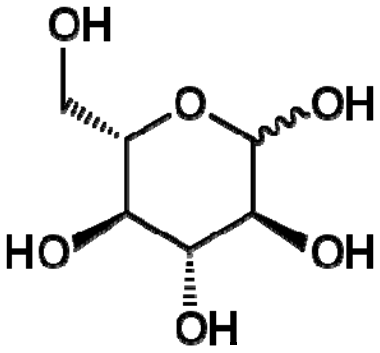

B

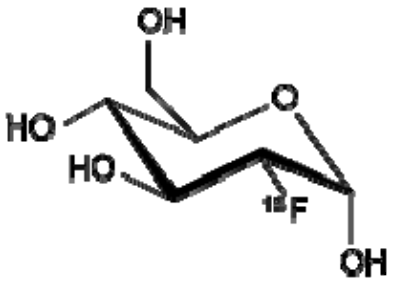

C

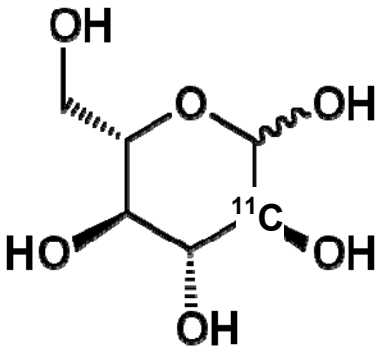

Figure 1.9: Chemical structures of glucose (A), FDG (B), and [^{11}C]glucose (C)

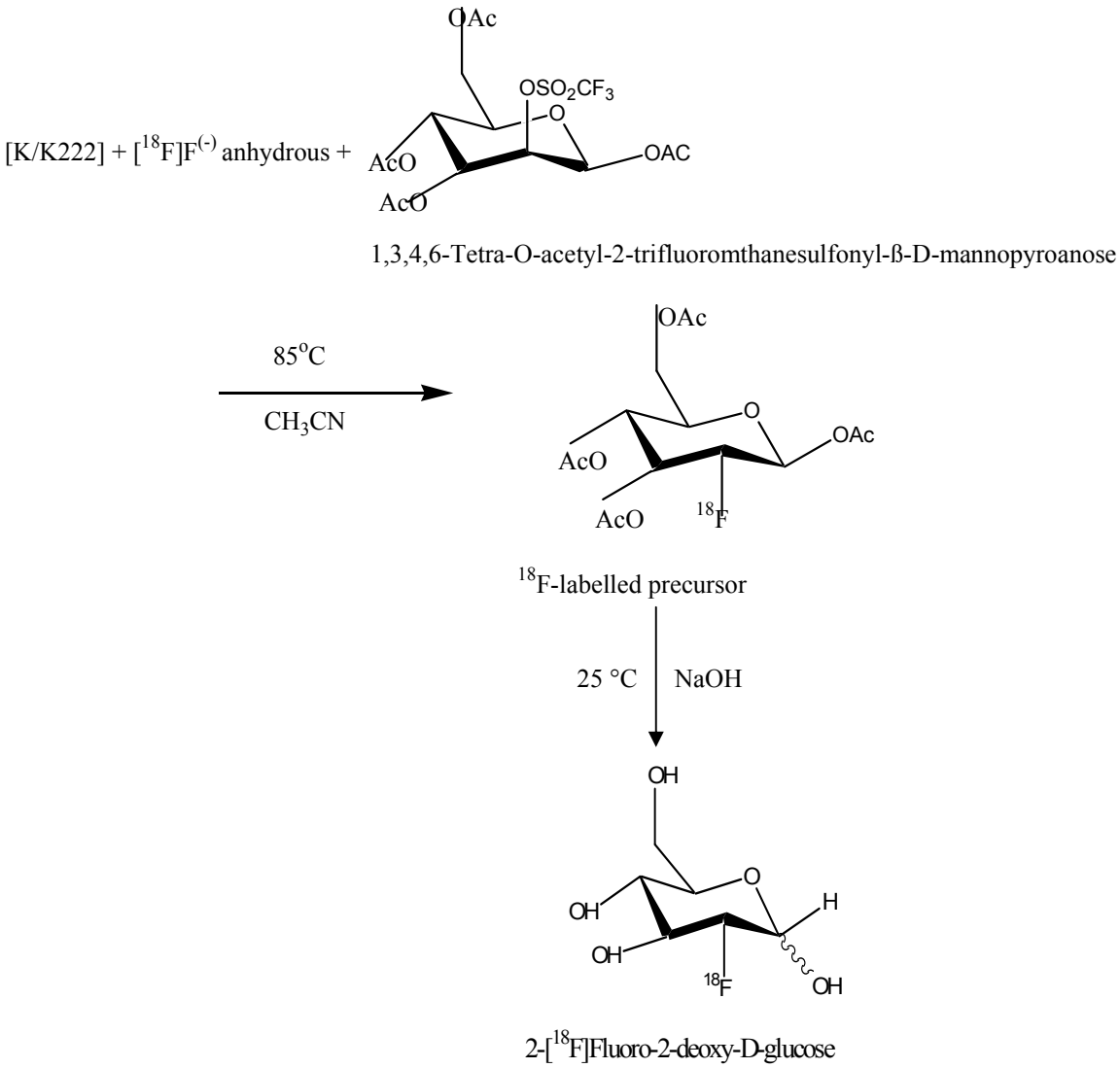

Figure 1.10: Synthesis of 2-[^{18}F]fluoro-2-deoxy-D-glucose (FDG)

(K1×k3)/(k2+k3), can be estimated using Patlak graphical kinetic analysis (Patlak and Blasberg, 1985), assuming there is negligible tracer washout (k4=0).

1.9.2 [^{11}C]Glucose

Radiolabeled [^{11}C]glucose (Figure 1.9C) provides an advantage over FDG as it follows the same metabolic fate and kinetics as unlabeled glucose in the myocardium resulting in a four compartment model (Herrero et al., 2002a; Herrero et al., 2002b). Radiolabeled glucose enters the cell via the GLUT transporters (k1 and k2) and similar to FDG is phosphorylated by hexokinase to glucose-6-phosphate (k3). Radiolabeled glucose can become a substrate for glycogen synthesis to form radiolabeled glycogen (k4) and/or enters glycolysis and oxidative metabolism (k5) to form radiolabeled carbon dioxide and lactate.

2.0 Hypotheses

The primary hypothesis of this thesis is that the progressive changes in the activity and expression levels of AMPK in the Arg302Gln PRKAG2 mutation result in alterations of cardiac glucose metabolism leading to excessive glycogen storage and development of cardiac hypertrophy. These hypotheses will be tested in a cardiac restricted transgenic model of the PRKAG2 disease (TGmut) against wildtype animals with the normal human AMPK gene (TGwt). We subsequently hypothesize that 1) mouse myocardial glucose uptake rates can be assessed with kinetic modeling; 2) Cardiac function will be decreased with increasing glycogen deposition; 3) Increased AMPK activity will cause an increase in GLUT4 transporter expression resulting in increased FDG uptake; 4) GS expression will be upregulated at early disease progression; 5) Reduced FDG uptake can be stimulated by insulin through insulin-independent pathways; 6) pharmacological inhibition of FA oxidation will decrease glycogen stores due to increased glucose oxidation.

3.0 Objectives

The primary objective of this project is to elucidate the mechanism of disease and abnormal metabolism due to changes in AMPK activity in the transgenic Arg302Gln mouse model serially with small animal PET with results validated by in vitro assays. The goal is to determine the ability of FDG to detect changes in glucose uptake, storage and metabolism in the heart in relation to AMPK activity and provide insights into the mechanism of PRKAG2 cardiac hypertrophy. Therefore, the objectives of this project are as follows: 1) Develop animal preparation standard operating procedures for FDG cardiac imaging; 2) Investigate methodologies for quantifying myocardial mouse FDG uptake; 3) Develop non-invasive methodology for blood input function measurements; 4) Determine image reconstruction

methodology for quantitative analysis of myocardial glucose uptake; 5) Evaluate FDG quantification methodology in a type 1 diabetes model induced with STZ known for reduced glucose uptake, at baseline, following induction, and after acute insulin treatment; 6) Evaluate FDG uptake in TGmut and TGwt mice with small animal PET at early and late stages of disease development; 7) Investigate the changes in cardiac function and development of cardiac hypertrophy serially with small animal echocardiography; 8) Determine the effect of insulin stimulation in the TGmut mouse hearts with measurements of FDG uptake; 9) Measure blood markers: insulin, glucose and FFA; 10) Perform *in vitro* validation studies in TGmut and TGwt hearts of AMPK activity, GS protein expression, GSK-3 protein expression, insulin receptor expression, glycogen deposition; 11) Evaluate alterations in ECG measurements of conduction system disease following chronic TMZ treatment with telemetry; 12) Determine if TMZ treatment attenuates glycogen storage disease in TGmut mouse hearts.

4.0 Introduction to manuscripts

The following four manuscripts are listed in the order of publications.

4.1 Manuscript #1

Transition of clinical FDG protocols to the small animal PET scanner, specifically with mice, involved several steps prior to manuscript #1: determining animal preparation, reconstruction algorithms (FBP vs iterative reconstruction) and analysis methodology (SUV vs Patlak vs 2-compartment model vs kmono). Additionally, there was significant development of our in-house Flowquant™ software as well as camera operations (originally the LabPET™, all final data for the manuscripts herein were acquired with the Siemens Inveon DPET). Manuscript #1 details methodology to determine an accurate blood input function in mice using the vena cava as the variation was statistically high with the LV image derived blood input function (coefficient of variability = 51%), most likely due to limitations of spatial resolution and myocardial spillover. As the radiotracer is injected into mouse tail vein, the vena cava is readily apparent in the initial frames after injection. We proposed, due to the high vascular rate of the mouse, that the distribution of tracer between the venous and arterial system is exceptionally fast permitting the use of the vena cava with little bias from the venous system. Additionally, the vena cava is a relatively large structure in the mouse with little spillover from adjacent organs and proving to be an accurate and reliable blood input function (coefficient of variability = ~23%). Therefore, with the use of the vena cava blood input function, we are able to accurately measure changes in myocardial FDG uptake with Patlak modelling in normal test-retest mice, and in a type 1 diabetic model with known reductions in myocardial FDG uptake.

4.2 Manuscript #2

The second manuscript in this thesis expands on the methodology presented in the previous publication, investigating myocardial glucose metabolism with FDG in the PRKAG2 mouse model. PRKAG2 mice were investigated at 1 month of age. At this age, the mice demonstrated increased myocardial wall thickness, heart mass and increased glycogen deposition. However, despite these changes, cardiac systolic function was not affected. FDG cardiac glucose uptake was decreased in TG mutant mice by 74% relative to TG wild-type, suggesting downregulation of glucose transport at this early stage of development. We proposed that the downregulation of exogenous glucose transport was due to a feedback pathway elicited from excessive intracellular glycogen stores which were increased by 83% in TGmut mice. Protein expression of AMPK, phosphorylated AMPK and phosphorylated ACC were significantly augmented indicating increased AMPK activity in the mutant mouse hearts. In line with excessive glycogen deposition, overall GS activity was increased, promoting glycogen storage (see Figure 1.3).

4.3 Manuscript #3

This manuscript is an extention of manuscript 2 and investigates if reduced cardiac glucose uptake could be augmented following insulin stimulation. Insulin should stimulate the translocation of GLUT4 to the plasma membrane increasing glucose uptake independent of AMPK activity (see Figure 1.2). Conversely, AMPK has been shown to independently increase the translocation of GLUT4. Myocardial FDG uptake was reduced 56% in TGmut mice compared to TGwt at baseline. Despite insulin stimulation in the skeletal muscle of both genotypes, there was no effect on cardiac FDG uptake in TGmut mice. There was no difference in cardiac insulin receptor expression between mouse genotypes. Concurrently,

we found that TGmut mice had a 47% reduction in systolic function, a 4-fold increase in cardiac glycogen stores with a 29% reduction in AMPK activity. These results demonstrate a link between insulin resistance and AMPK activity, such that despite the AMPK-independent regulation of glucose uptake by insulin, an increase in glucose uptake could not be achieved. Insulin resistance is commonly observed in HF patients and thus provides a basis for investigating metabolic therapy assessed in HF patients for treatment of affected PRKAG2 patients with the transgenic mouse model.

4.4 Manuscript #4

In this manuscript we targeted pharmacological metabolic intervention with TMZ for the attenuation of the PRKAG2 phenotype. Targeting FA oxidation in cardiac disease is attractive, theoretically preventing the uncoupling of glycolysis and lactate formation from glucose oxidation. We selected TMZ as it is currently undergoing clinical trials for treatment of heart failure patients and while showing promise, it has demonstrated no side effects in the patient population. We hypothesized that TMZ would increase glucose oxidation by inhibition of FA oxidation, shifting cardiac energy metabolism to an increased reliance on glucose metabolism. We treated mice from 1 month of age for 8 months. TMZ treatment reduced cardiac glycogen stores in TGmut mice by 55%. Using echocardiography, we evaluated cardiac function at baseline, 4 months and 8 months of treatment. TMZ-treated TGmut mice displayed improved systolic function at both timepoints with no significant difference to TGwt and TMZ-treated TGwt. In vivo monitoring of ECGs demonstrated that chronic TMZ treatment normalized cardiac rhythm in TGmut mice, with no evidence of ventricular preexcitation. This manuscript supports data from HF clinical research trials wherein TMZ improves systolic and electrophysiological function. These data suggest that

pharmacological modulation of cardiac metabolism to reduce glycogen stores may be beneficial in the attenuation of the PRKAG2 cardiac syndrome.

5.0 Statistics

All data reported in this thesis are expressed as mean +/- standard deviation. Dependent on experimental objectives, data were compared using either a F-test for variance, Z-test, Student's t-test or a one-way analysis of variance (ANOVA) with multiple comparisons between groups using a Bonferroni *post hoc* comparison; $p<0.05$ was considered significant.

CHAPTER 2: MANUSCRIPT #1

Repeatable Non-Invasive Imaging of

FDG PET in the Mouse Myocardium:

Evaluation of Tracer Kinetics in a Type 1 Diabetes Model

Stephanie L. Thorn,[1,2] Robert A. deKemp,[1] Tyler Dumouchel, [1] Ran Klein, [1] Jennifer M. Renaud, [1] R. Glenn Wells, [1] Michael H. Gollob,[2] Rob S. Beanlands,[1,2] Jean N. DaSilva[1,2]

[1]National Cardiac PET Centre, Division of Cardiology, University of Ottawa Heart Institute, 40 Ruskin St., Ottawa, Ontario, Canada, K1Y 4W7

[2]Department of Cellular and Molecular Medicine, Faculty of Medicine, University of Ottawa, 451 Smyth Rd., Ottawa, Ontario, Canada, K1H 8M5

Short Title: rMGU quantification in mice

Disclosures: RdK and RSB: DRAXImage; JDS and RSB:Lantheus Medical Imaging

Contributions of authors

FDG imaging, biodistribution, analysis of blood markers and preparation of the type 1 diabetic animal models described in this manuscript were conducted by myself, under supervision and guidance of Dr. Jean DaSilva. Dr Tyler Dumouchel designed and conducted the reconstructed image resolution experiments and assisted in the calibration of the microPET camera. Jennifer Renaud (MSc) and Dr. Ran Klein facilitated the analysis of the data by designing and optimizing the FlowQuant software. Dr Glenn Wells assisted with interpretation of data. Dr Michael Gollob and Dr Rob Beanlands participated in the clinical implications and perspective on the FDG imaging data. Dr. Robert deKemp facilitated the application of the vena cava blood input function, kinetic modeling and quantification.

ABSTRACT

A non-invasive and repeatable method for assessing mouse myocardial glucose uptake with FDG PET and Patlak kinetic analysis was systematically assessed using the vena cava image-derived blood input function (IDIF).

Methods: Contrast CT and computer modeling was used to determine the vena cava recovery coefficient. Vena cava IDIF (n=7) was compared to the LV cavity IDIF with blood and liver activity measured *ex vivo* at 60 min. The test-retest repeatability (n=9) of Patlak influx constant K_i at 10-40 min was assessed quantitatively using Bland-Altman analysis. Myocardial glucose uptake rates (rMGU) using the vena cava IDIF were calculated at baseline (n=8), following induction of type 1 diabetes (streptozotocin 50 mg/kg ip, 5 days), and following acute insulin stimulation (0.08 mU/kg body weight ip). These changes were analyzed with an SUV calculation at 20 and 40 min post-injection to correlate to the Patlak time interval.

Results: The proximal mouse vena cava diameter was 2.54 ± 0.30 mm. Using non-linear image reconstruction, the estimated recovery coefficient (RC) decreased from 0.76 initially (time 0 to peak activity) to 0.61 for the duration of the scan. There was a 17% difference in the image-derived vena cava blood activity at 60 min compared to the *ex vivo* blood activity measured in the gamma counter. The coefficient of variability for Patlak K_i values between mice was found to be 23% with the proposed method compared to 51% when using the LV cavity IDIF ($p<0.05$). No significant bias in Ki was found between repeated scans with a coefficient of repeatability of 0.16 mL/min/g. Calculated rMGU values were reduced by 60% in type 1 diabetic mice from baseline scans ($p<0.03$, ANOVA), with a subsequent

increase of 40% to a level not significantly different from baseline, following acute insulin treatment. These results were confirmed with SUV measured at 20 and 40 min.

Conclusions: The mouse vena cava IDIF provides repeatable assessment of the blood time activity curve for Patlak kinetic modeling of rMGU. Using this approach, an expected significant reduction in myocardial glucose uptake was demonstrated in a type 1 diabetic mouse model with significant recovery after acute insulin treatment.

Key Words: positron emission tomography, Patlak, myocardial glucose uptake, streptozotocin, test-retest repeatability.

INTRODUCTION

Myocardial metabolism has become an increasingly important target for treatment of cardiovascular diseases, with relatively little information known on the alterations of metabolism in cardiomyopathies (Horowitz et al., 2010; Lionetti et al., 2010; Wang and Lopaschuk, 2007). Transgenic, knockout, pharmacological, as well as surgical mouse models are used extensively to study cardiac metabolism. Although mouse models present many positive features such as the ease in producing customized transgenic or knockout lines as well as a lower expense in housing fees, the small size of the mouse can present challenging issues.

2-[^{18}F]fluoro-2-deoxyglucose (FDG) is a glucose analogue, commonly used in PET to assess cardiac glucose uptake and cell viability (Yoshinaga et al., 2005). FDG enters the cell via GLUT transporters (K1 and k2 rate constants) and is phosphorylated by hexokinase to [^{18}F]FDG-6-phosphate (k3 rate constant). The chemical structure of [^{18}F]FDG-6-phosphate traps the radiolabeled product within the cell. The FDG uptake rate constant, $K_i = (K1 \times k3)/(k2+k3)$, can be estimated using Patlak graphical kinetic analysis, assuming there is negligible tracer washout (k4=0) (Patlak et al., 1983). FDG has been modeled extensively with Patlak analysis in humans (Abraham et al., 2010; Anselm et al., 2011; Birnie et al., 2012; Ha et al., 2009; Mielniczuk et al., 2011; Shukla et al., 2012) and rats (Herrero et al., 2004; Menard et al., 2009; Menard et al., 2010; Shoghi et al., 2009; Shoghi et al., 2008). Studies in mice have evaluated the effects of diet (Kreissl et al., 2011), anaesthetic (Flores et al., 2008), mode of injection and blood glucose levels (Wong et al., 2011) on FDG uptake in mice. However, the inaccuracy of the left ventricle (LV) cavity blood image derived input

function (IDIF) (Fang and Muzic, 2008; Ferl et al., 2007; Locke et al., 2011) remains one of the most difficult impediments to obtaining reliable kinetic measurements in mice. The inaccuracy of the LV cavity IDIF is a particular phenomenon in mice PET imaging due to the relatively small cavity size on the order of the spatial resolution of the current microPET systems (~1.2 mm, Siemens Inveon DPET). Ferl et al (Ferl et al., 2007) were able to predict a blood input function using modeling by taking two arterial samples at approximately 10 and 60 minutes. Other groups have used serial blood sampling to determine the blood input function (Convert et al., 2007; Fang and Muzic, 2008; Kreissl et al., 2011). While manual blood sampling can provide accuracy, it incorporates invasive procedures, reducing the serial imaging capabilities. A hybrid image-derived input function has been proposed using the initial peak of the LV cavity IDIF, with the remainder of the curve derived from the liver time-activity curve normalized to a 60 min arterial blood sample (Tantawy and Peterson, 2010). Although this methodology reported reliable estimates of K_i using a 2 tissue-compartment model, sampling of arterial blood at 60 min is still required. Locke et al (Locke et al., 2011) recently reported an accurate IDIF with sampling of the LV cavity in mice. However, the accuracy was dependent on using gated iterative reconstruction (12 subset OSEM 2D 2 iterations, 18 MAP iterations). Although gated OSEM-MAP reconstructions allow accuracy at later time frames(Cheng et al., 2012), due to a reduction in spillover from the myocardium, the authors acknowledge that each reconstruction takes approximately 34 hr to complete (Locke et al., 2011). This methodology presents time issue constraints in high-output cardiac research centers. Additionally, gated reconstruction relies on accurate ECG gating that can be compromised in animal models with inherent (Sidhu et al., 2005) or induced arrhythmogenesis such as following myocardial ischemic injury. In

this study, we describe a novel method that provides a repeatable and accurate cardiac FDG Ki value using a corrected vena cava IDIF. This approach requires no invasive arterial blood sampling with non-gated dynamic iterative reconstruction algorithms. This methodology was tested for repeatability, and evaluated in a type 1 diabetic mouse model expected to exhibit decreased FDG cardiac uptake due to hyperglycemia.

MATERIALS AND METHODS

Animals

All animal experiments described herein were conducted according to the guidelines of the University of Ottawa Animal Care Committee and the Canadian Council on Animal Care for the use and care of laboratory animals. All animals were maintained on a 12-hour light/dark cycle with chow and water *ad libitum*. All animals used in this study were male FVB mice (25-34 g) purchased from Charles River Canada. Three groups of mice were used to determine i) the accuracy of the vena cava IDIF, ii) test-retest repeatability, and iii) ability to measure changes in a type 1 diabetes model. Type 1 diabetes was induced in male FVB mice by streptozotocin (STZ), dissolved in a 0.05M sodium-citrate solution, injected at 50 mg/kg ip once daily for 5 days (Rabbani et al., 2011). Mice were fasted 4-6 hrs prior to STZ injection to increase conversion. At 10 days post-STZ, fasting blood glucose levels (2-3 hr fast) were measured. Mice with levels higher than 15 mmol/L were categorized as having type 1 diabetes.

Reconstructed Image Resolution

Measurement of the partial volume effect in the vena cava will depend on the size of the vessel and scanner resolution. We therefore conducted experiments to determine the

recovery coefficient (RC) for the mouse vena cava. The size of the vena cava was determined in n=3 mice using CT contrast imaging (nanoSPECT/CT, BioScan, Washington, DC). Briefly, animals were anaesthetized with isoflurane (2% isoflurane, 2 mL/min oxygen) and injected iv with 0.2 mL of Exia^{TM} CT contrast (SKYSCAN, Kontich, Belgium). A 30s topogram was completed immediately after injection to select the field of view (FOV) over the proximal vena cava. A 9 min CT scan was reconstructed (45 kVp, 1500 ms exposure time, 360 projections) with 0.2 mm transaxial pixel size. The proximal vena cava diameter located above the kidneys and below the myocardium was measured by an average of three measurements on each of the coronal, sagittal and axial planes (Siemens IRW software). We subsequently determined the RC on the Inveon PET scanner for the vena cava by using the full width at half maximum (FWHM) of the Gaussian point spread function (PSF) scanner resolution with the perturbation technique (Fessler and Rogers, 1996). Briefly, a ^{22}Na point source (diameter = 0.25 mm, 1 kBq) embedded in a 1 cm^3 acrylic cube was placed within the PET scanner such that the point source location corresponded to the center of the vena cava on a reconstructed transaxial PET image. A five-minute acquisition was performed and the data binned into 3D sinograms. The high-count-density point source sinograms were scaled and added to the mouse sinogram data and reconstructed. The point source sinogram scaling ensures that only a small perturbation is introduced (i.e. < 1% of the counts in each mouse sinogram bin) so that the convergence properties of the reconstructed image are minimally affected. The perturbed images were reconstructed using the same parameters as the original mouse images and the difference was computed to obtain the PSF. The reconstructed image FWHM resolution was determined by fitting a Gaussian function to the PSF difference image.

Small Animal PET Imaging

Small animal PET FDG imaging was conducted with the Inveon™ DPET small animal scanner (Siemens, Knoxville, TN). A 60 min list-mode acquisition was started together with a 10-20 s tail vein injection of FDG (7-82 MBq in 150 μL). List data were sorted into 26 dynamic frames (12 x 10s, 3 x 60 s, 11 x 300s) and reconstructed using OSEM3D with 10 iterations, 16 subsets, zoom of 2.5 with a 128 x 128 matrix, resulting in 0.35 mm transaxial pixel size. Images were corrected for radioactive decay, random coincidences and dead-time losses using the vendor software (IAW version 1.5).

The average vena cava activity was determined from an ROI placed in the corresponding region of the PET image and thresholded to 50% of the local maximum vena cava activity (VC_{50}). The ROI was positioned manually above the kidneys and below the myocardial blood pool in the initial time frames, where the injected tracer bolus is clearly visible.

The RC for the measured vena cava activity was estimated by convolving a circular model of the vena cava with measured diameter, together with the 2D Gaussian point spread function (PSF) representing the reconstructed PET image resolution (Figure 2.1). Likewise, a complimentary uniform background activity was convolved with the same PSF to represent spill-in of activity from the liver into the vena cava ROI. An estimate of the true vena cava activity (A_{VC}) can then be obtained using the following relationship:

$$A_{VC} = \frac{VC_{50} - (1\text{-}RC_{50})B}{RC_{50}} \qquad \text{Eq. 1}$$

where B is the background activity determined by placing an ROI adjacent to the vena cava. The adjacent background used for this ROI is the liver (Figure 2.2A) which typically has homogenous FDG activity uptake and is the largest feature proximal to the vena cava.

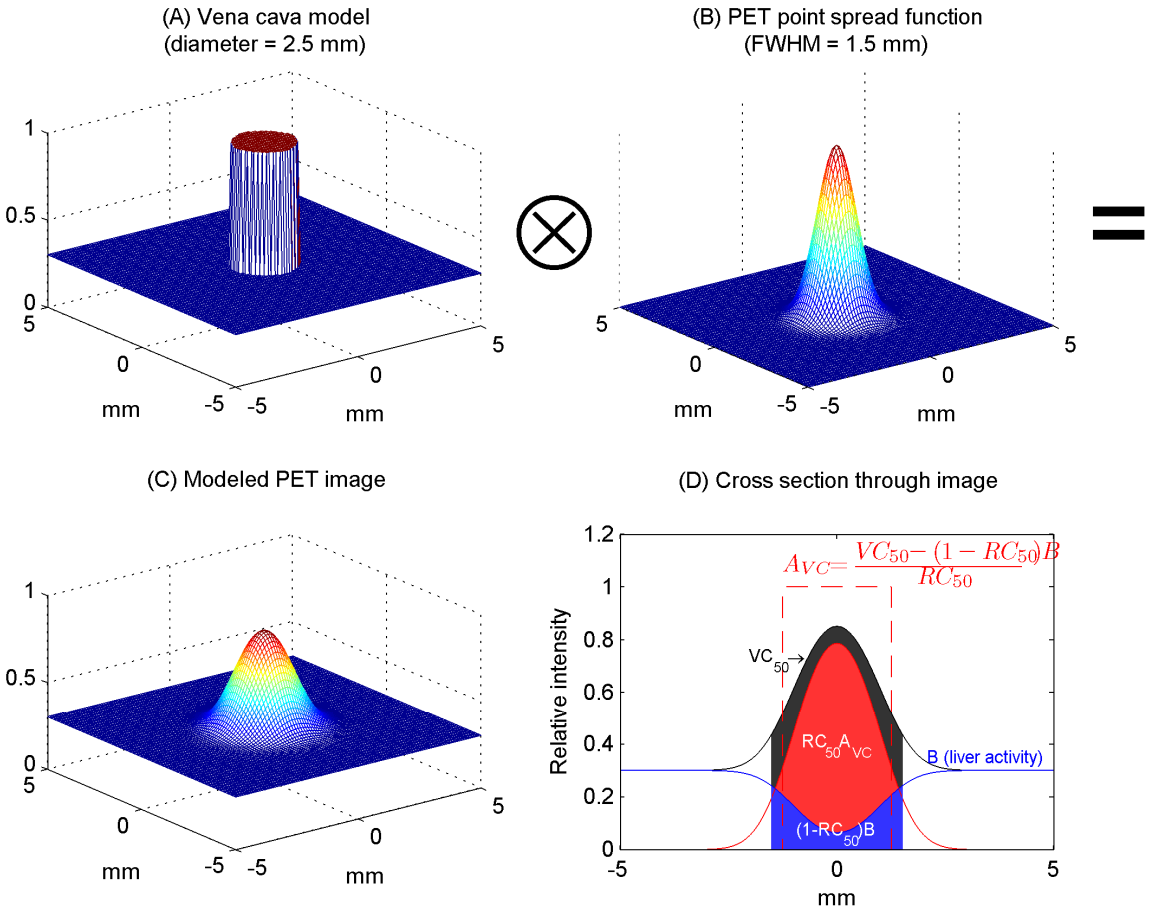

Figure 2.1: The vena cava recovery coefficient was estimated by modeling the vena cava as a long cylinder with uniform background activity (A) and convolving it with a previously derived PET point spread function (B) to model the PET image of the vena cava (C). The Recovery coefficient, *RC50*, was estimated as the integral activity above 50% peak activity in the modeled vena cava, relative to the integral modeled vena cava. As demonstrated in the cross section (D), the activity in a 50% peak activity thresholded ROI, *VC50*(black area) can be corrected for background activity spill in (blue area), and then corrected for recovery, *RC50*, to obtain the actual activity concentration in the vena cava, *AVC*, as shown in equation. Background activity, *B*, was obtained by sampling the liver activity.

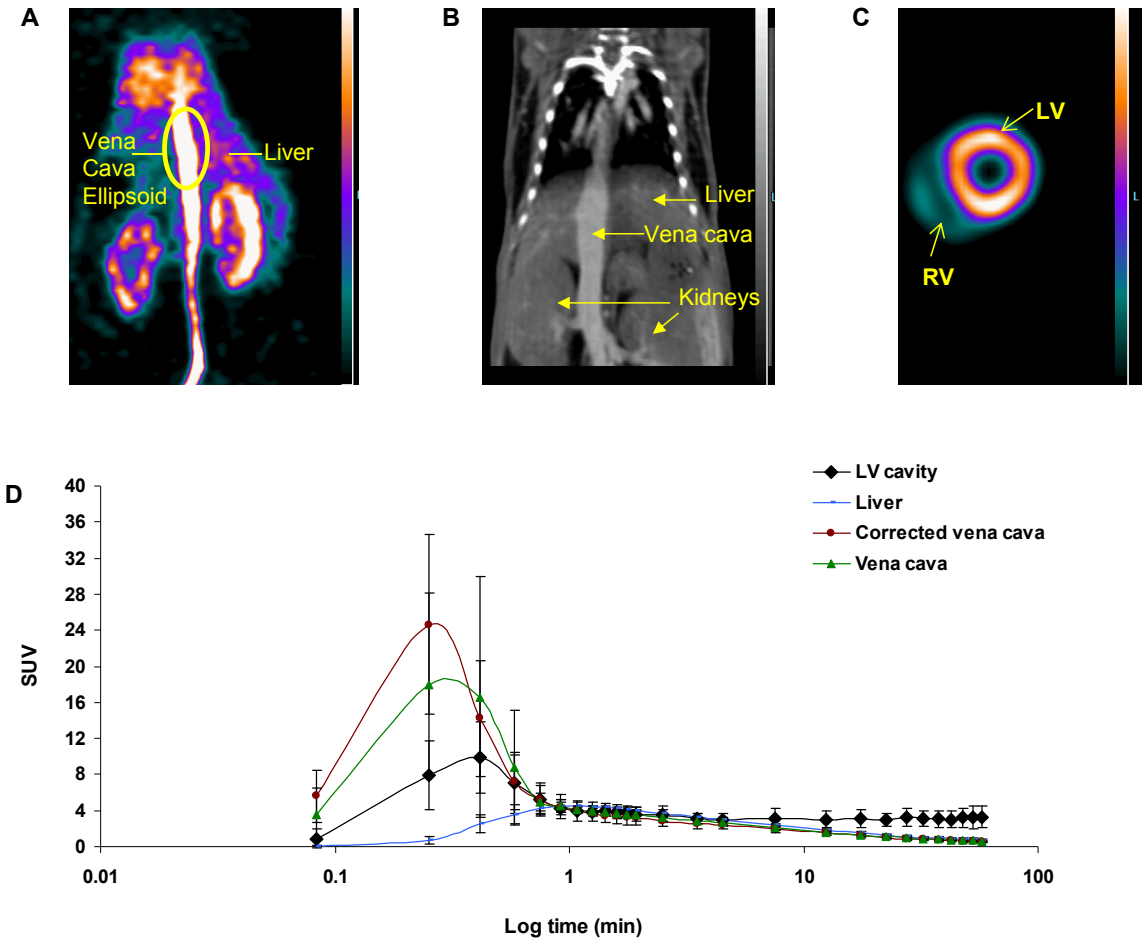

Figure 2.2: Representative images of (A) proximal mouse vena cava and background liver region in the early time frames of the FDG scan; (B) contrast CT of the mouse vena cava; (C) a mouse FDG heart at 60 min. Panel D displays the time activity curve displays the time activity curve displayed in SUV values for n=7 mice. The liver, LV cavity, vena cava and corrected vena cava blood activity curves are displayed over the log of time in 60 min.

Myocardial images were analysed and quantified with Patlak kinetic analysis (K_i) at 10-40 min from the reconstructed images using FlowQuant© semi-automated software (Klein et al., 2010; Lamoureux et al., 2012; Thomas et al., 2011). In brief, uptake images of the left ventricle were formed by using the last 5 min of scan data. The location, orientation and size of the LV were automatically determined by fitting ellipses to the myocardium in the transverse, vertical long axis and horizontal long axis planes. Transverse uptake images were reoriented automatically into short-axis sections generating LV slices from the apex to the base plane. Polar maps of the relative uptake activity (%) are formed from the sampled data. Blood regions of interest (ROIs) are automatically placed in the LV cavity. The sampling points are then applied to all time frames to generate myocardial and blood time-activity curves (TAC). Patlak kinetic analysis is applied to the myocardial data using either the blood input function from the FlowQuant© automated cavity measurement or the estimated vena cava blood input function (Eq.1) imported into FlowQuant©. This was done such that the exact same myocardium orientations and LV sampling were used with both blood input functions.

Regional rMGU was determined for each animal using the following standard equation:

$$rMGU = K_i \times BG / LC \text{ [mmol/min/g]} \qquad \text{Eq. 2}$$

where K_i is the Patlak uptake rate constant, BG is the blood glucose concentration [mmol/mL] obtained prior to FDG injection and LC is the lumped constant equal to 0.67, which accounts for differences in the uptake and phosphorylation of FDG vs glucose.

FDG uptake in the type 1 diabetic group was also quantified using a standardized uptake value (SUV) at 20 and 40 min to independently evaluate myocardial radiotracer uptake.

SUV was calculated according to the following standard equation:

$$SUV = \frac{\text{activity concentration in a region of interest (Bq/cc)}}{\text{Injected activity (Bq)/weight of the animal (g)}} \quad \text{Eq. 3}$$

Image Derived Input Function Accuracy

To determine the accuracy of the calculated IDIF, n=7 mice were scanned following iv injection of FDG with measurements of blood activity at 60 min compared to a manual blood sample following decapitation after the scan. Liver was also collected as a homogenous tissue region. FDG activity of the samples was measured with a Packard Cobra II gamma counter (Perkin Elmer, Boston, MA) and expressed as percent injected dose (activity) per gram of tissue (%ID/g). %ID/g of each sample was multiplied by the injected activity and divided by 100% to obtain the activity per cc of tissue (Bq/cc), assuming a tissue density of 1 g/cc.

Test-retest Repeatability

To evaluate the repeatability of Patlak Ki measurements using the calculated IDIF, n=9 mice were scanned twice three days apart, using the same procedures listed above. Blood glucose levels were sampled immediately prior to FDG injection. An additional blood sample was acquired to measure insulin and free fatty acid (FFA) levels. Patlak Ki values were compared to calculated 2-compartment model Ki values and SUV measurements.

Type I Diabetes

Mice (n=8) were scanned with FDG at baseline and 2 weeks post-STZ (Figure 2.3). An additional scan was conducted 3-4 days later with short-acting insulin (0.08 mU/kg body weight ip; Novolin R) injected 30 min prior to the FDG scan to assess insulin sensitivity

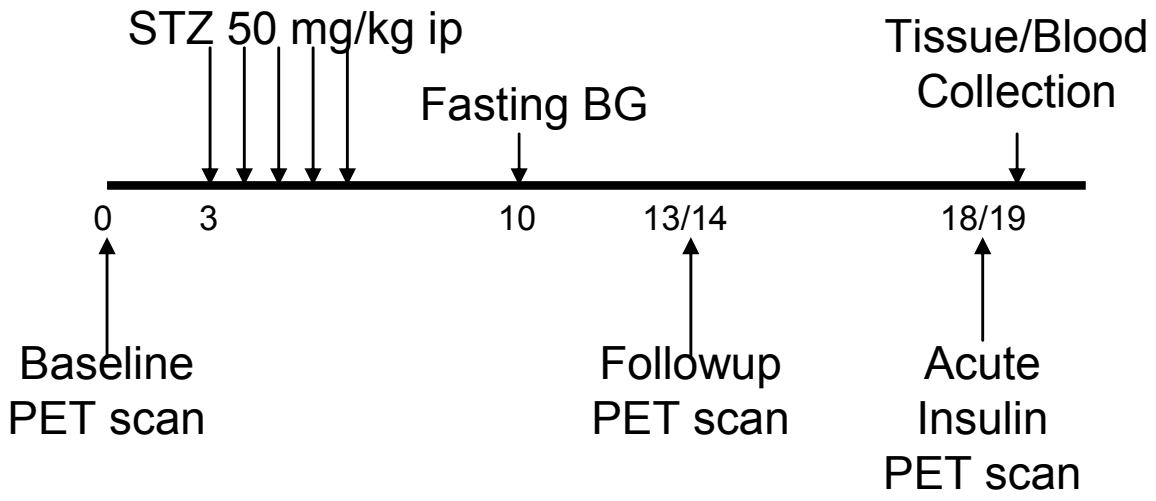

Figure 2.3: Schematic representation of the type 1 diabetic protocol

(Simoes et al., 2004). Blood glucose levels for all scans were measured immediately prior to FDG injection, with an additional blood sample acquired for measuring insulin and FFA levels.

Blood Markers

Blood glucose concentration was measured (mmol/L) with a small drop of blood from the saphenous vein using Advantage blood glucose strips (AccuChek, Roche Diagnostics, Laval, QC, Canada). Plasma insulin concentrations were measured with the Mouse Ultrasensitive Insulin ELISA kit (ALPCO Diagnostics, Salem, NH). Results were analyzed using the GraphPad Prism software (GraphPad Software, Inc.) and expressed in ng/mL.

The plasma FFA were measured with the commercially available Free Fatty Acid Quantification Kit (BioVision Inc., San Francisco, CA) with concentration of each sample expressed as mmol/L.

Statistical Analysis

Curve fitting with FlowQuant© Software was performed using MATLAB (The MathWorks, Natick, MA). All data are expressed as mean +/- standard deviation. Data were compared using either a F-test for variance, Z-test, student's t-test or a one-way

analysis of variance (ANOVA) with multiple comparisons between groups using a Bonferroni *post hoc* comparison; $p<0.05$ was considered significant.

RESULTS

Vena Cava Measurements

The measured average diameter of the mouse vena cava was 2.54 ± 0.30 mm (Figure 2.1B). The image FWHM resolution was estimated as 1.02 ± 0.04 mm in the early frames (from

time 0 to the peak vena cava activity), compared to 1.71 ± 0.12 mm in the subsequent times frames. This difference in image resolution is due to the known non-linear effects of OSEM image reconstruction that are dependent on temporal changes in local count-density and contrast. Using this time-dependent image PSF and the circular vessel dimension from CT, the vena cava RC value of 0.76 ± 0.036 estimated for the early frames was significantly higher than 0.61 ± 0.07 used for later time frames following the peak vena cava activity.

IDIF and Organ Activity Accuracy

The transaxial FOV on the Inveon DPET scanner is 10 cm, and the axial FOV is 12.8 cm, allowing for the whole mouse to be imaged in a single bed position. The LV when placed in the center of the FOV has excellent resolution and contrast. The RV is also apparent (Figure 2.1C). Table 2.1 presents the image-derived activities from the liver, vena cava and LV cavity compared with the tissue activities measured with the gamma counter. Evident in the liver, where there is relative homogeneity of signal and minimal partial volume effect due to the large size of the organ, there is a slight bias in measurements (20%) between the PET image vs the gamma counter. The blood activity from both the LV cavity and vena cava had lower population variability compared to gamma counter measurements of the trunk blood (23 and 20% vs 29% respectively; $p<0.01$, F-test). The LV cavity blood activity measured from the PET images at 60 min was almost 6-fold higher compared to the measured gamma counter activity, whereas the vena cava PET image activity was only 38% higher. When the vena cava activity was normalized using the image-to-gamma-counter activity ratio in the liver (liver ratio) this difference was further reduced to 17%. The full 60 min blood input functions (n=7 mice) were compared for the LV cavity, uncorrected vena cava, liver (background region) and calculated vena cava activity (Figure 2.1D). The early

Table 2.1: Image derived activity compared to gamma counter activity at 60 min

	Liver Activity (kBq/cc)		Blood Activity (kBq/cc)			
Mouse	**Image Derived**	**Gamma Counter**	**LV Cavity**	**Vena Cava**	**Vena Cava: Liver ratio**	**Gamma Counter**
1	952	1005	3366	811	750	589
2	907	801	2097	585	489	442
3	787	647	2095	539	432	316
4	833	711	2484	566	483	391
5	974	651	2875	507	366	557
6	866	637	3802	431	371	260
7	1018	845	3055	612	540	373
Mean	**905**	**757**	**2825**	**579**	**490**	**418**
Stdev	**82**	**136**	**643**	**118**	**131**	**121**
CV	**0.09**	**0.18**	**0.23**	**0.20**	**0.27**	**0.29**
Bias to Gamma Counter	**20%***		**575%***	**38%***	**17%**	

* t-test, p value <0.01

peak of the vena cava input function was higher than the LV cavity curve, and a slow decline in the later time frames as expected, whereas the LV cavity curve actually displays a slight increase potentially due to activity spilling in from the surrounding myocardium.

Test-retest repeatability

As there were only 3 days between scans, there was no difference in body weight. Blood glucose and insulin values were not significantly different between scans, however plasma FFA was significantly decreased approximately 41% (47.9 ± 11.1 vs 28.0 ± 5.4 mmol/L, $p<0.05$, t-test).

Figure 2.4 is representative polar maps and Patlak analysis curves from one mouse. Panel A and B are test-retest results in mouse 1 using the corrected vena cava blood input function. Patlak polar maps appear similar with an excellent linear fit observed at the specified interval of 10-40 min. Patlak K_i values had a range of 0.23 to 0.66 mL/min/g between mice with a mean of 0.5 ± 0.1 mL/min/g representing a 23% population coefficient of variability (COV) and good repeatability (Figure 2.5A, $r^2= 0.57$). Figure 2.4C and D show the same mouse test-retest scans using the LV cavity as the blood input function. There is a clear difference in the Patlak polar maps and a relatively poor fit to the data, with Ki values ranging from 0.08 to 0.37 mL/min/g between mice, and a COV of 51% (mean of 0.15 ± 0.08 mL/min/g). Bland-Altman plots of the Patlak K_i values from scan 1 and scan 2 using the corrected vena cava blood input function had no significant bias ($p>0.05$, t-test) (Figure 2.5B) and a coefficient of repeatability (CR) of 0.16 mL/min/g (32% of mean). We compared these results to Ki values derived from a 2-comparment 3K model and SUV at 30-60 min frames (Table 2.2). We found that the 2-compartment model has a higher population variability at 31% (compared to 23% with Patlak Ki) and a higher coefficient of repeatability at 39%

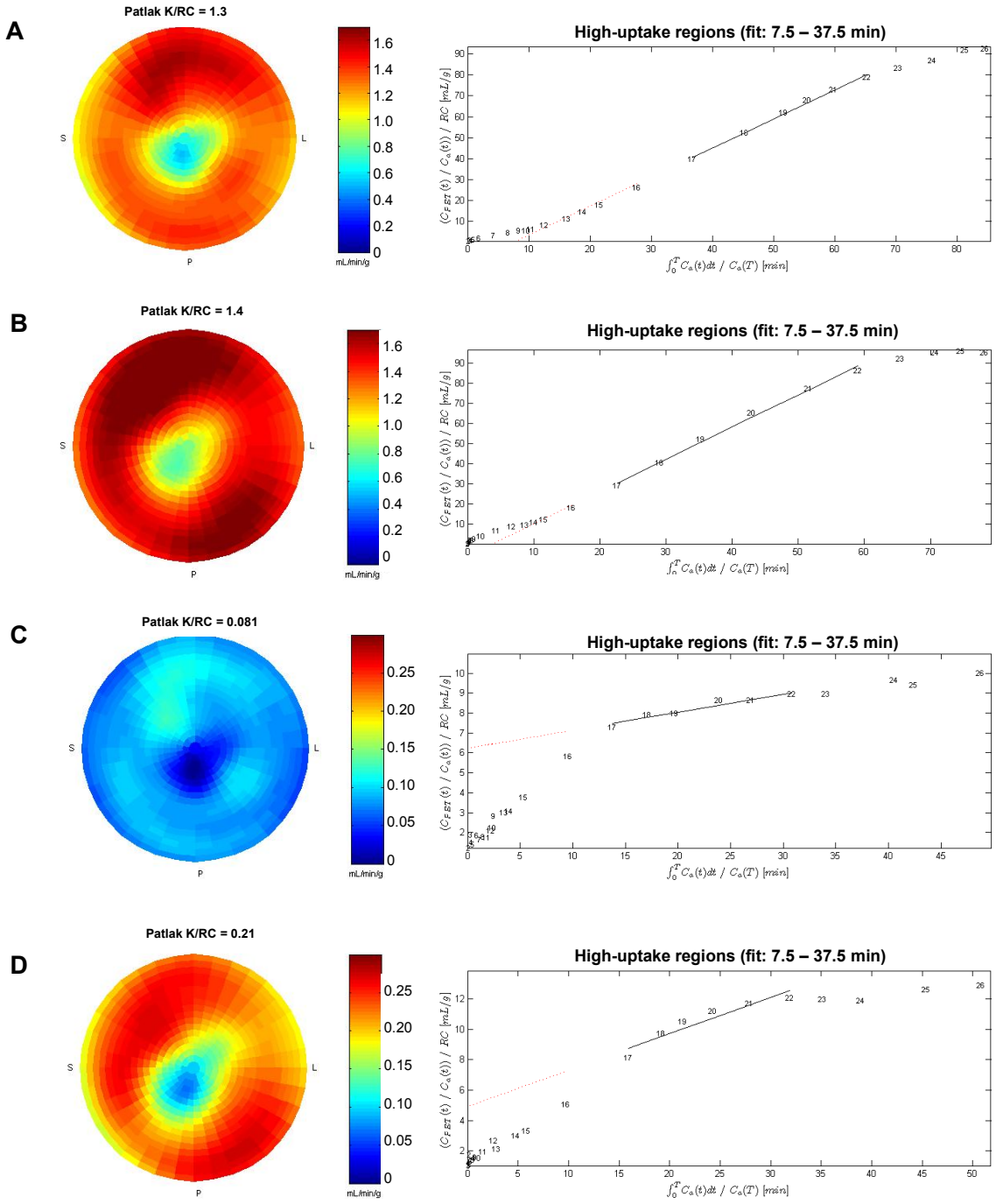

Figure 2.4: Patlak polar maps and plots of a representative test-retest mouse using the vena cava blood input function for scan 1 (A) and scan 2 (B) and using the LV cavity blood input function for scan 1 (C) and scan 2 (D).

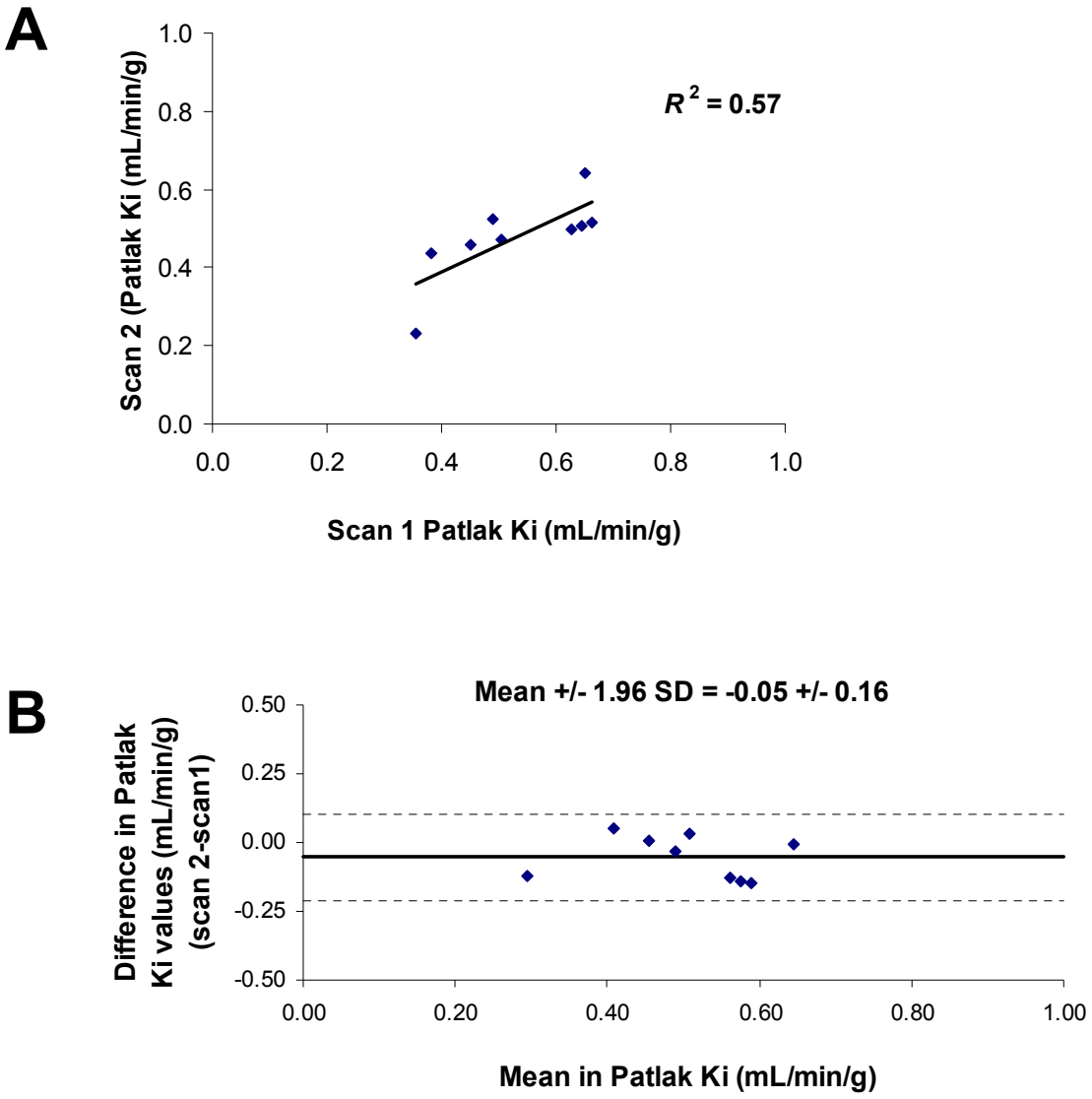

Figure 2.5: Comparison of test-retest Patlak Ki values using the vena cava IDIF (A) with a dashed line representing a line of identity. Bland-Altman plots of test-retest Patlak Ki using the vena cava IDIF (B).

Table 2.2: Comparison of kinetic modeling measurements

	Patlak Ki	**2-Compartment Model 3K Ki**	**SUV (30-60min)**
Mean ± stdev	0.50 ± 0.1	0.37 ± 0.1	15.46 ± 3.3
Population variability (%)	23	31	21
Coefficient of repeatability (%)	32	39	17

(compared to 32% with Patlak). SUV analysis provides the lowest values with 21% population variability and a coefficient of repeatability of 17% .

Type 1 Diabetes

Body weight and plasma insulin were significantly reduced in the type 1 diabetic state compared to baseline values (*$p<0.05$, ANOVA Bonferroni) (Table 2.3). Plasma FFA levels were increased significantly only during the acute insulin scan. As expected, blood glucose levels were significantly increased in the type 1 diabetic state, and reduced to baseline levels following acute insulin stimulation prior to FDG injection (Table 2.3). Representative images display an excellent fit using Patlak analysis with the corrected vena cava blood input at baseline (Figure 2.6A), during untreated type 1 diabetes (Figure 2.6B), and following acute treatment with insulin (Figure 2.6C). rMGU values were significantly reduced by 60% from baseline to type 1 diabetes. Following acute insulin treatment, rMGU increased by 40% towards baseline values (Table 2.4). Interpretation of these changes was confirmed with similar relative changes in SUV at 20 and 40 min (Table 2.4).

DISCUSSION

In this study, we developed a novel methodology for acquiring an accurate and repeatable blood IDIF using the vena cava in mice. Using a fed state with isoflurane as the anesthetic, we found as in previous studies (Ferl et al., 2007; Flores et al., 2008; Kreissl et al., 2011; Locke et al., 2011; Wong et al., 2011) that the myocardium has high tissue-to-background contrast. However, the small size of the mouse LV cavity on the order of the spatial resolution of the PET scanner with the high uptake in the myocardium resulting in substantial spillover of myocardial activity results in an inaccurate assessment of the blood

Table 2.3: Body weight and blood markers in type 1 DM mice

	Body Weight (g)	Blood glucose (mmol/L)	Insulin (ng/ml)	FFA (mmol/L)
Normal Controls	29.7 ± 1.8	11.3 ± 3.3	0.93 ± 0.32	40.2 ± 6.8
Type 1 DM	24.9 ± 1.5	22.6 ± 7.6*	0.08 ± 0.03*	65.4 ± 14.4
Type 1 DM + Insulin	25.2 ± 1.4	12.5 ± 6.2	0.18 ± 0.05*	92.1 ± 14.2*

* one way ANOVA, Bonferroni p value <0.05

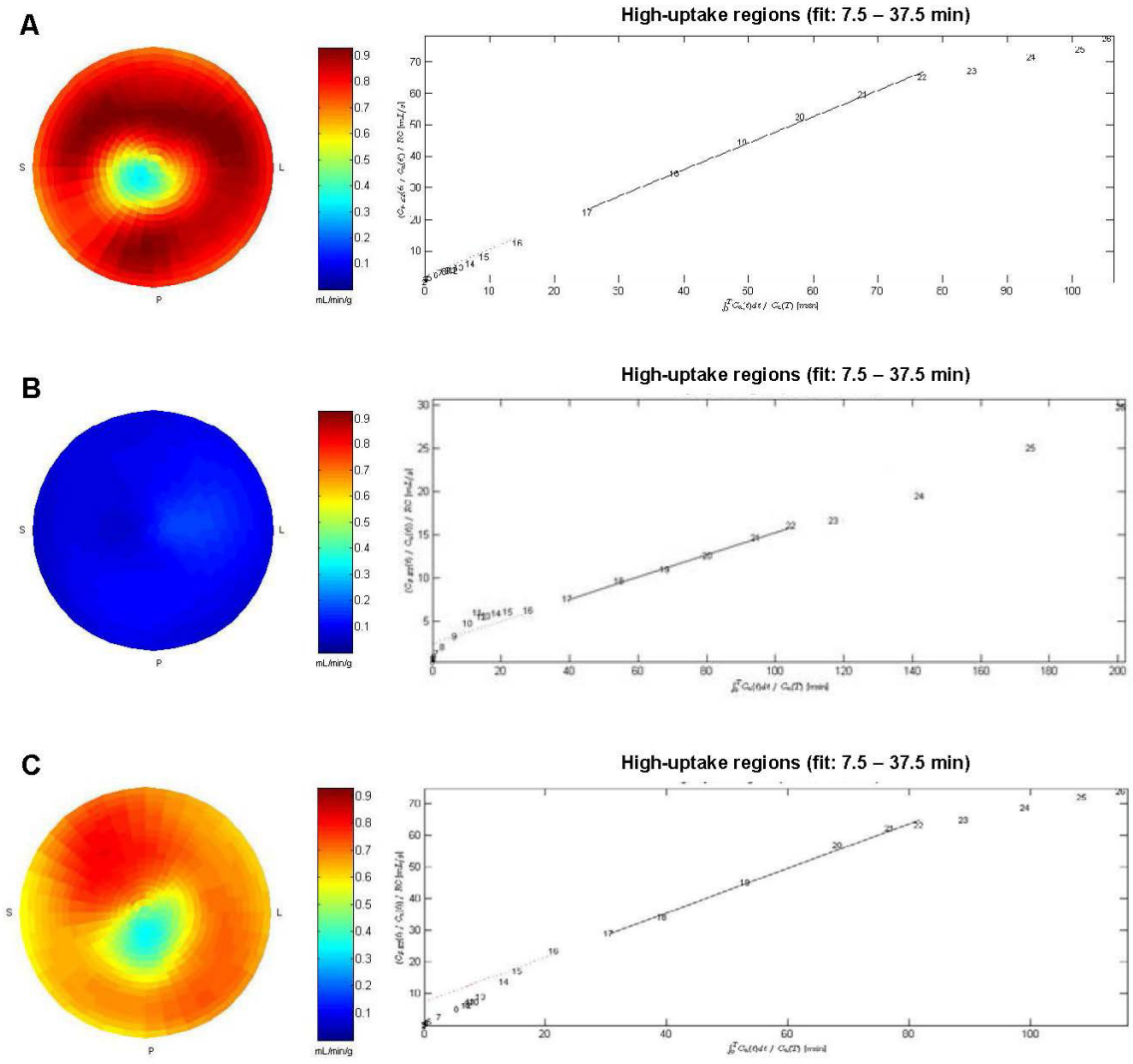

Figure 2.6: Representative Patlak polar maps and plots at baseline (A), following type 1 diabetes induction (B) and after acute insulin stimulation (C).

Table 2.4: rMGU and SUV values at baseline, type 1 diabetes and following acute insulin treatment

	Baseline	**Type 1 DM**	**Type 1 DM + Insulin**
rMGU	18.9 ± 6.4	7.7 ± 3.7*	12.8 ± 6.0
SUV 20 min	10.8 ± 2.9	2.9 ± 0.9*	7.7 ± 3.9
SUV 40 min	13.3 ± 3.8	3.6 ± 1.3*	8.3 ± 3.6

* one way ANOVA, Bonferroni p value <0.05

IDIF. Although an SUV can be used to compare activity concentration in a tissue of interest at one particular time-point, it has been noted that kinetic modeling is needed to assess even the simplest of changes in metabolic rate constants (Kreissl et al., 2011), such as increased FDG uptake rate with insulin stimulation.

We investigated the proximal portion of the vena cava for measurement of an IDIF. In human studies, venous and arterial concentrations of FDG are considered to be equal at 30-60 min post-injection of tracer (Cook et al., 1999). In mice, with their high cardiac output rate, we hypothesized that the distribution of tracer from venous to arterial blood occurs at a substantially higher rate. Additionally, the location of the vena cava for FDG scans removes most high-activity areas from proximity of the vena cava ROI, reducing activity spillover from adjacent background regions. The adjacent background used for this ROI is the liver which typically has homogenous FDG activity uptake. We were able to derive a RC for the vena cava using measured values of the reconstructed image resolution to estimate the true vena cava activity (Eq 1). Manual blood sampling was performed to confirm the accuracy of the calculated vena cava blood activity. We found a 17% difference between the measured blood activity compared to the image derived vena cava activity at 60 min when using the liver as a standard between the microPET camera and gamma counter. This was substantially lower compared to the blood input function derived from the LV cavity, which was approximately 575% higher than the gamma counter measured blood activity. To compare to previously published data from Locke et al (Locke et al., 2011), we reconstructed our data using their reconstruction parameters without gating. Despite an improvement from our calculated values, the IDIF from the LV cavity was 130% different from measured gamma counter activity. As stated in their paper, gating to reduce activity spillover from the

myocardium is essential to determine an accurate LV cavity IDIF (Locke et al., 2011). However, long reconstruction times (~34hr per mouse) and dependency on accurate ECG gating in all animal models render this method difficult to execute.

In cardiac studies the LV cavity ROI is commonly used to sample IDIFs since it is directly upstream from the blood supply to the myocardium, thus representing a good approximation of the blood input to the tissue. The vena cava curves look different in early time frames with earlier, sharper, and higher peaks compared to the LV cavity curves. We postulate, that this does not adversely impact the accuracy of the Patlak analysis since integral activity is used for the analysis and the shape of the curve outside the analysis time range (10-40 min) is of no consequence. Later time frames with the vena cava IDIF display a slow decline in activity concentration, consistent with FDG uptake and retention in tissue, rather than an the increase in activity concentration observed with the LV cavity. We presume that the increase in the LV cavity blood input function is due to myocardial spillover. Kreissl et al (Kreissl et al., 2011) noted that the initial time frames when the LV has low myocardial FDG uptake are appropriate for measurements of the LV cavity blood input function, while later frames of the blood IDIF can be derived through computer modeling with two blood samples.

Patlak K_i test-retest population variability was 23% with the vena cava blood input function, reduced from 51% when using the LV cavity blood input function ($p<0.05$). The Patlak Ki coefficient of repeatability with the vena cava blood input function was 32% with no significant bias between scan 1 and scan 2 ($p>0.05$). We additionally evaluated Ki for the 2-compartment model and found an increase in both the test-retest population variability and the coefficient of repeatability, which could be explained by larger number of free

parameters in the model. In our study we found no correlation with blood glucose levels ($R^2=4\times10^{-6}$) or plasma insulin levels ($R^2=0.03$) compared to Patlak Ki values. Although, we did find a significant reduction in plasma FFA levels from scan 1 and scan2, there was again no correlation with Patlak Ki values ($R^2=0.007$).

We validated this methodology in a streptozotocin induced Type 1 Diabetic mouse model. Type 1 diabetes is known to exhibit a reduction in insulin-stimulated glucose uptake due to an overall reduction in endogenous insulin. While the type 1 diabetes model will produce large perturbations in rMGU values, we chose this model as it is a well-established model of hyperglycemia and alterations in myocardial glucose uptake. Induction of type 1 diabetes significantly reduced rMGU by 60% compared to baseline scans ($p<0.05$). We further validated that we could measure an increased glucose uptake with an acute treatment of insulin in the type 1 diabetic mouse. A significant 40% increase in rMGU was observed, returning the measurement close to baseline pre-diabetic levels ($p>0.05$). These changes were supported by SUV values calculated at 20 and 40 min, capturing two time frames within the Patlak Ki time interval of 10-40 min.

In clinical studies, patients fast for a minimum of 6 hrs prior to scanning with non-diabetic patients receiving an oral glucose load prior to FDG injection, and diabetic patients an insulin-euglycemic clamp to ensure baseline blood glucose levels are not significantly different (Anselm et al., ; Birnie et al., ; Mielniczuk et al.). Kreissl et al (Kreissl et al., 2011) found that as in humans, fasting reduced cardiac FDG uptake rates in mice by approximately 5-6 fold. We did not perform our methodology under fasting conditions with an insulin-euglycemic clamp as the objective was to characterize the changes (if any) in the type 1 diabetic model from baseline, and the use of a clamp would normalize diabetic glucose

uptake as has been previously reported in human patients (vom Dahl et al., 1993). All FDG imaging protocols were conducted in the fed state.

One of our study's limitations is the fact that blood sampling for accuracy was only done at the 60 min time-point as opposed to sampling throughout the scan. Although the authors acknowledge this as a limitation, the 60 min time-point is representative of when the highest myocardial spillover is present and contaminating the LV cavity blood input curve. This method is also strongly dependent on the RC values which may change with alterations in the reconstruction parameters, both post-reconstruction filters as well as MAP priors, number of iterations and sizes of subsets. As such, the results are only applicable to the parameters used in this study. The degree that spill-over influences the measured values depends heavily on the distribution of the tracer background uptake. Extending this approach to other tracers or using this in models for which the uptake of FDG in the liver or blood clearance altered, should be approached with caution and may require additional validation.

CONCLUSION

A new methodology for measuring mouse FDG myocardial glucose uptake was developed by using an image derived blood input function with excellent repeatability. Additionally, this is the first study to demonstrate alterations in rMGU measurements of FDG in a mouse type 1 diabetic model. This methodology allows users to quantify changes in rMGU serially and non-invasively in mouse models with FDG and further translate this information directly to the clinical setting.

ACKNOWLEDGEMENTS

The authors thank Julia Lockwood for technical assistance with CT imaging, and the Animal Care and Veterinary services of the University of Ottawa for their assistance with animal health. This study was supported in part by the Heart and Stroke Foundation of Ontario (HSFO) Program Grant on Molecular Function and Imaging (grant # PRG6242). Stephanie Thorn was supported by a Heart and Stroke Foundation PhD Scholarship. Rob S. Beanlands is a Career Investigator supported by the Heart and Stroke Foundation of Ontario and Tier 1 Chair in Cardiovascular Research (University of Ottawa**).**

FUNDING SOURCES

Financial Support: Heart and Stroke Foundation of Ontario (HSFO) Program Grant on Molecular Function and Imaging (grant # PRG6242). S. L. Thorn was supported by a Heart and Stroke Foundation PhD Scholarship. R. S. Beanlands is a Career Investigator supported by the Heart and Stroke Foundation of Ontario and Tier 1 Chair in Cardiovascular Research (University of Ottawa).

CHAPTER 3: MANUSCRIPT #2

Early Alterations in Cardiac Glucose Metabolism in Mice Expressing the Human Arg302Gln-PRKAG2 Mutation Lead to the Development of Metabolic Cardiomyopathy.

Stephanie L. Thorn,[a,b] Jean N. DaSilva,[a,b] Robert A. deKemp,[a] Ran Klein,[a] Jennifer M. Renaud,[a] Rob S. Beanlands,[a,b] M.E. Harper,[c] Michael H.Gollob[b]

[a]National Cardiac PET Centre, Division of Cardiology, University of Ottawa Heart Institute, 40 Ruskin St., Ottawa, Ontario, Canada, K1Y 4W7; [b]Department of Cellular and Molecular Medicine, Faculty of Medicine, University of Ottawa, 451 Smyth Rd., Ottawa, Ontario, Canada, K1H 8M5; [c]Department of Biochemistry, Microbiology, and Immunology, Faculty of Medicine, University of Ottawa, 451 Smyth Rd., Ottawa, Ontario, Canada, K1H 8M5

Running Head: Alterations in PRKAG2 Cardiac Glucose Metabolism

Contributions of Authors:

Genotyping, FDG imaging, echocardiography, glycogen assay, westerns and all data analysis described in this manuscript were conducted by myself, under supervision and guidance of Dr. Jean DaSilva and Dr Michael Gollob. Dr. Robert deKemp facilitated the application of kinetic modeling and quantification. Jennifer Renaud (MSc) and Dr. Ran Klein assisted with the analysis of the data by designing and optimizing the FlowQuant software. Dr Rob Beanlands participated in the clinical implications and perspective on the FDG imaging data. Dr M.E. Harper assisted with interpretation of the biochemical assays within the context of the PRKAG2 model.

ABSTRACT

The PRKAG2 cardiac syndrome is characterized by excessive myocardial glycogen deposition, cardiac hypertrophy, frequent cardiac arrhythmias and progressive conduction system disease. The condition is often familial and is caused by genetic mutations in the γ2-subunit (PRKAG2) of AMP-activated protein kinase (AMPK). To study the pathogenesis and early cardiac metabolic alterations of this disease, we have assessed in vivo cardiac glucose uptake in young transgenic (TG) mice expressing the human disease-causing Arg302Gln PRKAG2 mutation.

At 4 weeks of age, in vivo cardiac glucose uptake was measured with 2-[^{18}F]-fluoro-2-deoxyglucose (FDG) over 60 minutes. Myocardial FDG uptake was decreased in TG mutant mice by 74% relative to TG wild-type, suggesting downregulation of glucose transport at this early stage of development. Echocardiography established no difference in cardiac contractility. However, a significant increase in left ventricle mass and wall thickness in TG mutant mice was observed, concurrent with an 83% increase in cardiac glycogen content. Protein expression of AMPK, phosphorylated AMPK and ACC were significantly increased in the myocardium of mutant mouse hearts. Protein levels of glycogen synthase and phosphorylated glycogen synthase, involved in glycogen synthesis in the heart were increased while phosphorylated levels of the glycogen metabolism regulator GSK3-β were reduced in mutant hearts as compared to wild-type. In the Arg302Gln PRKAG2 mouse model, changes in protein expression levels of key regulators of glucose metabolism promote an excess of myocardial glycogen storage, with an abnormal cardiac phenotype evident as early as 1 month of age.

Introduction

Th physiologic roles of adenosine monophosphate activated kinase (AMPK) in cardiac metabolism are diverse (Dolinsky and Dyck, 2006b; Zaha and Young, 2012). AMPK is a heterotrimeric kinase consisting of a catalytic subunit (α) and two regulatory subunits (β and γ). The γ-subunit contains the cystathionine-β-synthase (CBS) domains, which activate AMPK in response to energy deprivation primarily via allosteric regulation by AMP or ADP (Oakhill et al., ; Xiao et al.). The relationship between levels of AMP, ADP and ultimately ATP (Hardie and Sakamoto, 2006) regulate AMPK activity underlies the importance of AMPK in the rapid modulation of cardiac metabolism (Hardie, 2003; Young et al., 2005; Zaha and Young, 2012).

At rest, the predominant ATP producing pathway in the myocardium is mitochondrial oxidation of free fatty acids (FFA), generating 60-90% of ATP, with 10-40% generated by the oxidation of pyruvate (from glycolysis) (Dyck and Lopaschuk, 2006; Stanley et al., 2005). Glucose oxidation is minimized in the resting state due to inhibition by pyruvate dehydrogenase, a by-product of FFA oxidation. In response to metabolic stress, AMPK activation maintains adequate ATP levels by stimulating catabolism of both free fatty acid (FFA) and glucose substrates (Carling, 2004). The role of AMPK in maintenance of ATP levels via modulation of metabolic pathways has been investigated in various cardiomyopathies associated with diabetes, ischemia-reperfusion injury, cardiac hypertrophy and the chronic development of heart failure.

The clinical importance of AMPK function in the heart was demonstrated by discovery that genetic mutations in the *PRKAG2* gene, which encodes the gamma-2 regulatory subunit of

AMPK, causes a novel cardiac glycogenosis syndrome (Gollob et al., 2001a; Gollob et al., 2001b). Affected individuals exhibit varying degrees of cardiac hypertrophy, frequent and persistent cardiac arrhythmias, and progressive conduction system disease necessitating pacemaker implantation. In some cases, heart transplantation is required and in other cases, premature sudden death occurs (Gollob, 2003; Gollob et al., 2002; Gollob and Roberts, 2002). On gross pathologic and histologic assessment, the hallmark of the PRKAG2 cardiac syndrome is diffuse and extensive glycogen deposition (Arad et al., 2002).

To further study the pathogenesis of the PRKAG2 cardiac syndrome, various research groups have produced transgenic mouse models replicating the cardiac pathology and clinical features of the human genetic disease (Arad et al., 2003; Banerjee et al., 2010a; Davies et al., 2006; Sidhu et al., 2005). In all of these mouse models, excessive glycogen deposition, cardiac hypertrophy and Wolff-Parkinson-White syndrome are evident. What is particularly intriguing is the apparent biphasic alterations in AMPK activity (Banerjee et al., 2007). The age of the animals and extent of cardiac disease at the time of measurement appear to dictate whether AMPK activity is increased or decreased. Using 2-[^{18}F]fluoro-2-deoxyglucose (FDG) positron emission tomography (PET) imaging we previously investigated cardiac glucose uptake in adult human patients with the Arg302Gln mutation of PRKAG2 and a late stage of disease (Ha et al., 2009). FDG is a glucose analogue, commonly used in PET to assess cardiac glucose uptake and cell viability (Figure 3.1) (Yoshinaga et al., 2005). In the clinical investigation of adult PRKAG2 patients with a late stage of disease, we measured a 45% reduction in myocardial glucose uptake in patients versus control subjects (Ha et al., 2009).

In the current study, we use a transgenic mouse model expressing the Arg302Gln PRKAG2

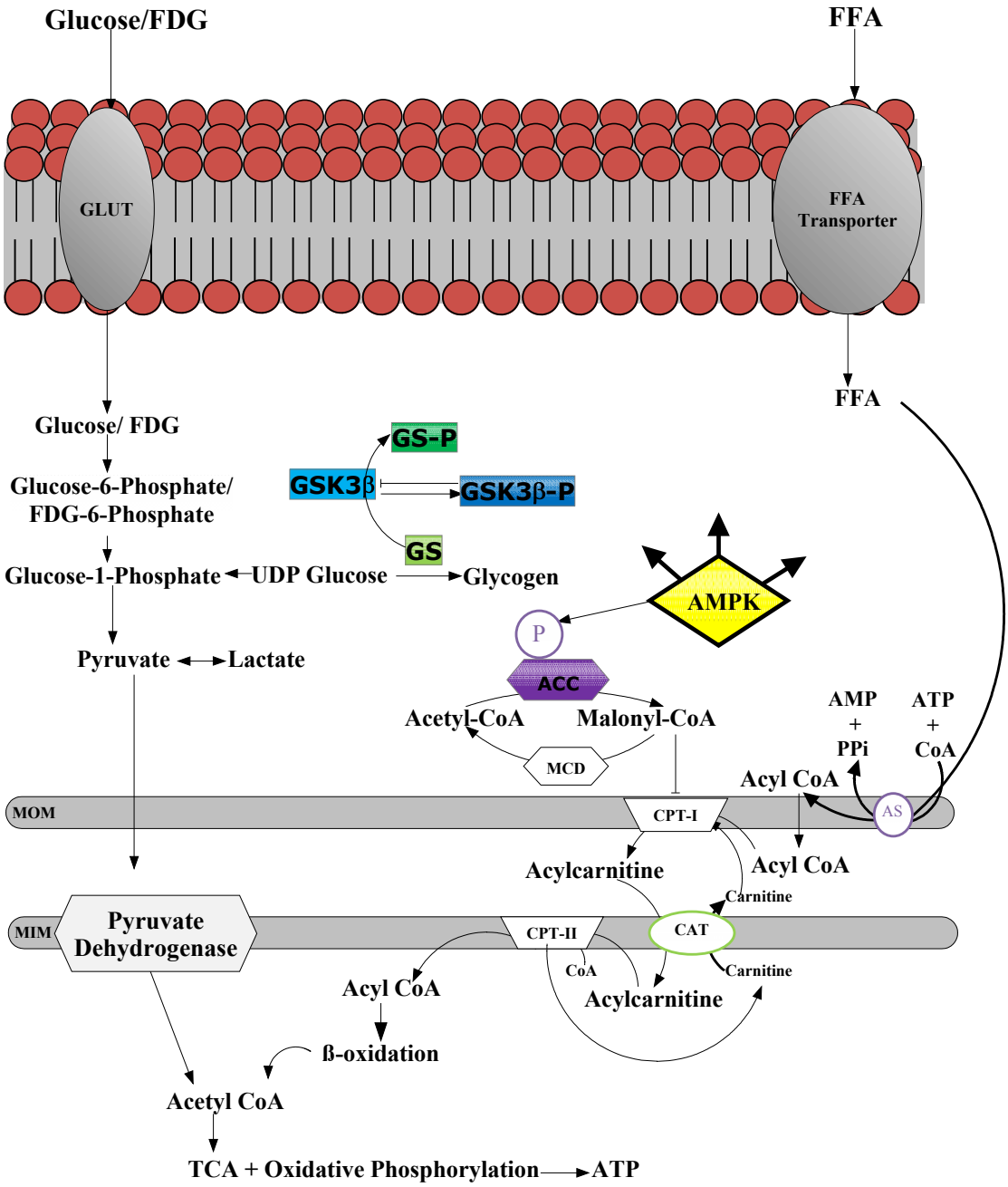

Figure 3.1: Schematic representation of cardiac metabolism.

mutation to investigate AMPK activity levels, *in vivo* myocardial glucose uptake and pertrubations in glycogen metabolism..Our aim was to address questions relating to disease development and the disordered metabolism that eventually causes heart failure and to this end, mechanisms were studied in one month old mice.

Materials and methods

Animals

All animal experiments described herein were conducted according to the guidelines of the University of Ottawa Animal Care Committee and the Canadian Council on Animal Care for the use and care of laboratory animals. All animals were maintained on a 12-hour light/dark cycle with chow and water *ad libitum*. Transgenic mice were generated as previously described (Sidhu et al., 2005) using an α-myosin heavy chain (MHC) promoter, PRKAG2 cDNA, 3'UTR human growth hormone. Transgenic mutant (TGmut) mice express the mutant PRKAG2 gene (substitute of arginine for glutamine at residue 302), with transgenic wildtype (TGwt) mice expressing the normal human PRKAG2 cDNA. PCR was performed on the genomic DNA isolated from weanling mouse tail snips with the QIAGEN DNeasy kit with the product sequenced. All studies herein were performed in mice at 4-5 weeks of age.

Echocardiography

Echocardiography images were obtained with the Vevo 770 imaging system (VisualSonics, Toronto, Canada) using a 707 transducer. Mice (TGwt n=6; TGmut n=6) were anaesthetized and maintained throughout experimental procedures with 1-2% isoflurane. Analysis of results was completed using the VisualSonics cardiac measurements program. Left ventricle

wall thickness, mass and fractional shortening were assessed using long axis B-mode images with the VisualSonics cardiac measurements formulas:

$$\text{Wall Thickness (mm)} = \sqrt{(\text{Epicardial Area(d)}/\pi)} - \sqrt{(\text{Endocardial Area(d)}/\pi)} \quad \text{Eq.1}$$

$$\text{LVmass (mg)} = 1.05 \times [{}^{5}/_{6} \times \text{Epicardial Area(d)} \times (\text{Epicardial Major(d)} + T)] - [{}^{5}/_{6} \times \text{Endocardial Area(d)} \times (\text{Endocardial Major(d)}] \quad \text{Eq.2}$$

$$\text{Fractional Shortening (\%)} = 100 \times \frac{[\text{Endocardial Area(d)} - \text{Endocardial Area(s)}]}{\text{Endocardial Area(d)}} \quad \text{Eq.3}$$

Small Animal PET Imaging

Small animal PET FDG imaging was conducted with the Inveon™ DPET small animal scanner (Siemens, Knoxville, TN) (TGwt n=3; TGmut n=6). A 60 min list-mode acquisition was started together with a 10-20 s tail vein injection of FDG (7-82 MBq in 150 μL). List data were sorted into 26 dynamic frames (12 x 10s, 3 x 60 s, 11 x 300s) and reconstructed using OSEM3D with 10 iterations, 16 subsets, zoom of 2.5 with a 128 x 128 matrix, resulting in 0.35 mm transaxial pixel size. Images were corrected for radioactive decay, random coincidences and dead-time losses using the vendor software (IAW version 1.5).

Myocardial Image Analysis

The rate of myocardial glucose uptake was calculated with Patlak kinetic analysis (Patlak et al., 1983) at 10-40 min from the reconstructed images using FlowQuant© semi-automated software (Klein et al., 2010; Lamoureux et al., 2012; Thomas et al., 2011; Thorn et al., 2013

(in press)). In brief, uptake images of the left ventricle were formed by averaging the last 5 min of scan data. The location, orientation and size of the LV were automatically determined by fitting ellipses to the myocardium in the transverse, vertical long axis (VLA) and horizontal long axis (HLA) planes. Transverse uptake images were reoriented automatically into short-axis (SA) sections generating LV slices from the apex to the base plane. Polar maps of the relative uptake activity (%) were formed from the sampled data. The sampling points were then applied to all time frames to generate myocardial time-activity curves (TACs). Blood regions of interest (ROI)

were derived with the Siemens IRW software using the proximal vena cava and the resulting blood TACs were imported into FlowQuant© image analysis software as previously described (Thorn et al., 2013 (in press)). Myocardial time activity curves were compared using standard uptake values calculated by:

$$\text{Standard Uptake Value} = \frac{\text{activity concentration in a region of interest (Bq/cc)}}{\text{injected activity (Bq)/weight of the animal (g)}} \quad \text{Eq.4}$$

The relationship after the initial input function (~time 0-2) between the myocardial activity ($C_m[t]$) corrected for blood activity (Cb[t]) and the integral of blood activity ($C_b[t]$) at time (t) becomes linear, with the slope representative of the uptake rate constant Ki.

Regional rMGU was determined for each animal using the following standard equation:

$$rMGU = K_i \times BG / LC \text{ [mmol/min/g]} \quad \text{Eq. 5}$$

where K_i [mL/min/g] is the Patlak uptake rate constant, BG is the blood glucose concentration [mmol/mL] obtained prior to FDG injection and LC is the lumped constant

equal to 0.67, which accounts for differences in the uptake and phosphorylation of FDG vs glucose. Blood glucose concentration was measured [mmol/L] with a small drop of blood from the saphenous vein using Advantage blood glucose strips (AccuChek, Roche Diagnostics, Laval, QC, Canada).

Glycogen Content and Protein Expression

Mice (TGwt n=6 and TGmut n=9) were euthanized by decapitation, and hearts were immediately removed and placed in liquid nitrogen for storage at -80°C. Tissue was ground using a mortar and pestle under liquid nitrogen. A separate group of mice (TGwt n=6; TGmut n=9) were used for for ex vivo heart weight to body weight measurements.

Glycogen content was determined using an amyloglucosidase digestion method as previously described (Zhou et al., 2008). Briefly, 10-50 mg of ground cardiac tissue was homogenized in a 1:9 (wt/vol.) ratio of PBM buffer (20mM KH_2PO_4, 10µM $CaCl_2$, 1mM $MgCl_2$, pH 6.1). Tissue homogenate (50µL) was boiled for 20 min in 30% KOH (wt/vol.) saturated with anhydrous Na_2SO_4. The remainder of tissue homogenate was used to determine protein concentration with a BCA assay. Glycogen was precipitated with 95% ethanol (vol./vol.), centrifuged at 4000 *g* for 15 min at 4°C. The glycogen pellet was dissolved in double distilled H_2O and incubated at 100°C for 20 min with 0.2% Anthrone (wt/vol.) in H_2SO_4. Absorbance was read at 595 nm to determine glycogen concentration of samples relative to an oyster glycogen standard curve (Sigma Aldrich Canada) and normalized to protein content (µg glycogen/µg of protein).

For quantification of protein expression, ground tissue was homogenized in buffer (10mM Tris-HCl, 50mM NaF, 1mM EDTA, 10mM dithiothreitol, 10% v/v glycerol, pH 7.5 at 4°C)

and a BCA assay performed to determine protein concentration. Tissue lysate (20 μg) was applied to each lane of an 8% SDS-polyacrylamide gel with separated bands of proteins transferred to a polyvinylidene fluoride membrane. In previous papers, the activity of AMPK measured with ex vivo substrate activity assays, expression of phosphorylated AMPK and phosphorylated ACC have been in agreement and used together as confirmation of AMPK activity (Folmes et al., 2009). Blocked membranes were incubated with either AMPKα (1:1000), phosphorylated AMPKα (1:500), phosphorylated ACC (Ser 79) (1:200), glycogen synthase (1:1000), glycogen synthase phosphorylase (1:500), GSK-3β (1:1000), and GSK-3β -phosphorylated (1:500) (Cell Signaling Technology). A mouse glyceraldehyde 3-phosphate dehydrogenase (GAPDH) antibody (Santa Cruz Biotechnology) was used as a loading control. Membranes were analysed using a Fluor Chem HD image system (Alpha Innotech, San Leandro, CA). Data were expressed as a ratio of target protein to GAPDH protein band intensities, normalized to the mean of TGwt controls for each membrane.

Statistical Analysis

Curve fitting with FlowQuant© software was performed using MATLAB (The MathWorks, Natick, MA). All data are expressed as mean +/- standard deviation. Data were compared using a Student's t-test; $p<0.05$ was considered significant.

RESULTS

Arg302Gln PRKAG2 increases LV mass and wall thickness with no change in LV function at 4 weeks of age

Cardiac function and dimensions, including left ventricle mass and wall thickness were assessed with echocardiography *in vivo*. Examples of M-mode (Figure 3.2A and B) and long axis B-mode (Figure 3.3A and B) echocardiography images are displayed for a TGwt and TGmut mouse. The Arg302Gln PRKAG2 TGmut mice at 4 weeks of age had no difference in left ventricle function as measured with fractional shortening compared to TGwt (53.63 ± 8.24 vs 55.81 ± 12.08, p=0.72) (Figure 3.2C). There was no measured difference in heart rates between groups (TGwt 454 bpm ± 58; TGmut 447 bpm ± 95, p=0.88). However, left ventricle mass was significantly increased by 53% in the TGmut mice (137.15 ± 37.1 vs 209.41 ± 33.11, p=.005) (Fig. 3.2D). TGmut left ventricle wall thickness was also increased by 30% (0.83 ± 0.17 vs 1.08 ± 0.19, $p<0.05$) (Figure 3.2E). The increase in TGmut wall thickness was most evident in the posterior wall (apical 0.79 ± 0.15 vs 1.09 ± 0.17, p=0.02; mid 1.14 ± 0.21 vs 1.54 ± 0.07, p=0.004; base 0.51 ± 0.12 vs 1.09 ± 0.44, p=0.02) with a trend towards increased wall thickness in the septal wall (Figure 3.3C).

In vivo Myocardial Glucose Uptake Rates are decreased in TGmut mice

In vivo myocardial glucose uptake rates were measured using non-invasive FDG PET scans. Although quantification of small animal PET images was conducted, reduced FDG uptake in the myocardium of TGmut mice relative to TGwt mice was readily apparent (representative cardiac images, Figure 3.4A). Analysis of the dynamic FDG uptake in the myocardium (y axis = standard uptake value vs x axis = time, Figure 3.4B) throughout the 60 min of acquired data shows a significant difference (49-65%, $p<0.05$) between the TGmut and TGwt mice at all time points after the initial peak activity following injection of the tracer (t=0 to 180s). Patlak kinetic analysis was used to assess the rate of myocardial glucose

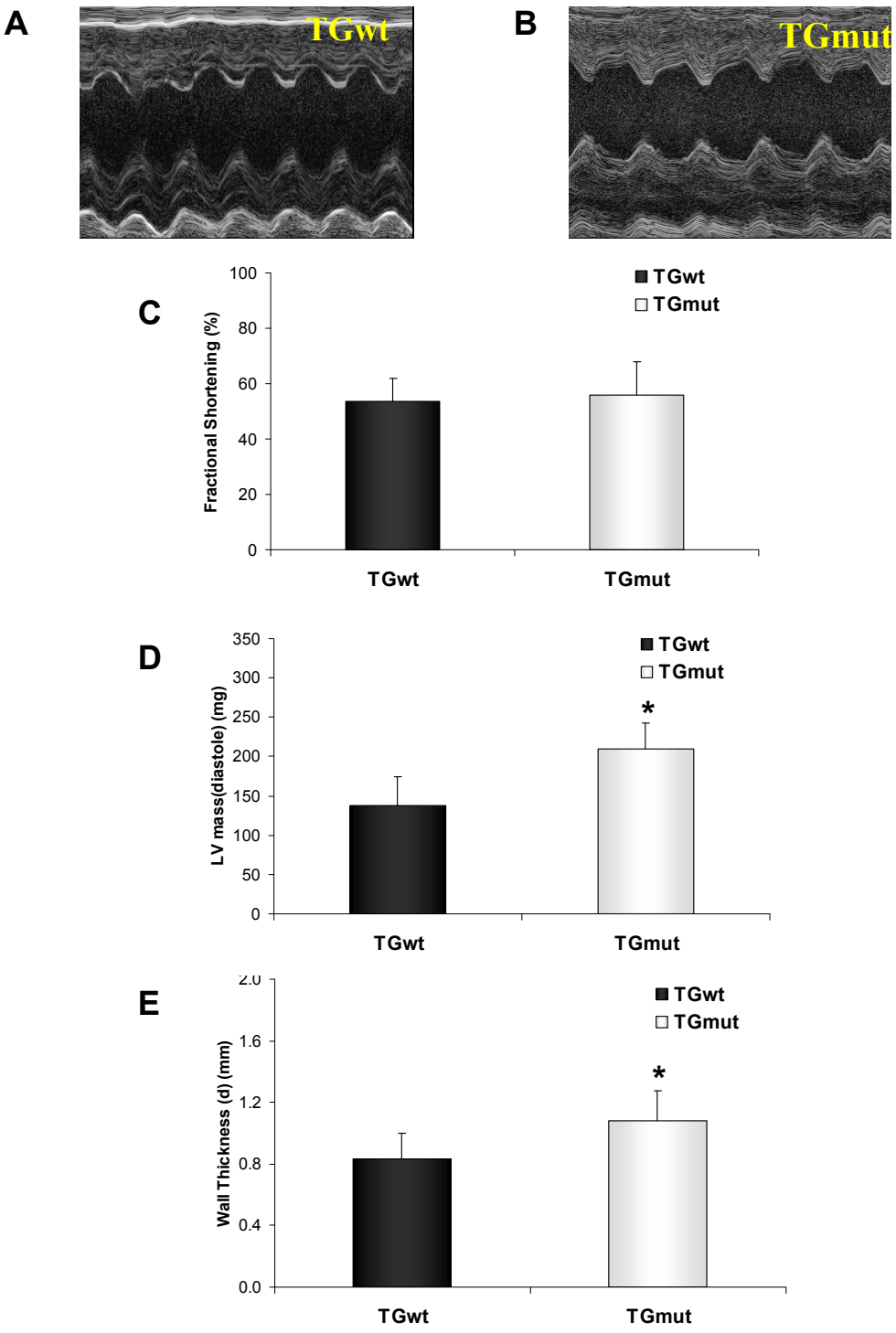

Figure 3.2: Representative echocardiography M-mode images of a TGwt (A) and TGmut (B) mouse. Using B-mode echocardiography measurements of the long axis, comparison of fractional shortening (C), LV mass (D), and wall thickness (E). TGwt n=6 and TGmut n=6. *p<0.05, Student's t-test.

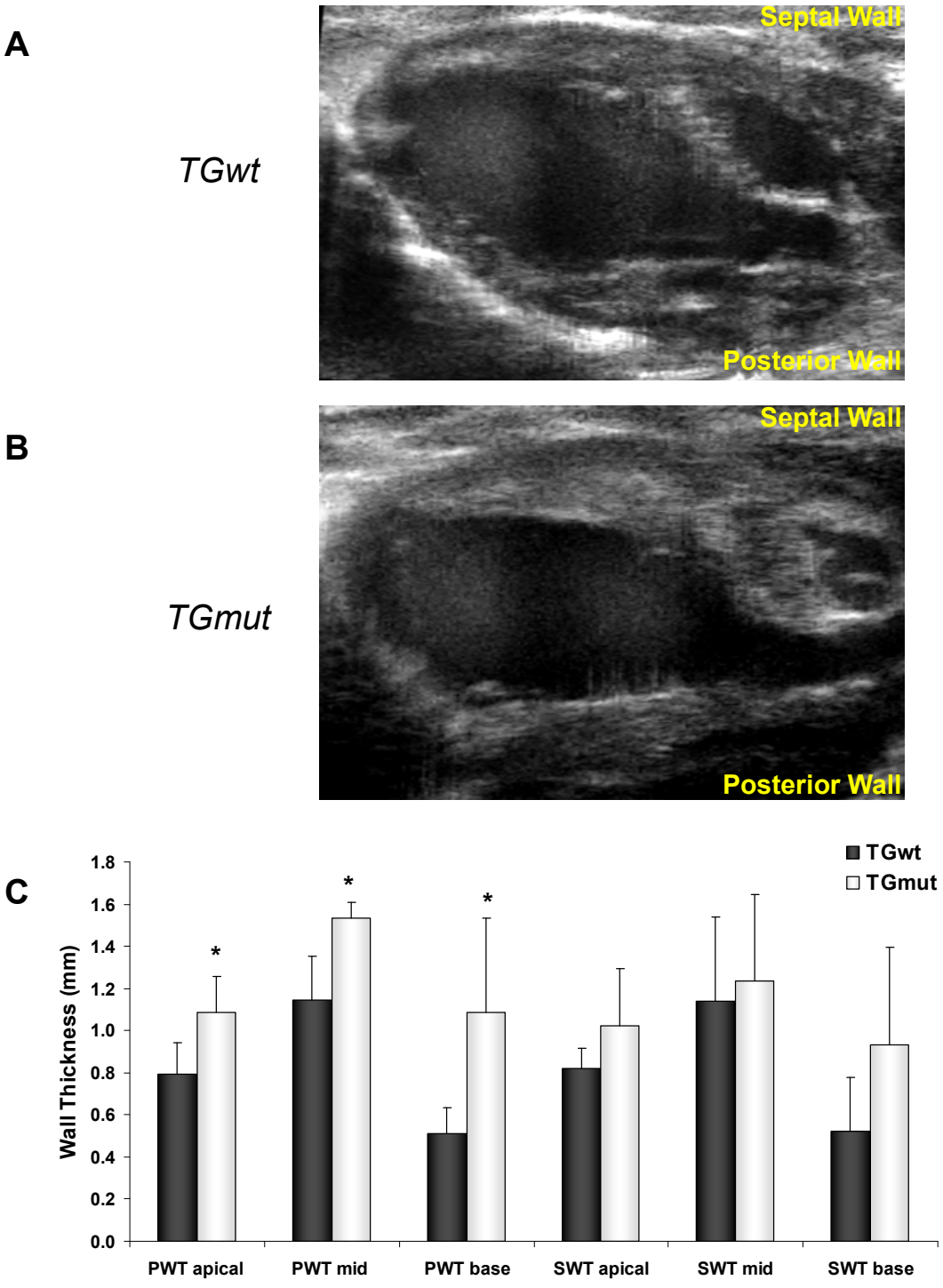

Figure 3.2: Representative echocardiography B-mode images of a TGwt (A) and TGmut (B) mouse. Comparison of posterior and anterior wall thickness at the apical, mid-lateral (mid) and base of the heart (C). TGwt n=6 and TGmut n=6 *p<0.05, Student's t-test.

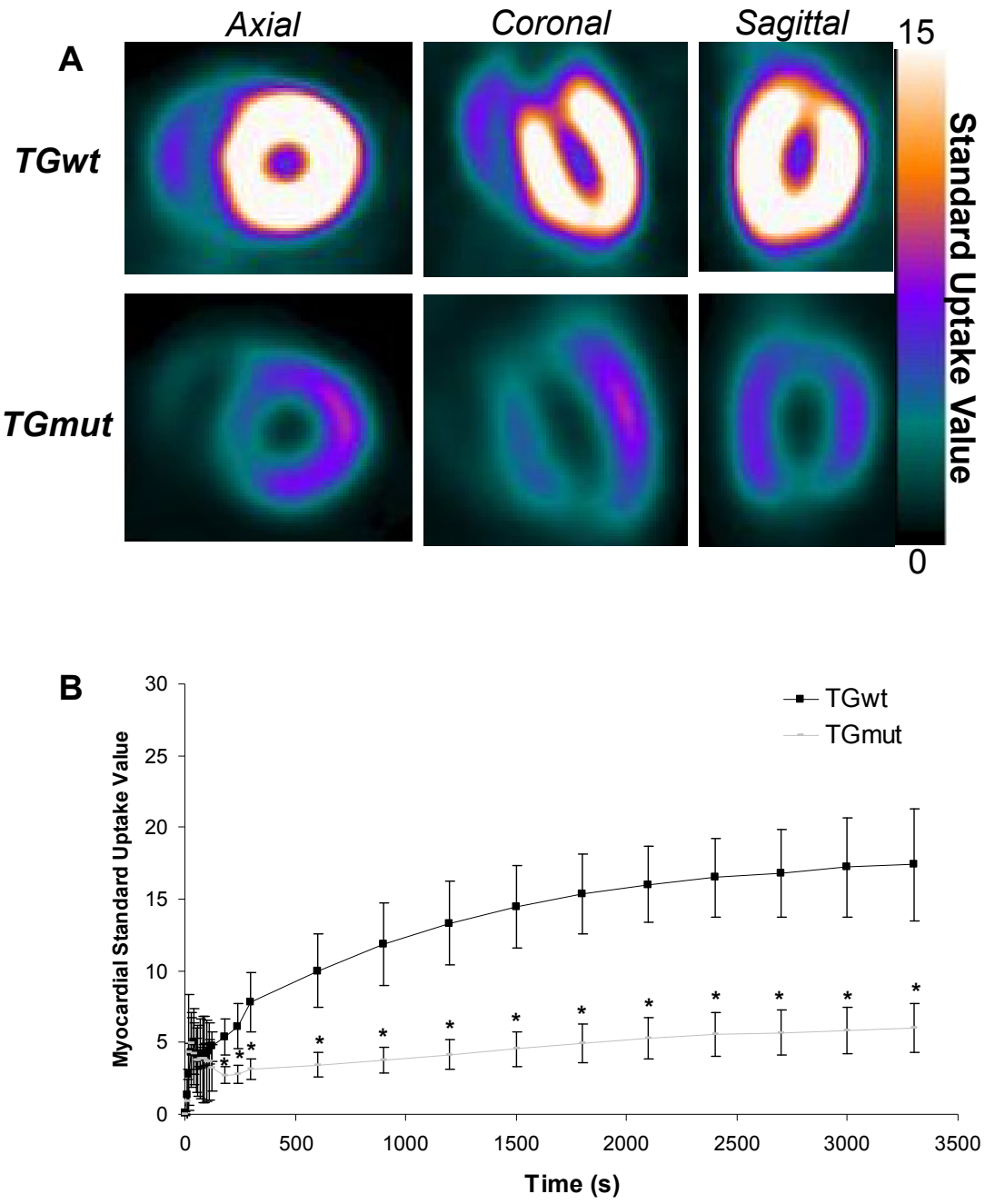

Figure 3.3: Representative FDG images of a TGwt and TGmut mouse (A). Images are presented in the axial, coronal and sagittal views and standardized to the same scale. Panel B displays the myocardial time activity curves for the TGwt and TGmut mice over 60 min using standard uptake values. TGwt n=3 and TGmut n=6 *$p<0.05$, Student's t-test.

uptake between 10 and 40 min. Representative Patlak kinetic analysis polar maps are shown in Figure 3.5A, where the surface of the left ventricle is displayed in a 2-D map with Patlak Ki values scaled to relative color intensities. The mean Patlak slopes for the linear fit at 10-40 min time interval for both the TGwt (slope= 0.70 ± 0.02) and TGmut (slope = 0.31 ± 0.01) groups were significantly different as shown in Figure 3.5B ($p<0.001$). Blood glucose levels were not significantly different between groups (not shown; $p=0.19$). Subsequently, the calculated rate of myocardial glucose uptake, rMGU, was reduced 74% in the TGmut heart compared to TGwt (11.79 ± 4.37 vs 2.90 ± 1.70; $p<0.01$ (Fig.ure 3.5C).

TGmut mice have a severe increase in cardiac mass relative to body weight correlated with excessive cardiac glycogen levels

We confirmed our findings of increased LV mass from echocardiography with ex vivo measurements of heart weight to body weight ratios. Body weights were not significantly different between the mouse groups (not shown; $p=0.18$). TGmut mice have an enlarged heart with a significant 49% increase in heart weight/body weight (mg/g) ratio compared to the age-matched TGwt mice (6.15 ± 1.42 vs 12.07 ± 1.11, $p=0.003$;) (Figure 3.6A). Previous groups have reported that only 4% of the increased cardiac mass in the transgenic mutant PRKAG2 mice at 4 weeks of age is due to glycogen stores and additional increases in mass may be due to development of cardiac hypertrophy and increased protein synthesis (Banerjee et al., 2010a). To control for any changes in total protein content, we normalized our glycogen content to protein levels. We found an increase of 83% in cardiac glycogen

levels in TGmut mice compared to TGwt controls (0.073 ± 0.034 vs 0.411 ± 0.142,$p<0.0001$) (Figure 3.6B).

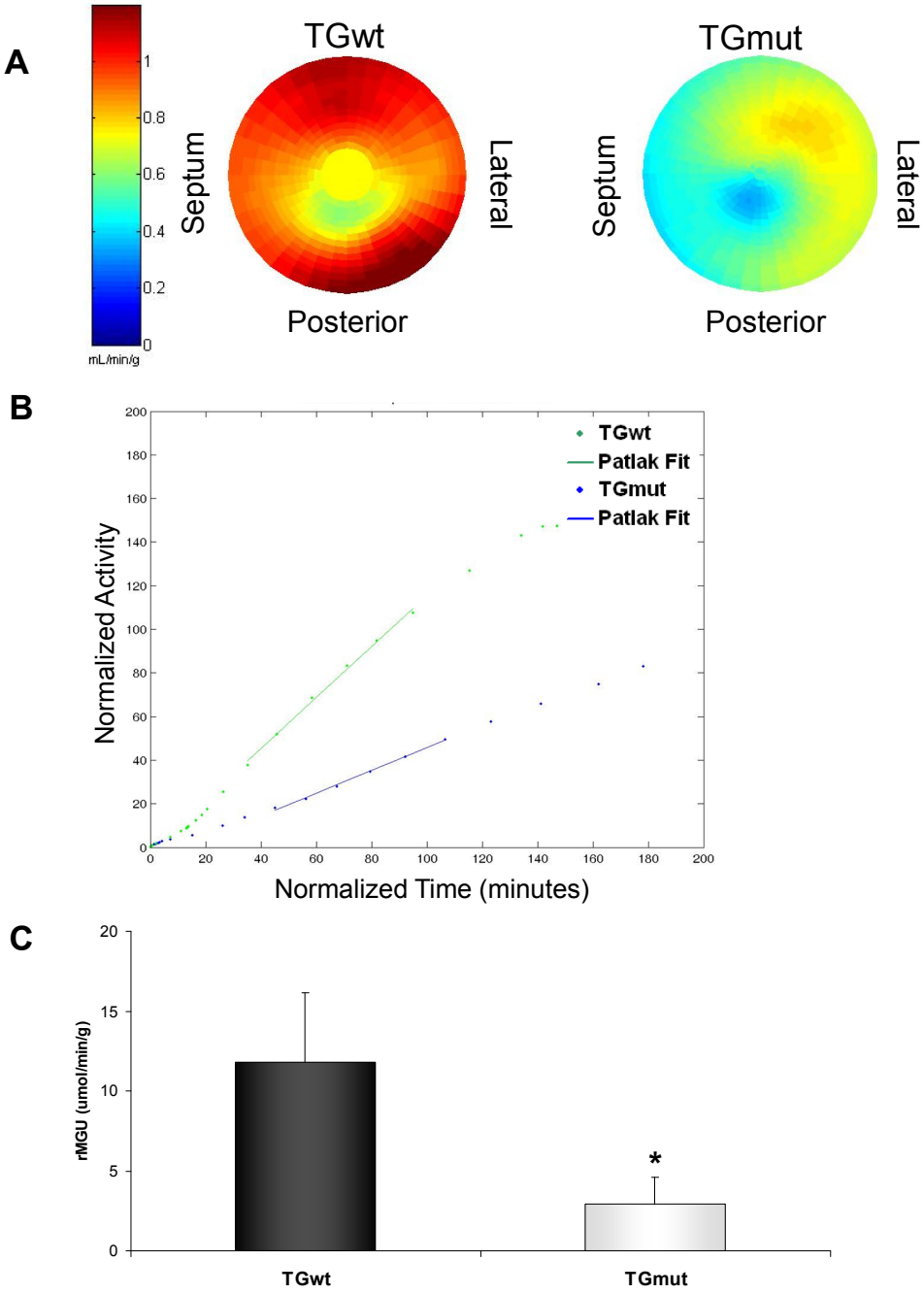

Figure 3.4: Representative FDG Patlak Ki polar maps for TGwt (A) and TGmut (B) mouse. Mean derivation of Patlak analysis showing a linear plot of normalized activity vs normalized time for the TGwt and TGmut mice (C). Solid lines represent the fit of the Patlak Ki to the linear curves at 10-40 min. The slope of this relationship Ki, is used to calculate the rate of myocardial glucose uptake (rMGU) (D). TGwt n=3 and TGmut n=6 *p<0.05, Student's t-test.

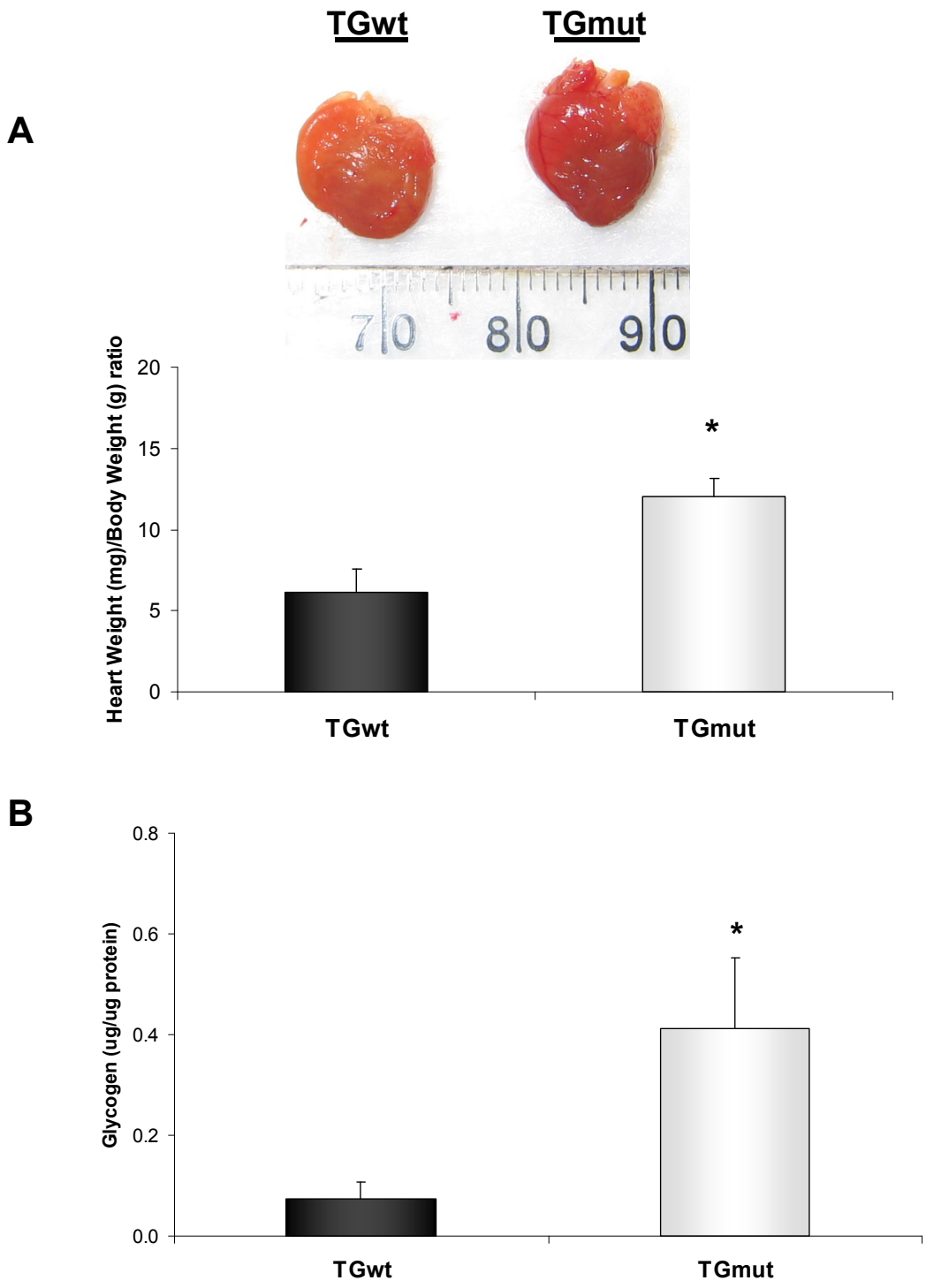

Figure 3.5: Whole heart necropsy images from a TGwt (left) and TGmut (right) mouse. Heart to body weight ratios (A). Cardiac glycogen levels determined with the amyloglucosidase digestion method. TGwt n=6 and TGmut n=9 (B)*$p<0.05$, Student's t-test.

TGmut mice expressing Arg302Gln have increased AMPK and phosphorylated AMPK expression at 4 weeks of age

AMPK protein levels were increased by 28% in TGmut mice ($p<0.001$) with a 22% increase in phosphorylated AMPK levels detected ($p<0.05$) (Figure 3.7A). Activated AMPK phosphorylates ACC, inhibiting the enzyme, thus allowing activation of carnitine palmitoyl transferase (CPT1), the rate limiting step for fatty acid uptake into the mitochondria for oxidation (Arad et al., 2007; Nagendran et al., 2012). We therefore used expression levels of phosphorylated ACC as a measurement of the intracellular activation of AMPK. We found that expression of phosphorylated ACC (Ser 79) (specific for both the ACCα and ACCβ isoforms) was increased by 36% ($p<0.01$) (Fig.ure 3.7B).

TGmut mice expressing Arg302Gln have increased glycogen synthase expression and reduced phosphorylated GSK-3β levels

AMPK activity is known to modulate glycogen synthesis and as such we evaluated the expression levels of both the active (non-phosphorylated) and inactive (phosphorylated) forms of glycogen synthase. Protein expression was significantly increased by 19 and 29%, respectively ($p<0.05$) (Figure 3.8A). We subsequently evaluated alterations in a secondary regulator of glycogen synthase activity, GSK-3β. We found that GSK-3β levels were not significantly altered, however the phosphorylated levels of GSK-3β were decreased by 60% ($p<0.001$) (Figure 3.8B).

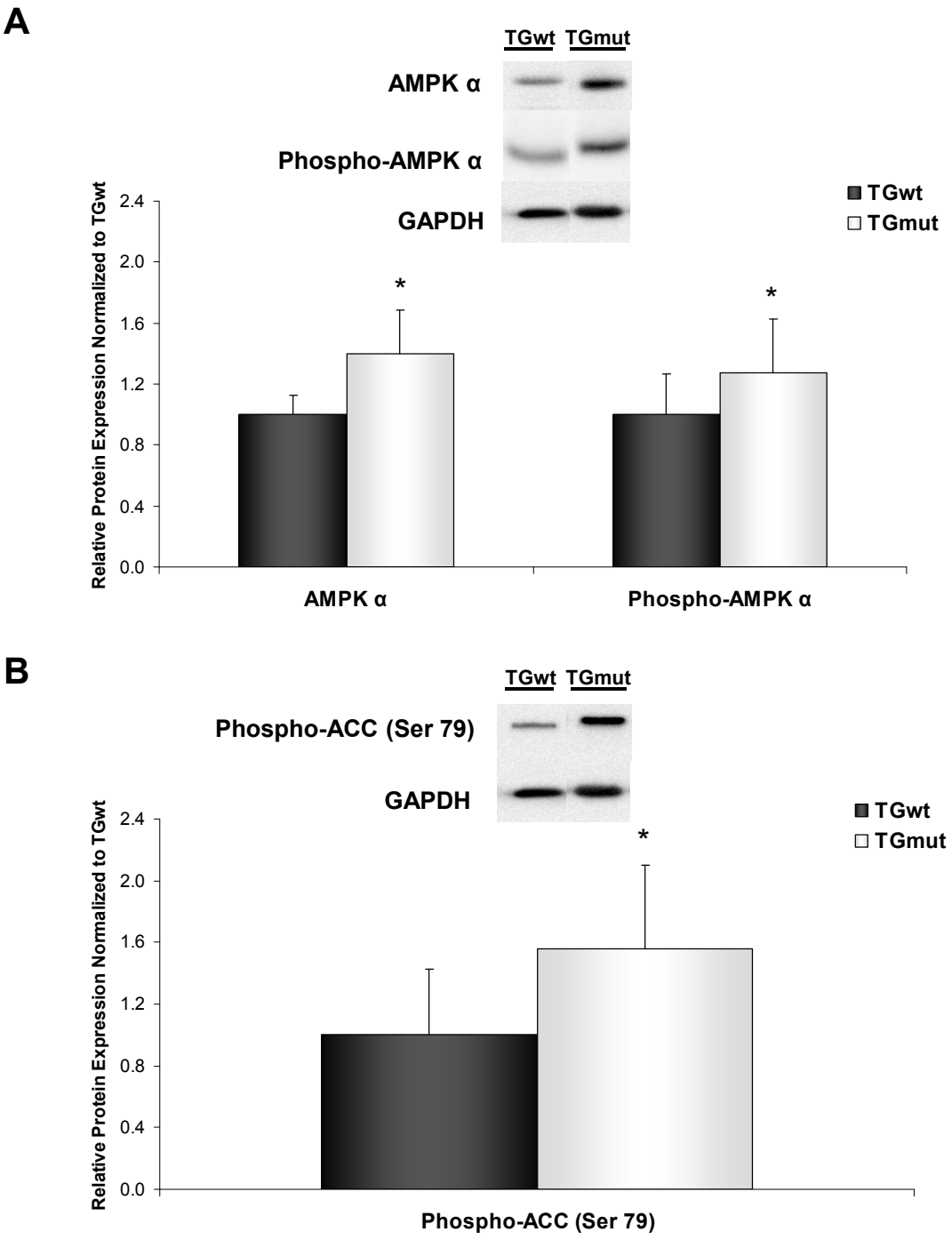

Figure 3.6: Relative protein expression normalized by measured GAPDH levels and then normalized to TGwt for AMPK and P-AMPK (A), and ACC-P (B). TGwt n=6 and TGmut n=9 *$p<0.05$, Student's t-test.

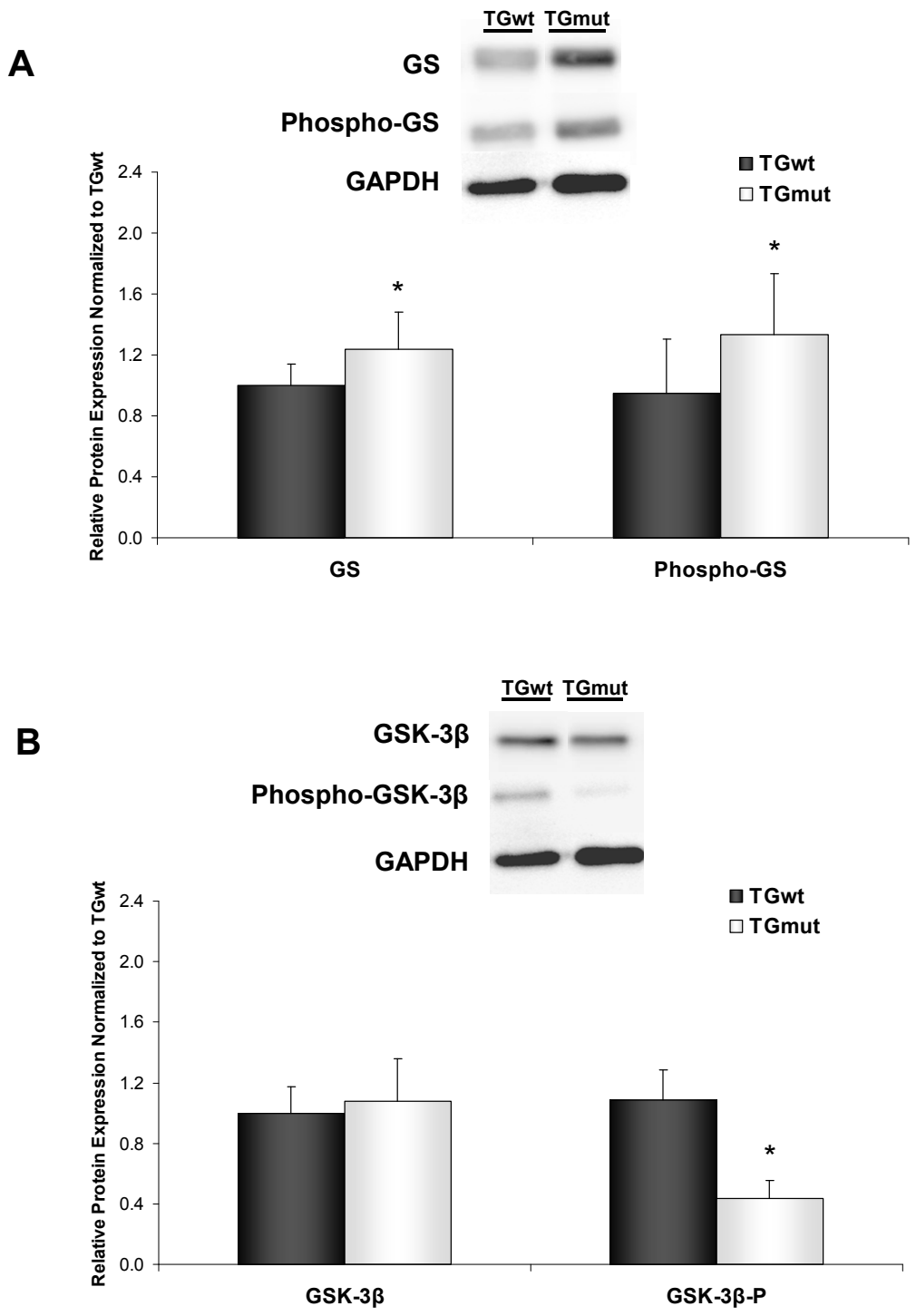

Figure 3.7: Relative protein expression normalized by measured GAPDH levels and then normalized to TGwt for GS and GS-P (A), and GSK-3β and GSK-3β-P (B). TGwt n=6 and TGmut n=9 *p<0.05, Student's t-test.

DISCUSSION

To study the effects of altered AMPK activity on glucose uptake and glycogen metabolism, we examined 4 week old mice expressing the disease-causing Arg302Gln PRKAG2 mutation. We chose mice at 4 weeks of age as they do not as yet have impaired cardiac function or contractility, confirmed by our echocardiography results. This allows for a more accurate assessment of the effect of mutant AMPK, as myocardial contractile dysfunction has been linked to alterations in glucose transport (Huang et al., 2009; Nagendran et al., 2012; Turdi et al.). Additionally, AMPK activity is reduced with age in normal control mice (Turdi et al., 2010). Thus assessing the transgenic mice at 4 weeks of age obviates confounding effects that can be due to either contractile dysfunction or other mechanisms in mice at older ages.

In this study, we demonstrate that the activated form of AMPK is increased in mice expressing the Arg302Gln mutation, prior to the onset of cardiac dysfunction. The elevated expression level of activated AMPK correlated with elevated levels of phosphorylated ACC, a downstream target of AMPK. These findings indicate that the development and progression of this genetic cardiomyopathy is preceded by enhanced AMPK activity. Previous studies in mice expressing Arg302Gln PRKAG2 were performed in mice from 8-40 weeks of age, and suggested a decrease in AMPK activity at the more advanced stage of disease (Folmes et al., 2009). Our present findings are consistent with those of Banjeree et al (Banerjee et al., 2007), who proposed a biphasic relationship of AMPK with age and disease progression. Their findings demonstrated elevated AMPK activity in young mice (< 2 weeks) but no difference in AMPK activity in mice at 5 months of age, compared to wild-type controls.

Activated AMPK is known to enhance translocation of GLUT4 to the cell membrane to facilitate glucose uptake (Russell et al., 1999). Thus, our observation of an increase in AMPK activity at 4 weeks of age might be predicted to increase cardiac uptake rate of glucose. However, the data from our transgenic mouse model using quantitative FDG-PET imaging indicated that glucose uptake is decreased at 4 weeks of age. Myocardial glucose uptake, as measured by FDG, is altered by changes in GLUT transporters and hexokinase activity, which phosphorylates FDG to FDG-6-phosphate where it becomes trapped in the cell. Recently, Banjeree *et al* (Banerjee et al., 2010b), using an alternative glucose tracer, reported an increase in relative 2-Deoxy-D-[^{14}C]glucose uptake in their PRKAG2 T400N mouse model at 2 and 8 weeks of age and associated the increase with a change in the glucose transporter, SGLT1. In itself, either FDG or its C-14 labeled counterpart, 2-Deoxy-D-[^{14}C] glucose, do not provide insight into the fate of glucose beyond the initial uptake and conversion to glucose-6-phosphate. These paradoxical results might be related to the complex feedback of cardiac glucose regulation and uptake caused by the excess glycogen levels that is evident in these young mice, which may serve to inhibit glucose transport into the cell even as early as 4 weeks of age.

To further investigate the observations of increased AMPK activity but decreased glucose uptake, we examined expression levels of key enzymes known to be involved in glycogen synthesis. We found that levels of both non-phosphorylated glycogen synthase and phosphorylated glycogen synthase were increased. Increased glycogen synthase activity would be linked to an increased turnover of glucose to glycogen, while the phosphorylated form of glycogen synthase should have an inhibitory effect on glycogen synthesis. Indeed, we found that glycogen levels were increased 5-fold in the TGmut hearts by 4 weeks. This

large magnitude of glycogen excess, and the accumulation of glycogen in muscle in general, have been hypothesized to inhibit glucose uptake and metabolism. (Wojtaszewski et al., 2002). Our observed increases in AMPK activity, decreases in glucose uptake and dysregulated glycogen synthase (in the presence of augmented glycogen stores), suggest disordered/competitive regulation in this complex system.

Accordingly we subsequently investigated GSK-3β expression levels. GSK-3β has long been recognized as a key regulator in glycogen metabolism as well as having a role in the development of cardiac hypertrophy (Antos et al., 2002; Cheng et al., ; Haq et al., 2000). We observed a significant decrease in phosphorylated GSK-3β (and therefore inhibition), with no change in total GSK-3β. Interestingly, a similar report was published in a model of the human Pompe lysosomal glycogen storage disease (Raben et al., 2010). Pompe disease is an inheritable diseased due to a deficiency in acid alpha-glucosidase (GAA), the enzyme responsible for breakdown of lysosomal glycogen to glucose. A marked decrease in expression of phosphorylated of GSK-3β was reported in $GAA^{-/-}$ mice with no change in total GSK-3β (Raben et al., 2010). This was also linked with both an increase in expression of GS and phosphorylated GS (Raben et al., 2010) similar to our current results. These data also support a possible competitive feedback pathway due to the excessive increase in glycogen stores.

Based on the results of this study, we conclude that in the Arg302Gln PRKAG2 transgenic mouse model, the excessive cardiac glycogen stores that accumulate early in development alter glucose uptake and glycogen metabolism pathways. We have shown that despite stimulation of AMPK, the affected TGmut mice show a decrease in myocardial glucose uptake at 4 weeks of age. We suggest that this reduction in glucose uptake may be due to a

feedback loop from the excessive cardiac glycogen stores already present. Subsequently, glycogen synthase and the inactivated form of glycogen synthase are both increased at this stage of development. Additionally, we report that a key regulator in glycogen formation, GSK-3β, was significantly reduced in its phosphorylated form with no change in total GSK-3β levels. Altogether our findings provides important mechanistic information on the progression of the glycogen storage disease present in the PRKAG2 cardiac syndrome prior to development of cardiac dysfunction.

Acknowledgments

The authors thank Julia Lockwood for assistance with echocardiography analysis and the Animal Care and Veterinary Services of the University of Ottawa for their assistance with animal health. This study was supported in part by the Heart and Stroke Foundation of Ontario Program Grant on Molecular Function and Imaging (grant # PRG6242), and by the Canadian Institutes of Health Research (M.Gollob). S. L. Thorn was supported by a Heart and Stroke Foundation PhD Scholarship. R. S. Beanlands is a Career Investigator supported by the Heart and Stroke Foundation of Ontario and Tier 1 Chair in Cardiovascular Research (University of Ottawa). M-E. Harper was supported by a Heart and Stroke Foundation of Ontario grant (NA6200).

CHAPTER 4: MANUSCRIPT #3

Chronic AMPK Activity Dysregulation Produces Myocardial Insulin Resistance in the Human Arg302Gln-PRKAG2 Glycogen Storage Disease Mouse Model

Stephanie L. Thorn,[1,2] Michael Gollob,[2] M.E. Harper,[3] Rob S. Beanlands,[1,2] Robert A. deKemp,[1] Jean N. DaSilva[1,2]

[1]National Cardiac PET Centre, Division of Cardiology, University of Ottawa Heart Institute, 40 Ruskin St., Ottawa, Ontario, Canada, K1Y 4W7; [2]Department of Cellular and Molecular Medicine, Faculty of Medicine, University of Ottawa, 451 Smyth Rd., Ottawa, Ontario, Canada, K1H 8M5; [3]Department of Biochemistry, Microbiology, and Immunology, Faculty of Medicine, University of Ottawa, 451 Smyth Rd., Ottawa, Ontario, Canada, K1H 8M5

Short title: PRKAG2 Myocardial Insulin Resistance

Contributions of Authors:

Genotyping, FDG imaging, echocardiography, glycogen assay, westerns and all data analysis described in this manuscript were conducted by myself, under supervision and guidance of Dr. Dr Michael Gollob and Dr Jean DaSilva. Dr M.E. Harper assisted with interpretation of the biochemical assays within the context of the PRKAG2 model. Dr Rob Beanlands participated in the clinical implications and perspective on the FDG imaging data. Dr. Robert deKemp facilitated the application of kinetic modeling and quantification.

ABSTRACT

Background — The PRKAG2 genetic mutations in the γ2-subunit of AMP-activated protein kinase (AMPK) are characterized by excessive myocardial glycogen deposition, cardiac hypertrophy, frequent cardiac arrhythmias and progressive conduction system disease. We investigated whether myocardial glucose uptake was augmented following insulin stimulation in a mouse model of the PRKAG2 cardiac syndrome.

Methods and Results — Myocardial glucose uptake was assessed with 2-[^{18}F]fluoro-2-deoxyglucose (FDG) positron emission tomography (PET) imaging in n=3 transgenic wildtype (TGwt) vs n=7 PRKAG2 mutant (TGmut) mice. Patlak Ki was reduced at baseline by 56% compared to TGwt (0.3 ± 0.2 vs 0.7 ± 0.1, t-test p=0.01). This reduction was confirmed with SUV measurements. A followup scan one week later with insulin stimulation augmented myocardial glucose uptake 71% in TGwt mice from baseline (0.7 ± 0.1 to 1.2 ± 0.2, t-test p<0.05), while no change was observed in TGmut mice. As this is a cardiac specific transgene, skeletal muscle was unaffected at baseline with a 33-38 % increase (SUV) for both genotypes following insulin stimulation. TGmut mice had a 47% reduction in systolic function. TGmut mice exhibited a 4-fold increase in cardiac glycogen stores that were correlated with a 29% reduction in phospho-AMPK α levels (0.8 ± 0.2 vs 1.1 ± 0.2, t-test p<0.05). There was no difference in cardiac insulin receptor expression between mouse genotypes.

Conclusions — These results demonstrate a link between insulin resistance and AMPK activity, and provide the basis for the use of this animal model for assessing metabolic therapy for treatment of affected PRKAG2 patients.

Key Words: positron emission tomography, FDG, Patlak, echocardiography, glucose

INTRODUCTION

Insulin resistance is strongly associated with the development of heart failure due to cardiotoxity induced by the hyperglycemic state with subsequent modification of contractile proteins (Ingelsson et al., 2005) and development of cardiac dysfunction (Raher et al., 2008). The potential to decrease insulin resistance and increase glucose uptake has recently been sought through the upregulation of adenosine monophosphate activated kinase (AMPK) activity (Horman et al.). AMPK acts as a cellular fuel gauge, tightly regulating glucose and fatty acid metabolism. Indeed, metformin, a common pharmacological treatment for type 2 diabetes, targets AMPK subsequently increasing insulin sensitivity (Ginion et al., ; Longnus et al., 2005; Yang and Holman, 2006).

The critical importance of AMPK function in the heart was highlighted by the observation that genetic mutations in the *PRKAG2* gene, encoding the gamma-2 regulatory subunit of AMPK, gives rise to a novel cardiac glycogenosis syndrome in humans (Gollob et al., 2001a; Gollob et al., 2001b). Affected individuals exhibit varying degrees of cardiac hypertrophy, frequent and persistent cardiac arrhythmias, and progressive conduction system disease leading to pacemaker implantation. In some cases, the need for heart transplantation or premature sudden death may occur (Gollob, 2003; Gollob et al., 2002; Gollob and Roberts, 2002). On gross pathologic and histologic assessment, the hallmark of the PRKAG2 cardiac syndrome is diffuse and extensive glycogen deposition throughout all four cardiac chambers (Gollob et al., 2006).

Using 2-[^{18}F]fluoro-2-deoxyglucose (FDG) and positron emission tomography (PET) imaging, human patients with the Arg302Gln mutation of PRKAG2 exhibited a 45%

reduction in myocardial glucose uptake in affected patients versus control subjects (Ha et al., 2009).

This study sought to evaluate whether the PRKAG2 myocardium is responsive to insulin-mediated cardiac glucose uptake. To address this, a transgenic mouse model of the human PRKAG2 cardiac syndrome was assessed with *in vivo* FDG PET imaging at baseline and one week later following insulin stimulation. We further evaluated whether this response correlated to changes in protein expression of activated AMPK, insulin receptors and cardiac glycogen content.

MATERIALS AND METHODS

Animal Model

All animal experiments described herein were conducted according to the guidelines of the University of Ottawa Animal Care Committee and the Canadian Council on Animal Care for the use and care of laboratory animals. All animals were maintained on a 12-hour light/dark cycle with chow and water *ad libitum*.

Transgenic mice were generated as previously described (Sidhu et al., 2005). The mice were generated using a cardiac specific α-myosin heavy chain (MHC) promoter, PRKAG2 cDNA, 3'UTR human growth hormone. These mice, therefore, have the transgene only in the myocardium. Transgenic mutant (TGmut) mice express the mutant PRKAG2 gene (substitute of arginine for glutamine at residue 302), with transgenic wildtype (TGwt) mice expressing the normal human PRKAG2 cDNA. PCR was performed on the genomic DNA isolated from weanling mouse tail snips with the QIAGEN DNeasy kit with the product

sequenced. All studies herein were performed in mice at 5-8 months of age (TGwt n=7, TGmut n=11).

Echocardiography

Echocardiography images were obtained with the Vevo 770 imaging system (VisualSonics, Toronto, Canada) using a 707 transducer. Mice (TGwt n=4; TGmut n=4) were anaesthetized and maintained throughout experimental procedures with 1-2% isoflurane. Long axis B-mode images were assessed with the commercially available VisualSonics cardiac measurements program to determine left ventricle fractional shortening and endocardial volume.

Small Animal PET Imaging

Small animal PET FDG imaging was conducted with the Inveon^{TM} DPET small animal scanner (Siemens, Knoxville, TN). Mice (TGwt n=3; TGmut n=7) were scanned at baseline and one week later 30 min following an intraperitoneal injection with short-acting insulin (Simoes et al., 2004) (8 mU/g body weight; Novolin ge Toronto, Novo Nordisk, Denmark). A 60 min list-mode acquisition was started together with a 10-20 s tail vein injection of FDG (25.3 ± 7.9 MBq in 150 μL). List data were sorted into 26 dynamic frames (12 x 10s, 3 x 60 s, 11 x 300s) and reconstructed using OSEM3D with 10 iterations, 16 subsets, zoom of 2.5 with a 128 x 128 matrix, resulting in 0.35 mm transaxial pixel size. Images were corrected for radioactive decay, random coincidences and dead-time losses using the vendor software (IAW version 1.5). Blood glucose concentration was measured [mmol/L] prior to FDG injection with a small drop of blood from the saphenous vein using Advantage blood glucose strips (AccuChek, Roche Diagnostics, Laval, QC, Canada).

Image Analysis

Myocardial uptake images of the left ventricle were formed by averaging the last 5 min of scan data using FlowQuant© semi-automated software (Klein et al., 2010; Lamoureux et al., 2012; Thomas et al., 2011; Thorn et al., 2012 (accepted, pending revisions)). The location, orientation and size of the LV were automatically determined by fitting ellipses to the myocardium in the transverse, vertical long axis (VLA) and horizontal long axis (HLA) planes. Transverse uptake images were reoriented automatically into short-axis (SA) sections generating LV slices from the apex to the base plane. Polar maps of the relative uptake activity (%) were formed from the sampled data. The sampling points were then applied to all time frames to generate myocardial time-activity curves (TACs). Myocardial TACs were compared using standard uptake values (SUV) calculated by dividing the activity concentration in the region of interest (Bq/cc) by the activity concentration per body weight injected into the animal (Bq/g). Skeletal muscle SUV values (Siemens IRW) were also evaluated at 7.5 and 60 min at both baseline and following insulin as a control region of interest for the cardiac genetic phenotype. Blood regions of interest (ROI) were derived with the Siemens IRW software using the proximal vena cava and the resulting blood TACs were imported into FlowQuant© image analysis software as previously described (Thorn et al., 2012 (accepted, pending revisions)). Patlak kinetic analysis (Patlak et al., 1983) was performed on the myocardium at 1.58- 7.5 min from the reconstructed images (FlowQuant©). The relationship after the initial input function between the myocardial activity ($C_m[t]$) corrected for blood activity (Cb[t]) and the integral of blood activity ($C_b[t]$) at time (t) becomes linear, with the slope representative of the uptake rate constant Ki.

Protein Expression and cardiac glycogen levels

Mice (TGwt n=4, TGmut n=4) were euthanized by decapitation with hearts dissected out, then placed immediately into liquid nitrogen for storage at -80°C. Tissue was ground using a mortar and pestle under liquid nitrogen. Glycogen content was determined using an amyloglucosidase digestion method as previously described.(Crawford et al., 2010; Lo et al., 1970; Zhou et al., 2008) Briefly, 10-50 mg of ground cardiac tissue was homogenized in a 1:9 (wt/vol.) ratio of PBM buffer (20mM KH_2PO_4, 10μM $CaCl_2$, 1mM $MgCl_2$, pH 6.1). Tissue homogenate (50μL) was boiled for 20 min in 30% KOH (wt/vol.) saturated with anhydrous Na_2SO_4. The remainder of tissue homogenate was used to determine protein concentration with a BCA assay. Glycogen was precipitated with 95% ethanol (vol./vol.), centrifuged at 4000 *g* for 15 min at 4°C. The glycogen pellet was dissolved in double distilled H_2O and incubated at 100°C for 20 min with 0.2% Anthrone (wt/vol.) in H_2SO_4. Absorbance was read at 595 nm to determine glycogen concentration of samples relative to an oyster glycogen standard curve (Sigma Aldrich Canada) and normalized to protein content (μg glycogen/μg of protein). Ground tissue was homogenized in buffer (10mM Tris-HCl, 50mM NaF, 1mM EDTA, 10mM dithiothreitol, 10% v/v glycerol, pH 7.5 at 4°C) and a BCA assay performed to determine protein concentration. Tissue lysate (20 μg) was applied to each lane of an 8% SDS-polyacrylamide gel with separated bands of proteins transferred to a polyvinylidene fluoride membrane. Blocked membranes were incubated with either AMPK α (1:1000), phosphorylated-AMPK α (Thr 172) (1:500), or Insulin receptor β (1:1000) (Cell Signaling Technology). A mouse glyceraldehyde 3-phosphate dehydrogenase (GAPDH) antibody (Santa Cruz Biotechnology, Inc) was used as a loading control. Membranes were analysed using a Fluor Chem HD image system (Alpha Innotech, San

Leandro, CA). Data were expressed as a ratio of target protein to GAPDH protein band intensities, normalized to the mean of TGwt controls for each membrane.

Statistical Analysis

Curve fitting with FlowQuant© software was performed using MATLAB (The MathWorks, Natick, MA). All data are expressed as mean +/- standard deviation. Data were compared using a student's t-test or a one-way ANOVA with Bonferroni correction; $p<0.05$ was considered significant.

RESULTS

Arg302Gln PRKAG2 increases left ventricle volume and reduces cardiac function

Cardiac function, volume and wall thickness were assessed with echocardiography *in vivo*. Examples of long axis B-mode (Figure 4.1A) images are displayed for a TGwt and TGmut mouse. The Arg302Gln PRKAG2 TGmut mice have a 96% increase in LV volume compared to TGwt controls (76.3 ± 29.3 uL vs 38.9 ± 7.3 uL, t-test $p<0.05$) (Figure 4.1B). Additionally, these mice display an overall reduction in cardiac systolic function with LV fractional shortening reduced 47% (TGwt 33.1 ± 5.1 % vs TGmut 17.7 ± 3.3 %, t-test $p<0.01$) (Figure 4.1C) with similarity in heart rates between groups (TGwt 407 ± 35 bpm; TGmut 360 ± 69 bpm, $p=0.27$). There was no difference in LV wall thickness in TGmut except for 30% significant reduction in the mid septal wall (1.4 ± 0.3 vs 0.9 ± 0.2, t-test $p<0.05$) (Figure 4.1D).

Myocardial Glucose Uptake is reduced in TGmut mice with no response to insulin stimulation

There was no difference between baseline and followup scans or between genotype with respect to body weight at time of scan ($p>0.05$ one way ANOVA, Bonferrroni Table 4.1).

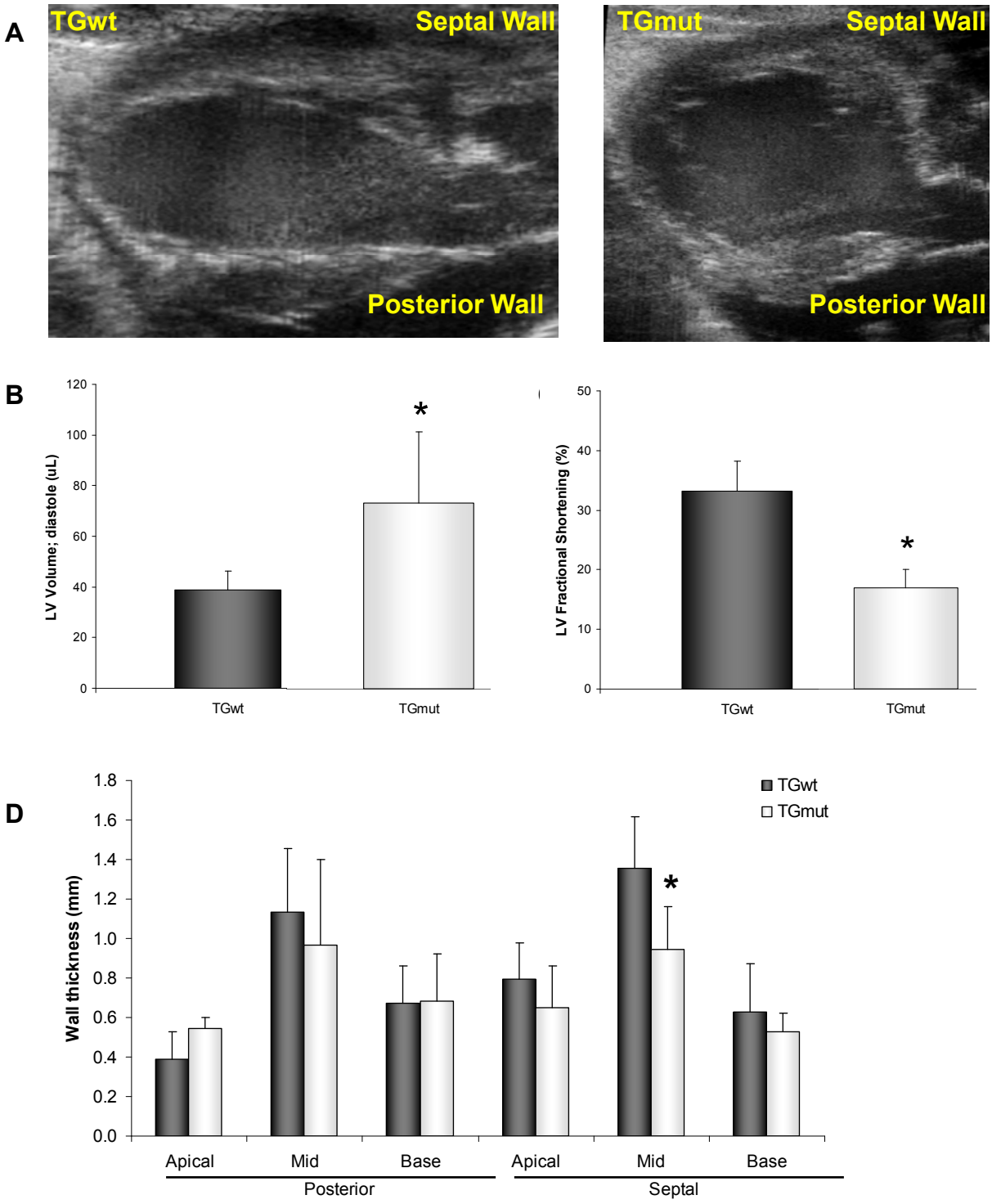

Figure 4.1: Representative echocardiography M-mode images (A)of a TGwt and TGmut mouse. Echocardiography B-mode measurements of the long axis, comparison of left ventricle volume (B), fractional shortening (C), and wall thickness (D). TGwt n=4 and TGmut n=4 *p<0.05, Student's t-test.

Blood glucose levels were not significantly different between TGwt and TGmut mice at baseline (Table 4.1). Both groups showing a similar decrease of 60-70% in blood glucose values following insulin pretreatment prior to FDG injection (Table 4.1). Representative cardiac images in TGwt (Figure 4.2A) and TGmut (Figure 4.2C) are depicted in axial, coronal and sagittal views at baseline and following insulin stimulation. Contrary to TGmut mice, SUV analysis of the myocardial curves displays an increase in initial uptake rate with insulin stimulation in TGwt mice (Figure 4.2B and 4.2D). In fact, a 43% reduction in myocardial glucose uptake following insulin stimulation at 60 min was observed in TGmut mice (Table 4.2). Both TGwt and TGmut show a 31-38% increase in skeletal muscle SUV values with insulin stimulation at both 7.5 and 60 min (Table 4.2). Patlak kinetic analysis was used to determine differences in myocardial glucose uptake rate. Representative Patlak Ki polar maps and linear plots of normalized activity in high uptake regions between 1.58 and 7.5 min are displayed (Figure 4.3: TGwt baseline (A), TGwt + insulin (B), TGmut baseline (C), TGmut + insulin (D)). Patlak polar maps qualitatively show an increase in Ki values with insulin in TGwt mice (Figure 4.3A and 4.3B), not observed in the TGmut mice (Figure 4.3C and 4.3D). In all cases, there was an excellent linear fit in the time frame of 1.5-7.5 min. At baseline, Patlak Ki was reduced 56% at baseline in TGmut mouse hearts compared to TGwt mice (Table 4.3). TGwt display an increase of 71% from baseline following insulin stimulation while TGmut showed no changed in cardiac uptake rates following insulin stimulation (Table 4.3).

Table 4.1: Body weight and blood glucose values prior to injection of FDG

	Body weight (g)	Pre-FDG blood glucose (mmol/L)
TGwt	36.4 ± 8.3	14.1 ± 1.3
TGwt insulin	37.7 ± 8.9	4.0 ± 0.3*
TGmut	32.2 ± 4.5	10.4 ± 3.4
TGmut insulin	33.2 ± 4.1	4.6 ± 1.9*

* $p<0.05$ by ANOVA and after Bonferroni correction

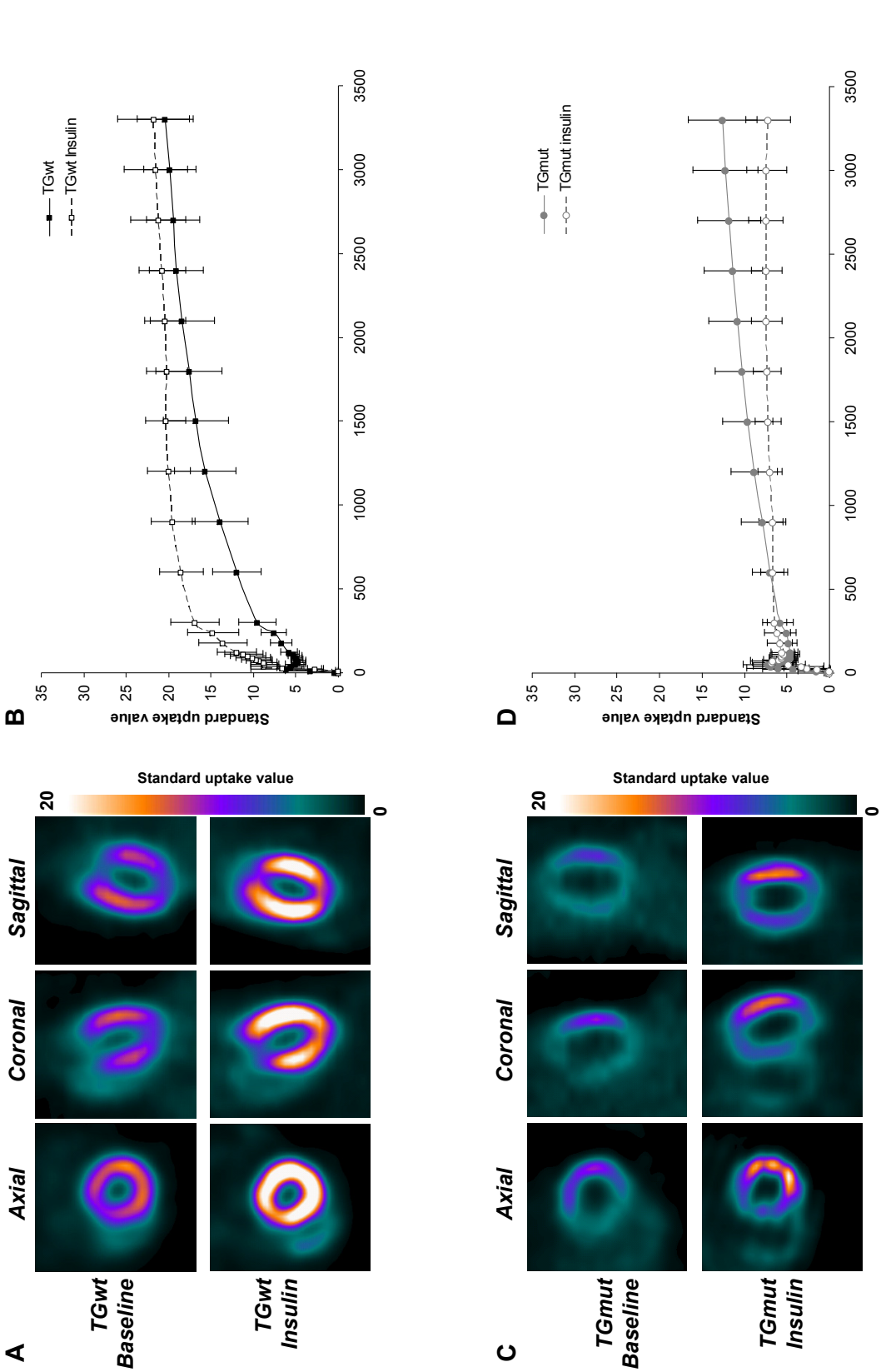

Figure 4-2: Representative cardiac FDG images of a TGwt (A) and TGmut mouse (C) at baseline and following insulin stimulation. Images are presented in the axial, coronal and sagittal views and standardized to the same scale. Panel B and D displays the myocardial TACs baseline and following insulin in TGwt and TGmut mice respectively over 60 min using SUV. TGwt n=3 and TGmut n=7 *p<0.05, Student t-test.

Table 4.2: Myocardium and skeletal muscle FDG SUV

	Myocardium	Muscle
SUV 7.5 min p.i.		
TGwt	9.6 ± 2.2	0.5 ± 0.1
TGwt insulin	16.9 ± 2.8*	0.8 ± 0.2*
TGmut	5.8 ± 1.6#	0.7 ± 0.1
TGmut insulin	6.4 ± 1.4	1.1 ± 0.5*
SUV 60 min p.i.		
TGwt	20.4 ± 3.3	0.7 ± 0.2
TGwt insulin	21.8 ± 4.3	1.1 ± 0.2*
TGmut	12.6 ± 4.1	1.0 ± 0.2
TGmut insulin	7.2 ± 2.6*	1.5 ± 0.6*

* $p<0.05$ vs non-insulin treated baseline with paired t-test
# $p<0.05$ vs TGwt with paired t-test

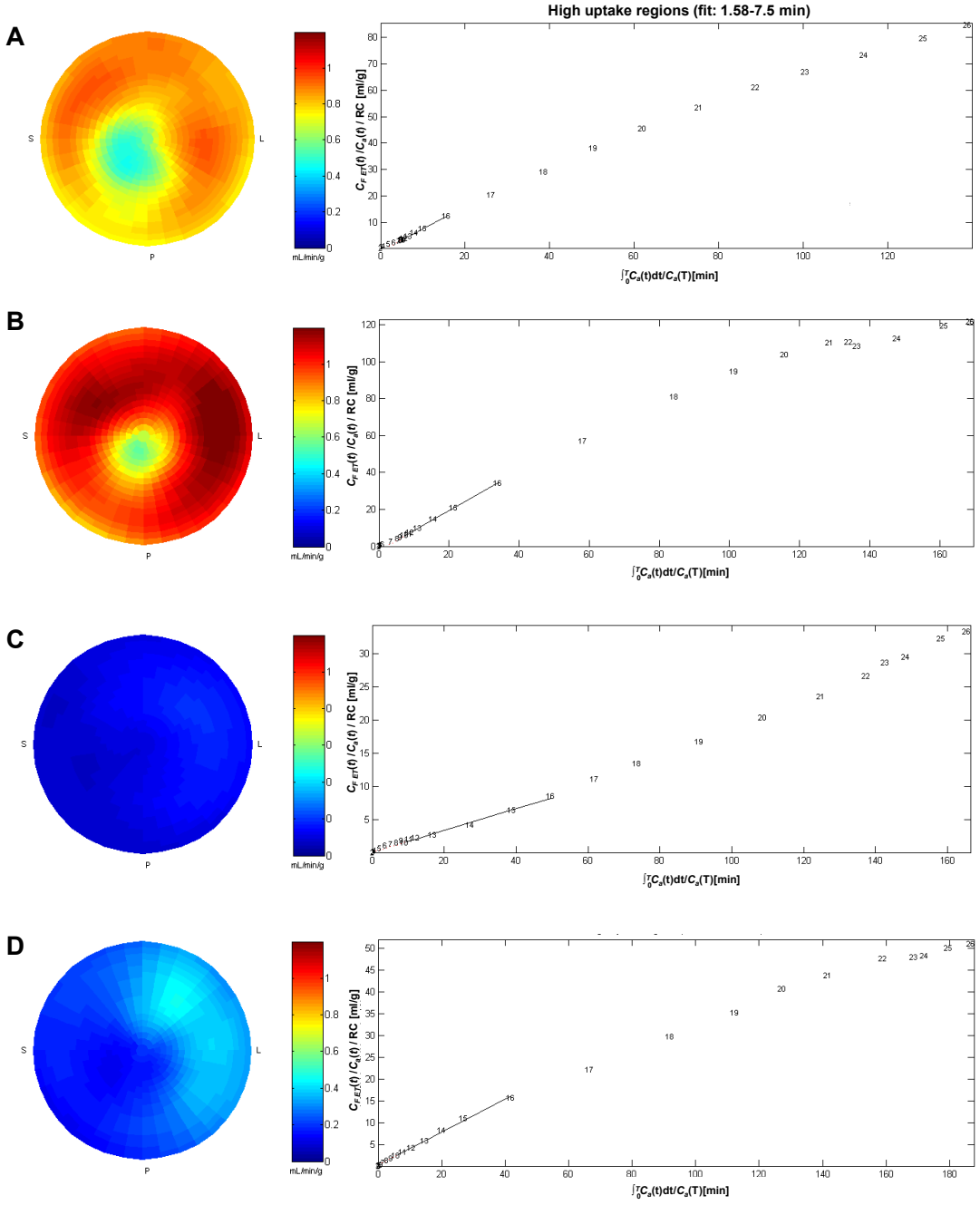

Figure 4.3: Representative FDG Patlak Ki polar maps for TGwt baseline(A), TGwt with insulin (B), TGmut baseline (C) and TGmut following insulin (D). Representative mean derivation of Patlak analysis showing a linear plot of normalized activity vs normalized time are shown beside the polar map for each state. Solid lines represent the fit of the Patlak Ki to the linear curves at 1.58-7.5 min. The slope of this relationship quantifies Patlak Ki. TGwt n=3 and TGmut n=6

Table 4.3: Myocardial FDG Patlak kinetic analysis (1.58-7.5 min)

	Baseline	**Insulin**
TGwt	0.7 ± 0.1	1.2 ± 0.1*
TGmut	0.3 ± 0.2[#]	0.4 ± 0.2

* $p<0.05$ vs non-insulin treated baseline with paired t-test
[#] $p<0.05$ vs TGwt with paired t-test

Glycogen Deposition and Protein Expression

There was a 4-fold increase in cardiac glycogen levels in the TGmut mice compared to TGwt hearts (0.46 ± 0.07 vs 0.11 ± 0.05, t-test $p<0.001$). A 29% reduction in phosphorylation of AMPK α on Thr^{172} normalized to total AMPK expression levels was found in TG mut mice compared to TGwt hearts (1.1 ± 0.2 vs 0.8 ± 0.2, t-test $p<0.05$) (Figure 4.4A). Protein expression of cardiac insulin receptor β was not affected by the PRKAG2 genotype with no difference found between groups (Figure 4.4B).

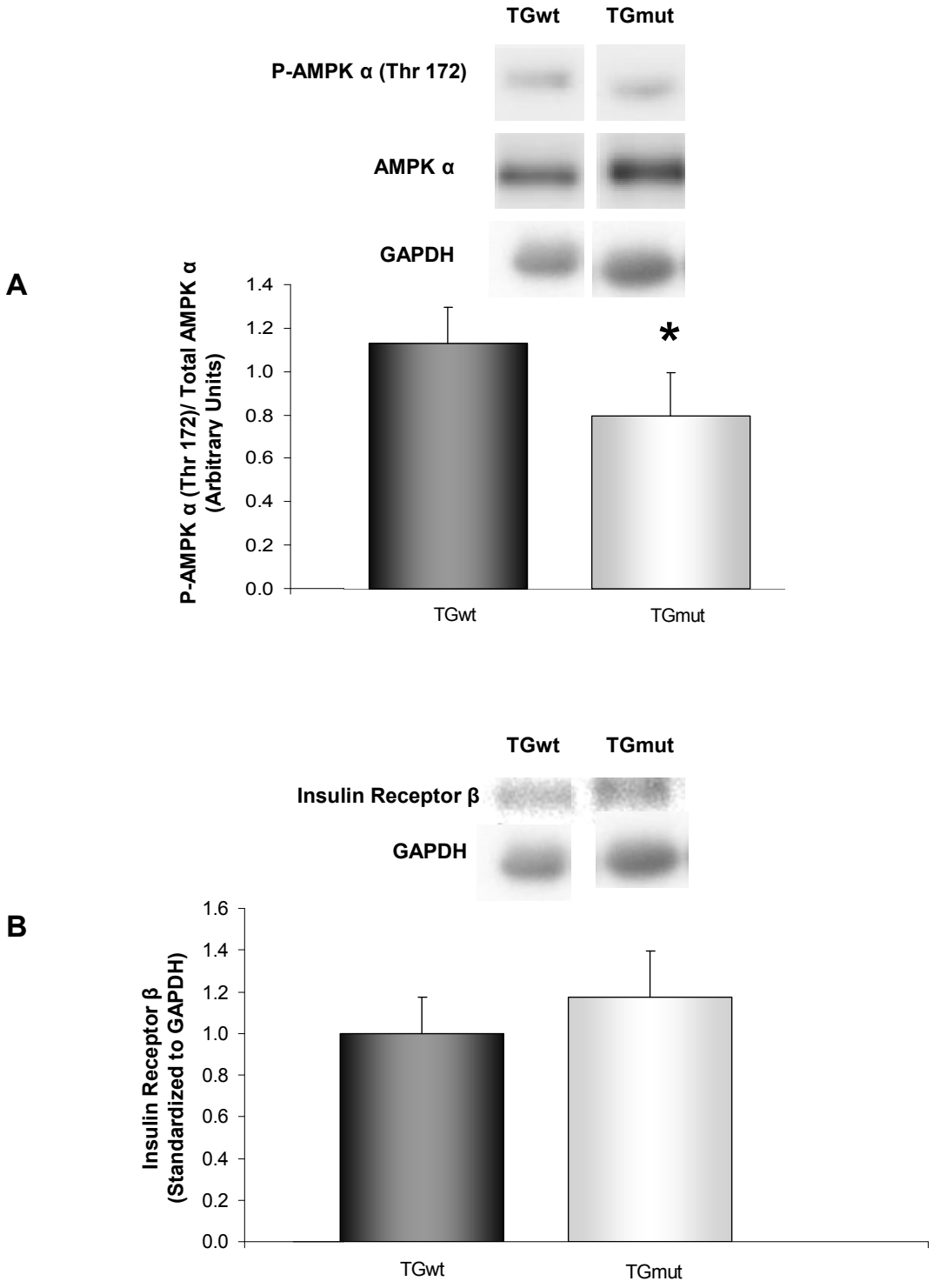

Figure 4.4: Relative protein expression normalized by measured GAPDH levels and then normalized to TGwt for phospho-AMPK α levels expressed to total AMPK (A), and insulin receptor protein expression (B). TGwt n=4 and TGmut n=4 *$p<0.05$, Student's t-test.

DISCUSSION

Central to cardiac metabolism, AMPK is activated in response to energy deprivation to rapidly modulate cardiac metabolism (Zaha and Young, 2012). Activated AMPK is known to enhance translocation of GLUT4 to the cell membrane to facilitate glucose uptake (Coven et al., 2003). In the current study, we evaluated mice at 5-8 months of age and demonstrated a reduction in the phosphorylation of the α subunit of AMPK of 29% that agrees with a previously published study using the Arg302Gln PRKAG2 mice at >8 weeks of age (Folmes et al., 2009). With a reduction in AMPK activity, our data establishes a 56% reduction in glucose uptake with FDG PET imaging in TGmut mice compared to TGwt.

As GLUT transporter efficiency is the rate limiting step for glucose uptake, and the insulin dependent transporter GLUT4 is the most abundant transporter in the mouse myocardium, we sought to determine if FDG uptake could be increased in the PRKAG2 mutant mouse hearts following acute insulin stimulation. We found that unlike TGwt mice, where there was a 71-76% increase in Patlak Ki and SUV values from baseline, TGmut mice displayed no increase in FDG uptake following insulin stimulation. We additionally determined that the protein expression of the cardiac insulin receptor β is not altered between TGwt and TGmut mice. As the transgene is cardiac specific, we compared the myocardial FDG data with skeletal muscle uptake at baseline and following insulin. As expected, this alteration affects the heart only, with skeletal muscle SUV values increased similarly 31-38% following insulin in both genotypes. This increase correlates with previously published data in control mice with insulin pretreatment (Kreissl et al., 2011).

The lack of responsiveness to cardiac insulin stimulation in the PRKAG2 mutant mice, where AMPK activity is dysfunctional, is intriguing where a link between insulin stimulation

and AMPK is currently under investigation with regards to type 2 diabetes (Horman et al., 2012). The limiting factor in our model may be the excess glycogen levels. In a normal myocardium, insulin promotes glucose uptake and glycogen synthesis (Towler and Hardie, 2007). Previous groups have shown that when saturated with glucose, skeletal muscle will display insulin resistance matched with a reduction in AMPK activity (Kraegen et al., 2006; Saha et al., 2010). In the current study, an approximate 4-fold increase in cardiac glycogen stores was observed in TGmut mice. From this data, we would hypothesize, that the increased glycogen stores are causing a negative feedback reducing AMPK activity and thus reducing glucose uptake. The lack of insulin stimulation appears to agree with the theory that inhibition of AMPK activity ameliorates insulin stimulation even in the presence of glucose deprivation.

In this study, we used FDG as a measurement of glucose uptake. Glucose uptake can be affected by multiple factors including but not limited to: GLUT and SGL transporter translocation to the cell membrane, hexokinase activity and glucose-6-phosphate levels. We did not measure directly the sarcolemmal protein expression, mRNA or whole cell activity of these factors in this study.

The current findings indicate that the PRKAG2 mouse model has reduced cardiac glucose uptake at 5-8 months of age, correlating with previous work (Ha et al., 2009) from our group with reduced uptake in affected PRKAG2 patients. This reduction in cardiac uptake occurs with reduced cardiac function, increased glycogen stores and reduced AMPK activity. Furthermore, the PRKAG2 mouse model exhibits myocardial insulin resistance. The findings of this study not only provide insight of the PRKAG2 cardiac syndrome, but also emphasize the potential role of AMPK in insulin resistance observed in other

pathological cardiac states. Conversely, with similarities to pathologic cardiac states such as type 2 diabetes, these findings provide further information on the role that metabolic therapeutic targets may have in the affected PRKAG2 patients.

ACKNOWLEDGEMENTS

The authors thank the Animal Care and Veterinary services of the University of Ottawa for their assistance with animal health. We would also like to thank the PET radiochemistry lab for the FDG used in this study and the microPET facilities.

GRANTS

This study was supported in part by the Heart and Stroke Foundation of Ontario Program Grant on Molecular Function and Imaging (grant # PRG6242), and by the Canadian Institutes of Health Research (M.Gollob). S. L. Thorn was supported by a Heart and Stroke Foundation PhD Scholarship. R. S. Beanlands is a Career Investigator supported by the Heart and Stroke Foundation of Ontario and Tier 1 Chair in Cardiovascular Research (University of Ottawa**).**

DISCLOSURES

Drs Rob deKemp and Rob Beanlands are consultants with DRAXImage; Dr Jean DaSilva and Dr Rob Beanlands are consultants with Lantheus Medical Imaging. Dr Rob deKemp receives revenue shares from FlowQuant sales.

CHAPTER 5: MANUSCRIPT #4

Attenuation of the Arg302Gln-PRKAG2 Cardiac Syndrome and Ventricular Preexcitation with Trimetazidine Treatment

Stephanie L. Thorn, MSc,[1,2] Jean N. DaSilva, PhD,[1,2] Qiuju Li, MSc,[2] Michael H.Gollob, MD[2]

[1]National Cardiac PET Centre, Division of Cardiology, University of Ottawa Heart Institute, 40 Ruskin St., Ottawa, Ontario, Canada, K1Y 4W7; [2]Department of Cellular and Molecular Medicine, Faculty of Medicine, University of Ottawa, 451 Smyth Rd., Ottawa, Ontario, Canada, K1H 8M5; [3]Department of Biochemistry, Microbiology, and Immunology, Faculty of Medicine, University of Ottawa, 451 Smyth Rd., Ottawa, Ontario, Canada, K1H 8M5

Running Head: Attenuation of PRKAG2 cardiac syndrome with trimetazidine

Key Words: Wolf-Parkinson White, arrhythmia, AMPK, echocardiography, telemetry

Contributions of Authors:

Genotyping, echocardiography, glycogen assay, and all data analysis described in this manuscript were conducted by myself, under supervision and guidance of Dr Jean DaSilva and Dr Michael Gollob. Qiuju Li (MSc) implanted all telemetry devices used for this study. All telemetry data analysis was conducted by myself.

ABSTRACT

The PRKAG2 cardiac syndrome is characterized by excessive myocardial glycogen deposition, cardiac hypertrophy, frequent cardiac arrhythmias and progressive conduction system disease. The condition is often familial and is caused by genetic mutations in the γ2-subunit (PRKAG2) of AMP-activated protein kinase (AMPK). Trimetazidine (TMZ), is a novel anti-ischemic agent that selectively inhibits the fatty acid β-oxidation pathway. This leads a concurrent increase in glucose oxidation shifting cardiac energy metabolism to an increased reliance on glucose metabolism. The present study aims to investigate whether chronic pharmacologic intervention with trimetazidine in the Arg302Gln PRKAG2 mouse model would attenuate cardiac glycogen stores and therein normalize cardiac function and electrical conduction.

Mice at 4-5 weeks of age were provided either control water (TGwt, TGmut) or treated chronically with TMZ water for 8 months at 10 mg/kg/day po ($TGwt^{TMZ}$, $TGmut^{TMZ}$). TMZ reduced cardiac glycogen levels by 55% in $TGmut^{TMZ}$ vs TGmut mice (0.21 ± 0.13 vs 0.46 ± 0.07, p=0.008). $TGmut^{TMZ}$ displayed improved systolic function compared to TGmut mice at both 20 (19.8 ± 5.2 vs 29.5 ± 7.5, t-test p=0.02) and 36 weeks (19.2 ± 5.8 vs 26.2 ± 2.4, t-test p=0.04) with no significant difference to TGwt and $TGwt^{TMZ}$. TGmut mice manifested ventricular preexcitation as noted by the short PR interval (16 ± 5 vs 33 ± 2 ms in TGwt; $p<0.05$) and wide QRS (22 ± 3 vs 14 ± 2 ms in TGwt; $p<0.05$). TMZ treatment significantly reduced the QRS interval ($TGmut^{TMZ}$ 17 ± 2 ms) with normalized sinus rhythm and no presentation of delta waves. The present data indicates that chronic TMZ treatment reduces cardiac glycogen stores in the PRKAG2 mutant mice while improving systolic function and

abolishing ventricular preexcitation. These data suggest that pharmacological modulation of cardiac metabolism may be beneficial in the attenuation of the PRKAG2 cardiac syndrome.

INTRODUCTION

Glycogen Storage Diseases are inherited metabolic diseases characterized by excessive glycogen accumulation (storage) in various tissues (Shin, 2006). At least 15 genetic forms of this disease have been described, with at least half known to affect the heart leading to a progressive cardiomyopathy, arrhythmia, and mortality (Shin, 2006).

The most recent glycogen storage disease was described by our research group in Ottawa in 2001(Gollob, 2003; Gollob et al., 2001a; Gollob et al., 2002; Gollob and Roberts, 2002; Gollob et al., 2001b), and is referred to as the PRKAG2 Cardiac Syndrome. Affected PRKAG2 patients progressively develop cardiomyopathy, arrhythmias and conduction system disease. Presently, about 70% of our patients have cardiac devices, including pacemakers and defibrillators.

A mutation in the protein kinase AMPK gamma 2 (*PRKAG2*) gene encoding for the gamma-2 regulatory subunit of the heterotrimeric AMP-activated protein kinase (AMPK) is responsible for the pathology of this syndrome (Gollob et al., 2001a; Gollob et al., 2001b). AMPK is a heterotrimeric kinase consisting of a catalytic subunit (α) and two regulatory subunits (β and γ). The γ-subunit contains the cystathionine-β-synthase domains (CBS) whereby AMPK is activated in response to energy deprivation primarily via allosteric regulation by AMP or ADP (Oakhill et al., 2011; Xiao et al., 2011). AMPK activation increases the catabolism of free fatty acids (FFA) (Carling, 2004; Kudo et al., 1995; Luiken et al., 2003), and accelerates glucose uptake (Russell et al., 1999) stimulating glycolysis (Marsin et al., 2000).

In the present study, we investigate reversing the severity of the glycogen storage in the PRKAG2 cardiac syndrome with use of trimetazidine, a therapeutic agent known to function as a "myocardial energy switch" in the heart, shifting myocardial metabolism from fatty acid oxidation to enhanced utilization of glucose oxidation. Trimetazidine (1-(2,3,4-trimethoxybenzyl) piperazine dihydrochloride, or TMZ), is a novel anti-ischemic agent that selectively inhibits the activity of long chain 3-ketoacyl-coenzyme A thiolase (3-KAT), the final enzyme of the fatty acid β-oxidation pathway (Figure 5.1) (Kantor et al., 2000). This leads to a partial inhibition of fatty acid β-oxidation, thereby shifting cardiac energy metabolism to an increased reliance on cardiac glucose metabolism (Kantor et al., 2000). Heart failure clinical trials have indicated a potential benefit of TMZ therapy in reducing mortality and even-free survival in patients (Cera et al., 2010; Fragasso et al., 2012; Gunes et al., 2009b; Zhang et al., 2012).

Thus, in the setting of altered cardiac metabolism promoting pathologic glycogen storage, TMZ may be efficacious in offsetting disease severity by enhancing glucose utilization and promoting glycogen breakdown, countering the metabolic propensity for glycogen storage in the PRKAG2 cardiac syndrome. It has recently been shown that reduction of cardiac glycogen stores in a PRKAG2 mouse model with a tetracycline-reversible promoter resulted in reversal of the cardiomyopathy, cardiac and electrophysiological dysfunction (Wolf et al., 2008).

We have constructed transgenic mice overexpressing the human wild-type PRKAG2 gene and the Arg302Gln PRKAG2 mutation (Gollob et al., 2002; Gollob and Roberts, 2002; Gollob et al., 2001b; Ha et al., 2009). Transcription of the transgene is under the

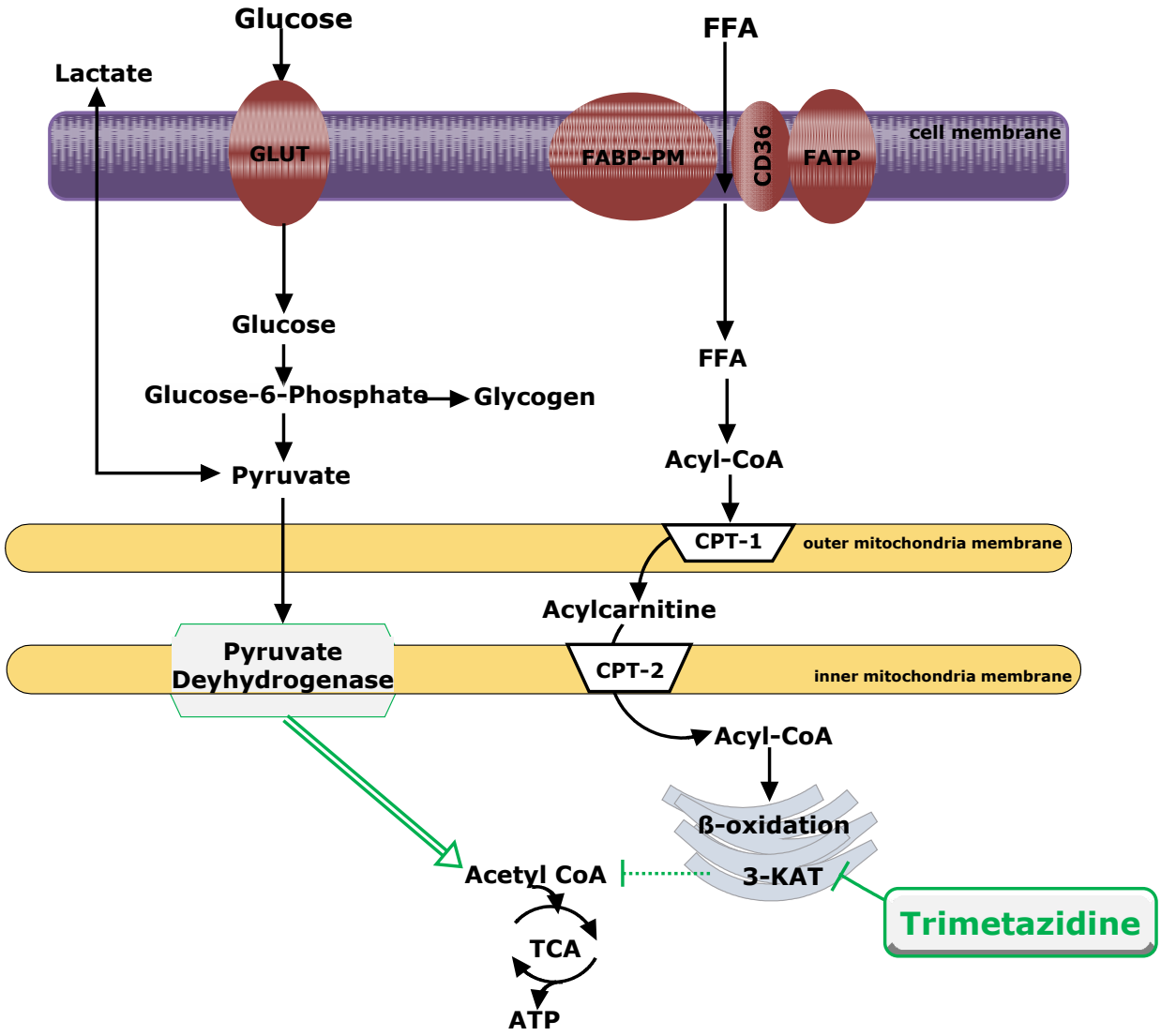

Figure 5.1: Trimetazidine inhibition of 3-KAT inhibits Acetyl-CoA contribution by FA oxidation therebye stimulating glucose oxidation via pyruvate dehydrogenase.

control of the cardiac-specific alpha-myosin heavy chain promoter, thereby restricting expression of the gene to the mouse myocardium. These mice recapitulate the phenotypic features of the human PRKAG2 cardiomyopathy including glycogen accumulation and frequent cardiac arrhythmias (Sidhu et al., 2005).

The present study aims to investigate whether chronic pharmacologic intervention with trimetazidine in the Arg302Gln PRKAG2 mouse model would attenuate cardiac glycogen stores and therein normalize cardiac function and electrical conduction.

MATERIALS AND METHODS

Animals

All animal experiments described herein were conducted according to the guidelines of the University of Ottawa Animal Care Committee and the Canadian Council on Animal Care for the use and care of laboratory animals. All animals were maintained on a 12-hour light/dark cycle with chow and water *ad libitum*. Transgenic mice were generated as previously described(Sidhu et al., 2005) using an α-myosin heavy chain (MHC) promoter, PRKAG2 cDNA, 3'UTR human growth hormone with the FVB mouse strain. Transgenic mutant (TGmut) mice express the mutant PRKAG2 gene (substitute of arginine for glutamine at residue 302), with transgenic wildtype (TGwt) mice expressing the normal human PRKAG2 cDNA. PCR was performed on the genomic DNA isolated from weanling mouse tail snips with the QIAGEN DNeasy kit with the product sequenced.

Study Protocol

Mice at 4-5 weeks of age were provided either plain water (controls TGwt, TGmut) or treated chronically with TMZ water for 8 months at 10 mg/kg/day po ($TGwt^{TMZ}$, $TGmut^{TMZ}$). An 8 month treatment regime was selected to evaluate animals at 9 months of age, at which point the TGmut mice are at full morbidity.

Echocardiography

Cardiac function was assessed with echocardiography (Vevo 770,VisualSonics, Toronto, Canada) using a 707 transducer at baseline (n= 6 TGwt, n= 6 TGmut), mid-treatment (5 months of age) (n= 6 TGwt, n= 9 $TGwt^{TMZ}$, n= 7 TGmut, n=7 $TGmut^{TMZ}$) and endpoint (9 months of age) (n=6 TGwt, n= 7 $TGwt^{TMZ}$, n= 5 TGmut, n=6 $TGmut^{TMZ}$). Mice were anaesthetized and maintained throughout experimental procedures with 1-2% isoflurane. Analysis of results was completed using the VisualSonics cardiac measurements program. The average left ventricle wall thickness (mm) and fractional shortening (%) were assessed using long axis B-mode images with the standard VisualSonics cardiac measurement formulas.

Telemetry

Monitoring of ECGs and arrhythmias were conducted in the conscious state with implantable telemetry units (DSI Dataquest ART 4.1, Minnesota, USA) in mice at treatment endpoint (9 months of age). Briefly, mice (n= 6 TGwt, n= 6 $TGwt^{TMZ}$, n= 8 TGmut, n=6 $TGmut^{TMZ}$) were anaesthetized and maintained with 1-2% isoflurane for surgical implantation of the telemetry units (TA10EA-F20). Buprenorphine (0.05 mg/kg, sc) was administered bid on day of surgery and 2 days post for pain management. Telemetry units were implanted in the abdominal cavity with ECG leads positioned in the thoracic cavity (positive lead positioned

1 cm to the right of the xyphoid process, negative lead positioned on the right pectoral muscle). After 3 days for recovery from surgery, animals were placed on receivers and telemetry units were turned on (magnetic switch). ECG waveforms were recorded continuously for 24 hr over 3 days for each animal. Software analysis was used to quantify heart rate (HR), PR interval, QRS interval, and for qualitative assessment of percentage of arrythmias (Ponemah Physiology Platform, P3 Plus, Software).

Glycogen Content

Mice (n= 7 TGwt, n= 4 $TGwt^{TMZ}$, n= 4 TGmut, n=6 $TGmut^{TMZ}$) were euthanized by decapitation with hearts dissected out, and placed immediately into liquid nitrogen for storage at -80°C. Tissue was ground using a mortar and pestle under liquid nitrogen. Glycogen content was determined using an amyloglucosidase digestion method as previously described.(Crawford et al., 2010; Lo et al., 1970; Zhou et al., 2008) Briefly, 10-50 mg of ground cardiac tissue was homogenized in a 1:9 (wt/vol.) ratio of PBM buffer (20mM KH_2PO_4, 10μM $CaCl_2$, 1mM $MgCl_2$, pH 6.1). Tissue homogenate (50μL) was boiled for 20 min in 30% KOH (wt/vol.) saturated with anhydrous Na_2SO_4. The remainder of tissue homogenate was used to determine protein concentration with a BCA assay. Glycogen was precipitated with 95% ethanol (vol./vol.), centrifuged at 4000 *g* for 15 min at 4°C. The glycogen pellet was dissolved in double distilled H_2O and incubated at 100°C for 20 min with 0.2% Anthrone (wt/vol.) in H_2SO_4. Absorbance was read at 595 nm to determine glycogen concentration of samples relative to an oyster glycogen standard curve (Sigma Aldrich Canada) and normalized to protein content (μg glycogen/μg of protein).

Statistical Analysis

All data are expressed as mean +/- standard deviation. Data were compared using a student's t-test or ANOVA with Bonferroni's correction; $p<0.05$ was considered significant.

RESULTS

TMZ systemic parameters

Mice were treated with either water (controls) or TMZ at 10 mg/kg/day for 8 months. We found no difference in body weight gain and no effect on mortality between control and treated mice.

TMZ treatment reduces cardiac glycogen levels

Cardiac glycogen levels were reduced 55% in $TGmut^{TMZ}$ vs TGmut mice (0.21 ± 0.13 vs 0.46 ± 0.07, $p=0.008$) (Figure 5.2). There was no difference in glycogen levels between $TGmut^{TMZ}$ hearts compared to either TGwt or treated controls ($TGmut^{TMZ}$ 0.21 ± 0.13 vs TGwt 0.08 ± 0.03 vs $TGwt^{TMZ}$ 0.21 ± 0.07, One way ANOVA, $p>0.05$).

TMZ Treatment Improves Systolic Function

Cardiac dimensions and function were assessed at baseline, 20 and 36 weeks with echocardiography *in vivo*. Left ventricle wall thickness was increased by 30% in TGmut mice vs TGwt at 1 month of age (0.8 ± 0.2 vs 1.1 ± 0.2, $p<0.05$) (Figure 5.3B). However, there was no difference between any of the groups at 20 or 36 weeks. There was no difference in systolic function at baseline (4 weeks) between TGmut and TGwt mice (53.6 ± 8.2 vs 55.8 ± 12.1, $p=0.72$) (Figure 5.3C). With progression of time, the TGmut mice show reduced systolic function compared to TGwt mice at both 20 (19.8 ± 5.2 vs 31.5 ± 15.3) and

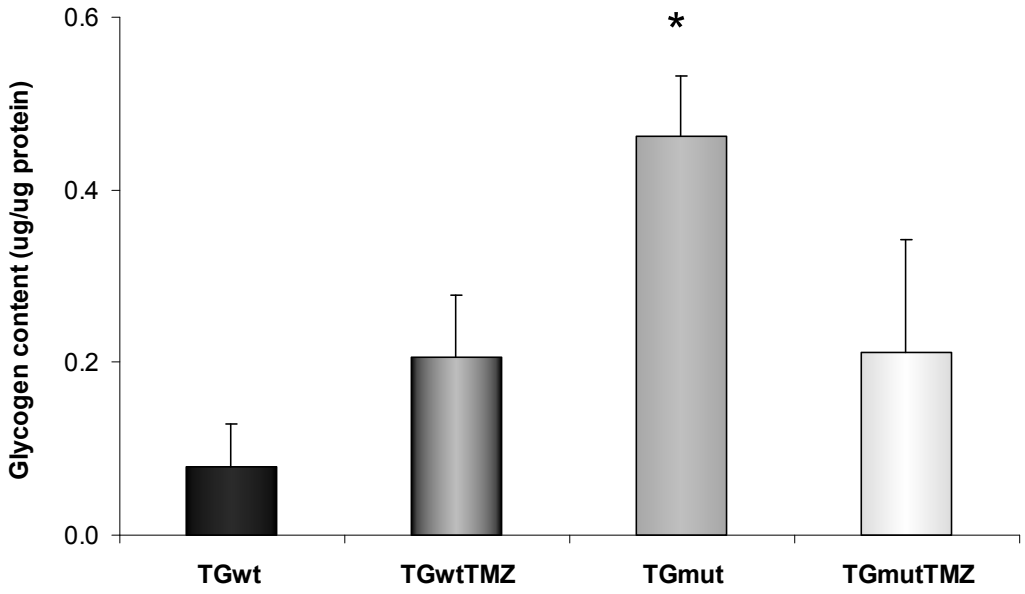

Figure 5.2: Cardiac glycogen levels determined with the amyloglucosidase digestion method. TGwt n=7, TGwt^{TMZ} n= 4, TGmut n=6, TGmut^{TMZ} n=4* $p<0.05$ by ANOVA, Bonferroni correction

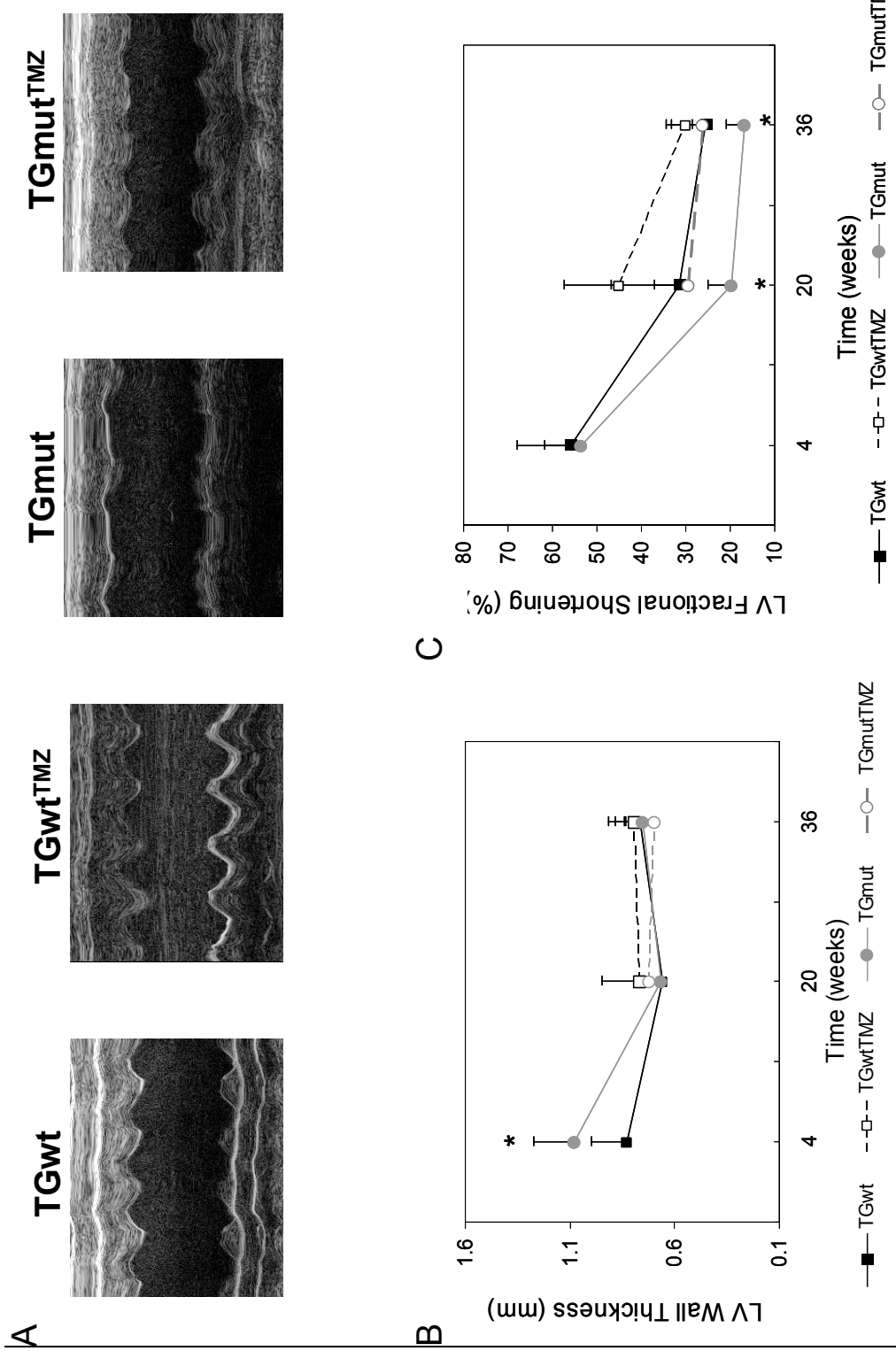

Figure 5.3: Representative M-mode images of the left ventricle for each group (A); Echocardiography assessment of left ventricle wall thickness (B) and fractional shortening (C) at baseline (n= 6 TGwt, n= 6 TGmut), mid-treatment (5 months of age) (n= 6 TGwt, n= 9 $TGwt^{TMZ}$, n= 7 TGmut, n=7 $TGmut^{TMZ}$) and endpoint (9 months of age) (n=6 TGwt, n= 7 $TGwt^{TMZ}$, n= 5 TGmut, n=6 $TGmut^{TMZ}$). * $p<0.05$ by

36 weeks (19.2 ± 5.8 vs 25.6 ± 7.8) (Figure 5.3C). While TGmut^{TMZ} have improved systolic function compared to TGmut mice at both 20 (19.8 ± 5.2 vs 29.5 ± 7.5, t-test p=0.02) and 36 weeks (19.2 ± 5.8 vs 26.2 ± 2.4, t-test p=0.04) with no significant difference to TGwt and TGwt^{TMZ} (One way ANOVA, $p<0.05$). Although a trend towards an increase, there was no significant improvement in LV function in TMZ treated TGwt mice to TGwt controls at either timepoint.

TMZ normalizes electrophysiological dysfunction

In situ ECG waveform recordings demonstrated significantly reduced HR in the TGmut mice (Table 1) compared to all other groups (One way ANOVA, $p<0.05$). TGmut mice were identified as manifesting ventricular preexcitation as noted by the short PR interval (16 ± 5 vs 33 ± 2 ms in TGwt; $p<0.05$) and wide QRS (22 ± 3 vs 14 ± 2 ms in TGwt; $p<0.05$) (Figure 5.4). Treatment with TMZ did not significantly alter any of these parameters in the TGwt mice. However, treatment with TMZ reduced the QRS interval in affected mice (TGmut^{TMZ} 17 ± 2 ms)

Although the PR interval in TGmut^{TMZ} mice was not normalized with treatment (19 ± 8 ms), qualitative assessment demonstrates that treatment normalized sinus rhythm with no presentation of delta waves (Figure 5.5).

DISCUSSION

TMZ is a common angina treatment throughout Europe, although still under clinical trials in the US. TMZ has recently come to the forefront in metabolic therapy, specifically

Table 5.1: Effects of TMZ treatment on cardiac conduction

	TGwt	TGwt^{TMZ}	TGmut	TGmut^{TMZ}
HR (bpm)	560 ± 75	512 ± 98	432 ± 49 *	487 ± 59
QRS (ms)	14 ± 2	15 ± 1	22 ± 3 *	17 ± 2
PR (ms)	33 ± 2	31 ± 2	16 ± 5 *	19 ± 8 *

* $p<0.05$ by ANOVA, Bonferroni correction

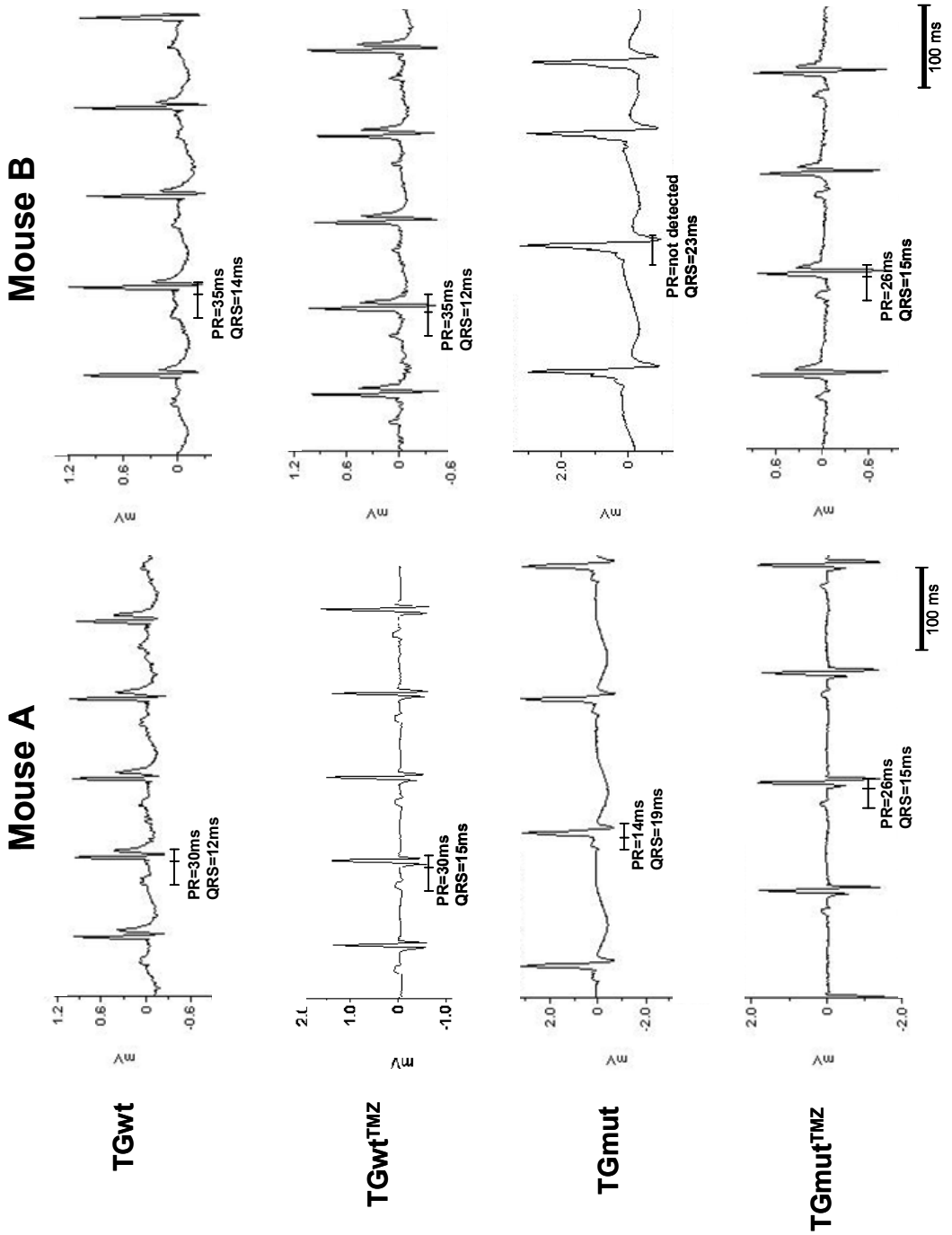

Figure 5.4: Representative ECG captures. Note the attenuation of ventricular preexcitaton with TMZ treatment in TGmut^{TMZ}

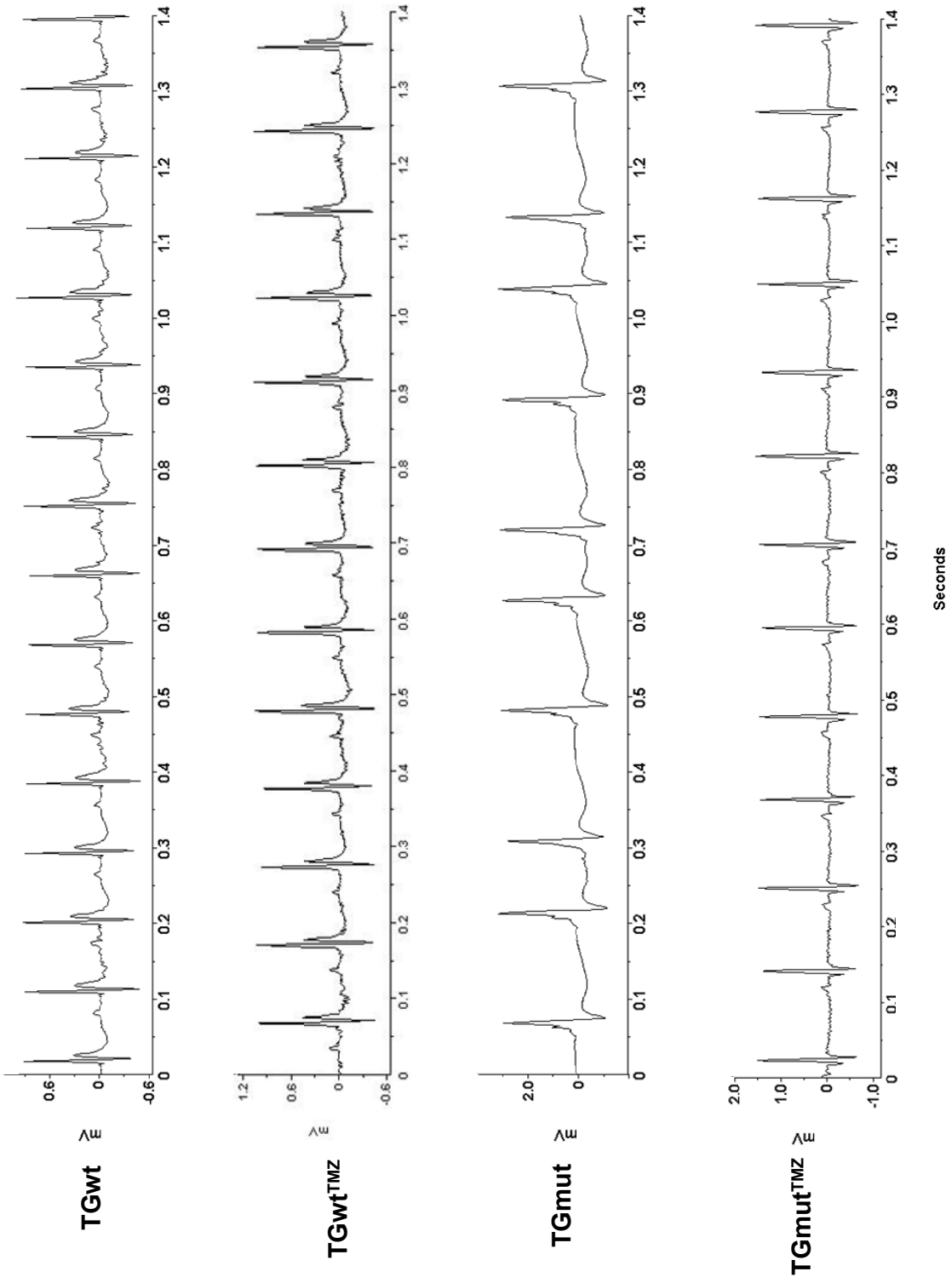

Figure 5.5: Representative images of sinus rhythm. Note the normal sinus rhythm without evidence of preexcitation or delta waves following TMZ treatment in the TGmut^{TMZ} animal

investigated as to whether it improves morbidity and mortality in chronic heart failure patients.(Cera et al., 2010; Fragasso et al., 2012; Gunes et al., 2009b; Zhang et al., 2012; Zhao et al.) In clinical trials, TMZ recovers systolic function in both heart failure patients(Gunes et al., 2009a; Zhang et al., 2012) and patients with diabetic cardiomyopathy.(Zhao et al., 2012) Additionally, TMZ treatment improves/prevents the onset of atrial fibrillation in heart failure patients.(Gunes et al., 2009b) In all, the data points to increased event free survival in TMZ treated cardiac patients through an improvement in both mechanical and potentially electrical function.(Fragasso et al., 2012; Gunes et al., 2009b; Zhang et al., 2012)

The biochemistry behind the apparent "rescuing" from heart failure by TMZ is particularly intriguing for PRKAG2 patients. In the PRKAG2 cardiac syndrome, the arrythmogenic nature of the disease is due to a dysregulation in AMPK function. The mutation in the AMPK gamma 2 subunit appears to cause a gain of function in the early stages of the disease(Folmes et al., 2009) leading to abhorrent glycogen stores and the phenotypic arrythmogenic dysfunction. The upregulation of AMPK activity would increase both FFA and glucose uptake pathways. Thus the production of acetyl-CoA from fatty acid oxidation will inhibit the glucose oxidation pathway, causing an uncoupling from glycolysis.(Lopaschuk et al., 1988; Lopaschuk et al., 1993; Neely and Morgan, 1974; Saddik and Lopaschuk, 1994) This uncoupling would promote lactate production with a subsequent decrease in cellular pH.(Liu et al., 1996; Lopaschuk, 1997; Lopaschuk et al., 1993) Additionally, excess glucose may be shuttled into glycogen stores, also contributing to a reduction in cellular pH. Recently, Wolf and colleagues(Wolf et al., 2008) presented

compelling data that the unifying mechanism for the PRKAG2 arrythmogenic dysfunction is the presence of excessive glycogen stores. By using a tetracycline-repressible PRKAG2 transgenic mouse model, this data demonstrated that by `shutting off the mutant human AMPK transgene, glycogen stores are reduced and cardiac ECGs are normalized in TGmut mice. Although AMPK in itself has been implicated to have direct regulation of ion channel gating,(Light et al., 2003) the reduction in cellular pH due to both excessive lactate and glycogen production could disrupt ion channel kinetics. Excessive glycogen stores also appear to disrupt the development of the annulus fibosus, contributing to the predominance of atrial fibrillation in the PRKAG2 cardiac syndrome.(Wolf et al., 2008) These data demonstrate that a pharmacological therapy that targets the metabolism of glycogen stores may be effective in alleviating the phenotypic manifestations of the PRKAG2 cardiac syndrome.

As TMZ directly inhibits fatty acid oxidation subsequently increasing glucose oxidation,(Lopaschuk et al., 2003) we hypothesized that TMZ treatment would reduce cardiac glycogen stores and consequently improve cardiac function and electrical conductance. Indeed, we demonstrated that chronic TMZ treatment reduces cardiac glycogen stores by 55% in TGmut mice. Although we saw no improvement in cardiac hypertrophy, the reduction in cardiac glycogen stores was accompanied by a normalization in cardiac systolic function. Perhaps most compelling, in vivo telemetry data demonstrated an attenuation of ventricular prexcitation, with TGmut^{TMZ} mice exhibiting normal sinus cardiac rhythm. While further studies need to be conducted to determine the exact impact of TMZ on the biochemical milieu involved in glycogen synthesis, degradation, as well AMPK

activity, our data agrees with current clinical trials which exhibit a positive effect of TMZ on cardiac function and arrthymogenesis. Our data further suggests that reduction in glycogen deposition improves the phenotypic outcomes of the PRKAG2 cardiac syndrome.

In summary, we have evaluated the efficacy of TMZ, a fatty acid oxidation inhibitor, on the attenuation of the PRKAG2 cardiac syndrome. The present data indicates that chronic TMZ treatment reduces cardiac glycogen stores in the PRKAG2 mutant mice. This reduction in glycogen stores parallels an improvement in cardiac systolic function with attenuation of ventricular preexcitation. This data suggests that pharmacological modulation of cardiac metabolism may be beneficial in the attenuation of the PRKAG2 cardiac syndrome.

ACKNOWLEDGEMENTS

The authors thank the Animal Care and Veterinary services of the University of Ottawa for their assistance with animal health.

GRANTS

This study was supported in part by the Heart and Stroke Foundation of Ontario Program Grant (grant # PRG6242), and by the Canadian Institutes of Health Research (M.Gollob). S. L. Thorn was supported by a Heart and Stroke Foundation PhD Scholarship.

DISCLOSURES

Dr Jean DaSilva is a consultant with Lantheus Medical Imaging.

CHAPTER 6: GENERAL DISCUSSION

6.0 General Discussion of Project

Despite FDG being one of the most widely used clinical tracers in PET imaging, translation of techniques for assessment of myocardial glucose uptake in small animals has proven difficult. Transgenic mice provide a model in which to assess the development and pathology of the disease in a living organism where tissues can be readily harvested for molecular assessment. However, the small size of the mouse heart on the spatial resolution of even the most advanced microPET cameras has limited the development of a reliable technique for quantitative assessment of MGU.

Quantitative assessment of MGU requires the use of kinetic modeling such as Patlak (Patlak et al., 1983). Patlak kinetic modeling calculates the rate constants of FDG entering the cell via GLUT transporters (K1 and k2 rate constants) and phosphorylated by hexokinase to the trapped product [^{18}F]FDG-6-phosphate (k3 rate constant). As with all kinetic modeling, an accurate blood input function is required to determine the concentration of tracer delivered to the tissue region of interest. As previously stated, the small size of the mouse heart on the spatial resolution of the camera does not permit the sampling of an IDIF within the LV cavity, as typically seen in clinical and large animal research studies (Abraham et al., 2010; Anselm et al., 2011; Birnie et al., 2012; Ha et al., 2009; McFalls et al., 2002; Mielniczuk et al., 2011; Shukla et al., 2012). In this thesis, we have described methodology to determine an accurate blood input function in mice using the vena cava. Wherein the variation was statistically high with the LV cavity IDIF (coefficient of variability = 51%), the use of the vena cava IDIF yielded a reliable blood input function (coefficient of variability = ~23%) in test-retest studies. Furthermore, using this novel procedure we demonstrated that a reduction

in FDG uptake could be assessed in a mouse type 1 diabetic model, as well as an increase in FDG following acute insulin stimulation.

This approach to mouse myocardial quantitative FDG analysis was then applied to investigating the glucose metabolism perturbations within the PRKAG2 mouse model. PRKAG2 mice were investigated at 1 month of age whereby mice demonstrated increased myocardial wall thickness, heart mass and increased glycogen deposition. We were able to determine a significant decrease in FDG cardiac glucose uptake in TGmut mice, suggesting downregulation/dysfunction of glucose transport at this early stage of development. We proposed that the downregulation/dysfunction of exogenous glucose transport was due to a feedback pathway elicited from excessive intracellular glycogen stores significantly augmented by increased AMPK activity and overall GS activity.

To challenge glucose uptake, we inititated acute insulin studies in the PRKAG2 mice. Insulin should stimulate the translocation of GLUT4 to the plasma membrane increasing glucose uptake independent of AMPK activity (see Figure 1.2). However, despite increased FDG uptake in skeletal muscle following insulin stimulation, there was no effect of insulin on cardiac FDG uptake in TGmut mice. These results provide a basis for investigating metabolic therapy in the transgenic mouse model for treatment of affected PRKAG2 patients.

In continuation of this theory, we targeted the attenuation of the PRKAG2 disease characteristics with TMZ. Targeting FA oxidation in cardiac disease is attractive, theoretically preventing the uncoupling of glycolysis and lactate formation from glucose oxidation. We selected TMZ, as it is currently undergoing clinical trials for treatment of

heart failure patients and while showing promise, has demonstrated no side effects in the patient population. We hypothesized that TMZ would increase glucose oxidation by inhibition of FA oxidation, shifting cardiac energy metabolism to an increased reliance on glucose metabolism. TMZ-treated TGmut mice displayed improved systolic function, normalized cardiac rhythm with no evidence of ventricular preexcitation and a reduction in total glycogen stores. This data suggest that pharmacological modulation of cardiac metabolism to reduce glycogen stores may be beneficial in the attenuation of the PRKAG2 cardiac syndrome.

6.1 Development of a Reliable Mouse Cardiac FDG Imaging Procedure

This project developed a novel method for acquiring an accurate and repeatable Patlak Ki for mouse FDG imaging with the vena cava as the blood IDIF. The small size of the mouse LV cavity is on the order of the spatial resolution of the PET scanner, in combination of high myocardial activity spillover produces an inaccurate assessment of the blood IDIF and reliable quantitative value. Although an SUV can be used to compare activity concentration in a tissue of interest at one particular time-point, kinetic modeling is required to assess glucose uptake rates, which may be altered under stimulatory conditions and cannot be detected with SUV analysis.

In mice, with their high cardiac output rate, the distribution of tracer from venous to arterial blood appears to occur within the initial input function of the scan, unlike in humans where the venous and arterial concentrations of FDG are not considered to be equal until 30-60 min post-injection of tracer (Cook et al., 1999). The initial peak input function of the vena cava is

higher than observed in the LV cavity. This is due to the injection of the radiotracer via the tail vein, however this does not adversely impact the accuracy of the Patlak analysis as integral activity is used for the analysis. Therefore, the shape of the curve outside the Patlak analysis time range (10-40 min) is of little consequence. The location of the vena cava is easily visualized and is not surrounded by any high-activity areas, reducing activity spillover from adjacent background regions. The adjacent background for this ROI is the liver which typically has homogenous FDG activity uptake.

We were able to derive a RC for the vena cava using measured values of the reconstructed image resolution to estimate the true vena cava activity, and confirmed with manual blood sampling. We found a 17% difference between the measured blood activity compared to the image derived vena cava activity at 60 min when using the liver as a standard between the microPET camera and gamma counter. This was substantially lower compared to the blood input function derived from the LV cavity, which was approximately 575% higher than the gamma counter measured blood activity. We hypothesized that this difference in accuracy was due to myocardial activity spillover into the LV cavity, substantially compounding the IDIF activity measurements.

Patlak K_i test-retest population variability was 23% with the vena cava blood input function, reduced from 51% when using the LV cavity blood input function. The Patlak Ki coefficient of repeatability with the vena cava blood input function was 32% with no significant bias between scan 1 and scan 2. We additionally evaluated Ki for the 2-compartment model and found an increase in both the test-retest population variability and the coefficient of repeatability, which could be explained by larger number of free parameters in the model.

There was no correlation with blood glucose levels ($R^2=4\times10^{-6}$) or plasma insulin levels ($R^2=0.03$) compared to Patlak Ki values. Although, we did find a significant reduction in plasma FFA levels from scan 1 and scan 2, there was again no correlation with Patlak Ki values ($R^2=0.007$).

We validated this methodology in a STZ induced T1DM mouse model. T1DM is known to exhibit a reduction in insulin-stimulated glucose uptake due to an overall reduction in endogenous insulin. While the T1DM model will produce large perturbations in rMGU values, we chose this model as it is a well-established model of hyperglycemia and alterations in myocardial glucose uptake. With our novel quantitative approach, induction of T1DM significantly reduced rMGU by 60% compared to baseline values. Following insulin stimulation, there was a 40% increase in rMGU, returning the values close to baseline pre-diabetic levels. These changes were supported by SUV values calculated at 20 and 40 min, capturing two time frames within the Patlak Ki time interval of 10-40 min.

6.2 Assessment of myocardial glucose metabolism in the PRKAG2 mouse model

Despite recognition over a decade ago of the gene causative for the condition, there is currently no therapy for patients with the PRKAG2 cardiac syndrome. This disease has a debilitating morbidity with patients developing cardiac arrhythmias in their adolescence and requiring pacemaker implantation by their early 40`s or 50`s (Gollob, 2008). A portion of this population will develop dilated cardiomyopathy due to the destruction of cardiac tissue by excessive glycogen stores, leading to the requirement of a heart transplant. The elucidation in affected patients of the biochemical processes that underlie the disease

development are limited due to the invasiveness of in vitro techniques. FDG PET imaging provides a method to reliably and quantitatively assess myocardial glucose uptake in the patients. AMPK activity has been proposed to be upregulated in the PRKAG2 model, thereby increasing translocation of GLUT4 to the plasma membrane increasing glucose uptake. As enhanced AMPK activity will increase FA oxidation, the underlying mechanism of the PRKAG2 disease may be the uncoupling of glucose oxidation from glycolysis in the presence of increased glucose uptake, promoting excessive glycogen stores. The pathological glycogen stores potentiate the development of cardiac hypertrophy leading to dilated cardiomyopathy and most likely the electrophysiological manifestations of the disease. Characterization of glucose metabolism in the transgenic mouse model and correlating with FDG PET provides a non-invasive translational tool for applications in clinical monitoring of disease progression and therapy development, as discussed in this thesis.

Clinical investigation of adult PRKAG2 patients measured a 45% reduction in myocardial glucose uptake in affected patients versus control subjects (Ha et al., 2009). In mouse models, a common method to assess cardiac metabolism is isolated perfused hearts. A previous study has demonstrated an increase in myocardial glucose uptake of 2-deoxyglucose in TGmut mice at 19 and 49 days of age using an isolated perfused heart. In our study, we demonstrate a reduction in myocardial glucose uptake in TGmut mice at 28 days of age, similar to the FDG PET results from our patient population. A potential difference between our in vivo and the previously published in situ results could be the lack

of hormones, FFA fluctuations and other competing substrates that are not present in the isolated perfused heart model (Depre et al., 1999).

Interestingly, we found that the one month PRKAG2 mice demonstrated no systolic dysfunction. We believed that this was beneficial, as it eliminated any possible alterations in glucose transporters due to myocardial dysfunction or age related decreases in AMPK activity in itself (Huang et al., 2009; Nagendran et al., 2012; Turdi et al., 2010). We demonstrated elevated expression level of activated AMPK correlated with elevated levels of phosphorylated ACC. These findings indicate that the development and progression of this genetic cardiomyopathy is first the result of enhanced AMPK activity in agreement with previously published studies (Banerjee et al., 2007; Folmes et al., 2009). The work of Banerjee et al (Banerjee et al., 2007) suggested a biphasic relationship of AMPK with age and disease progression, where young mice (<2 weeks) demonstrated elevated AMPK activity but no difference in AMPK activity compared to wild-type animals by 5 months of age. In mice 8-40 weeks of age, expressing the Arg302Gln mutation, a decrease in AMPK activity was determined (Sidhu et al., 2005). Our current work agrees with this, as the 5-8 month old mice demonstrated reduced AMPK activity (see Manuscript #3).

Activated AMPK is known to enhance translocation of GLUT4 to the cell membrane to facilitate glucose uptake (Coven et al., 2003). Thus, our observation of an increase in AMPK activity at 4 weeks of age might be predicted to increase the cardiac uptake rate of glucose. However, excess glycogen stores are known to inhibit glucose-6-phosphate and would therefore downregulate glucose uptake (Richter and Galbo, 1986). Further investigation into this pathway is required to determine if the enhanced AMPK activity increases in vivo

glucose uptake at an earlier age in the PRKAG2 mouse model, and whether glucose-6-phosphate regulation reduces glucose uptake at 1 month of age.

In the presence of increased AMPK activity but decreased glucose uptake, we then investigated the protein expression of key enzymes known to be involved in glycogen synthesis. Our data demonstrate increased GS activity, which may provide inhibitory feedback on exogenous glucose uptake (Wojtaszewski et al., 2002; Wojtaszewski et al., 2003) (see Figure 1.3).

6.3 Myocardial Insulin Resistance in the PRKAG2 Mouse Model

The interplay of insulin signaling and AMPK appears to be through the Akt and AS160 proteins. The activation of Akt by insulin has been demonstrated to inhibit AMPK via the phosphorylation of the AMPK α-subunits on Ser485 or Ser491 (α-1 and α-2 respectively) (Horman et al., 2006) subsequently blocking phosphorylation of Thr^{172} by upstream kinases. Conversely, AMPK has been shown to phosphorylate and thereby inhibit AS160 independently of insulin, which in turn prevents Rab GAP function and thus increases translocation of GLUT4 (Treebak et al., 2006) (see Figure 1.2). As GLUT transporter efficiency is the rate limiting step for glucose uptake, and the insulin dependent transporter GLUT4 is the most abundant GLUT in the mouse myocardium, we sought to determine if FDG uptake could be increased in the PRKAG2 mutant mouse hearts following insulin stimulation. We found that unlike TGwt mice where there was a 71-76% increase in Patlak Ki and SUV values, TGmut mice displayed no increase in FDG uptake following insulin

stimulation. We additionally determined that the protein expression of the cardiac insulin receptor β is not altered between TGwt and TGmut mice.

The lack of responsiveness to cardiac insulin stimulation in the PRKAG2 mutant mice, where AMPK activity is dysfunctional, is intriguing where a link between insulin stimulation and AMPK is currently under investigation with regards to type 2 diabetes (Horman et al., 2012). The limiting factor in our model may be the excess glycogen levels. In a normal myocardium, insulin promotes glucose uptake, glycogen synthesis and storage (Towler and Hardie, 2007). Previous groups have shown that when saturated with glucose, skeletal muscle will display insulin resistance matched with a reduction in AMPK activity (Kraegen et al., 2006; Ruderman and Prentki, 2004; Saha et al., 2010). In the current study, an approximate 4-fold increase in cardiac glycogen stores was observed in TGmut mice. The increased glycogen stores may be causing an inhibitory feedback pathway, reducing AMPK activity and thus reducing glucose uptake. The lack of insulin stimulation appears to agree with the theory that inhibition of AMPK activity ameliorates insulin stimulation even in the presence of glucose deprivation (Chopra et al., 2012).

The findings of this study provide insight into the PRKAG2 cardiac syndrome, but also emphasize the potential role of AMPK in insulin resistance observed in other pathologically cardiac states.

As the transgene is cardiac specific, skeletal muscle SUV values increased similarly 31-38% following insulin in both genotypes. This increase correlates with previously published data in control mice with insulin pretreatment (Kreissl et al., 2011).

6.4 Blocking FFA oxidation to Attenuate the PRKAG2 Disease Characteristics

TMZ is a prescribed treatment for angina throughout Europe, although still under clinical trials in the US. TMZ has recently come to the forefront in metabolic therapy, specifically investigated as to whether it improves morbidity and mortality in chronic heart failure patients (Cera et al., 2010; Fragasso et al., 2012; Gunes et al., 2009b; Zhang et al., 2012; Zhao et al., 2012). We selected TMZ, as it has demonstrated no side effects in the patient population. In clinical trials, TMZ recovers systolic function in both heart failure patients (Gunes et al., 2009a; Zhang et al., 2012) and patients with diabetic cardiomyopathy (Zhao et al., 2012). Additionally, TMZ treatment improves/prevents the onset of atrial fibrillation in heart failure patients (Gunes et al., 2009b). In all, the data point to increased event free survival in TMZ treated cardiac patients through an improvement in both mechanical and potentially electrical function (Fragasso et al., 2012; Gunes et al., 2009b; Zhang et al., 2012). Based on the above research, we used a moderate TMZ dose of 10 mg/kg/day. Due to the chronic period of treatment proposed (8 months-attenuation; 6 months-reversal), TMZ therapy was administered via water bottles as chronic treatment for this time frame via injections or gavage would not be sanctioned by CCAC guidelines (dose is estimated per average body weight of animals every two weeks and based on drinking 5 mL of water per day, with water consumption monitored to ensure accurate drug dosage). In animal studies, the drug dosage varies from 1-30 mg/kg/day (Li et al., 2010; Liu et al., 2010; Mody et al., 1998; Szkilnik et al., 2005; Unal et al., 2005). In humans, the dose regime has been either 20 mg 3 x daily (Cera et al., 2010; Fragasso et al., 2006a; Fragasso et al., 2006b; Fragasso et al., 2006c) or 35 mg 2 x daily with the modified-release formula (Barre et al., 2003; Genissel et

al., 2004; Sellier and Broustet, 2003; Tuunanen et al., 2008). The variation in human dose regime is due to the pharmacokinetics of TMZ in order to maintain a therapeutic plasma concentration (Onay-Besikci and Ozkan, 2008). The higher dose cited for animal research is due to both: i) the route of entry, with the drug not provided in a slow release capsule, but rather through a single injection or via drinking water; ii) higher animal metabolic rates. These distinctions require, as cited in the literature above, a higher dose/kg than currently used in human studies to maintain a therapeutic plasma concentration.

The direct inhibition of FA oxidation by TMZ and subsequent augmentation of glucose oxidation (Lopaschuk et al., 2003), appears to reduce cardiac glycogen stores and consequently improve cardiac function and electrical conductance. In this study we demonstrated that chronic TMZ treatment reduces cardiac glycogen stores by 55% in TGmut mice with an improvement in cardiac systolic function. Perhaps most compelling, TMZ attenuates the development of ventricular preexcitation, with TGmut^{TMZ} mice exhibiting normal sinus cardiac rhythm.

The present data indicates that chronic TMZ treatment reduces cardiac glycogen stores in the PRKAG2 mutant mice. This reduction in glycogen stores parallels an improvement in cardiac systolic function with attenuation of ventricular preexcitation, suggesting that pharmacological modulation of cardiac metabolism may be beneficial in the attenuation of the PRKAG2 cardiac syndrome.

6.5 Conclusions

Small animal FDG imaging studies using the vena cava IDIF methodology, demonstrate reliable and accurate quantification of myocardial glucose uptake in normal controls. Furthermore, we have validated this methodology in a type 1 diabetic model demonstrating reduced FDG uptake that is enhanced following acute insulin treatment. We employed this novel approach to characterize quantitative glucose uptake in the PRKAG2 mouse model. Despite imaging at 1 month of age, cardiac glucose uptake appears to be reduced in the PRKAG2 mice. We have hypothesized that this decrease in glucose uptake is due to pathological glycogen stores developed from augmented GS activity. We further hypothesize that the augmented GS activity results from dysregulation in AMPK activity due to the γ2-subunit mutation. This reduction in MGU appears to be consistent with the results of the human PRKAG2 population. A possible mechanism by which glycogen levels inhibit glucose-6-phosphate, and thereby reduce glucose uptake, will need to be further investigated. Despite an AMPK-independent pathway by which insulin could stimulate exogenous glucose uptake, PRKAG2 display myocardial insulin resistance. The insulin resistance is correlated with a reduction in systolic function and AMPK activity. The link between insulin resistance and cardiac diseases such as heart failure and diabetes led to the assessment of metabolic modulation by TMZ treatment. TMZ treatment normalized cardiac glycogen stores in the PRKAG2 mouse model, preventing cardiac dysfunction and attenuating ventricular preexcitation.

As a result of the research presented in this thesis, quantitative cardiac FDG imaging can be assessed in multiple mouse models. We have further demonstrated that the PRKAG2 mice

have a myocardial insulin resistance and that pharmacological targeting of metabolic pathways can be used to attenuate the disease. Additionally, we have demonstrated alterations in cardiac glucose uptake in the transgenic mouse model that mirror the human PET imaging data. This outcome allows for transition of therapy assessment in the PRKAG2 mouse model to the human clinical patients with FDG PET imaging.

6.6 Future direction

Prior to these experiments, quantitative and reliable FDG imaging in mice was not available without invasive serial blood withdrawals (Convert et al., 2007; Fang and Muzic, 2008; Ferl et al., 2007; Kreissl et al., 2011) or with the use of ECG gated dynamic iterative reconstruction (Locke et al., 2011) with reconstruction times exceeding thirty hours per mouse. The use of the vena cava input function allows for FDG studies in any mouse model with high reliability previously not possible. In order to detect a significant difference of 20% between groups, with a 23% test-retest reliability, we would require a minimum of six subjects per group.

FTHA, the FA uptake and metabolism tracer, is now regularly synthesized and produced at the University of Ottawa Heart Institute. The evaluation of the FA metabolism pathway in the PRKAG2 cardiac syndrome is novel, and may provide further information on how the dysregulation of AMPK activity promotes pathological glycogen storage. We would hypothesize that FTHA uptake would be increased in PRKAG2 1 month old mice, correlating with increased AMPK activity. We would further expect that TMZ treatment would reduce FA oxidation. PET imaging may be used in the future to clarify the impact of

TMZ or other metabolic therapies on both cardiac glucose uptake (FDG) and FFA metabolism (FTHA). However, as FTHA images both FA uptake and oxidation, a tracer such as [^{11}C]palmitate may be more beneficial. [^{11}C]palmitate has bi-exponential kinetics such that the uptake and storage into triglycerides (slower washout component) and the component of [^{11}C]palmitate incorporated into oxidative metabolism (faster washout) can be quantified separately (Schelbert et al., 1986). Additionally, [^{11}C]acetate can be utilized to assess alterations in oxidative metabolism. However, it should be noted that due to the tight regulation of the Randle cycle, other groups have noted that a decrease FA oxidation is tightly regulated to an increase in glucose oxidation, with no alterations in total acetyl-CoA concentration, and therefore, no difference in [^{11}C]acetate (Mody et al., 1998).

A secondary direction will be to further evaluate myocardial glucose uptake in PRKAG2 mice younger than 1 month of age. The FVB strain develops early, and it may be possible, with careful manipulation of anaesthetic and tracer injections to image mice as early as 2 weeks of age. This would allow the in vivo assessment of glucose uptake when it may be accelerated. Assessment of myocardial neonatal cellular metabolism may also provide an insight into the initial progression of the PRKAG2 metabolic cardiomyopathy.

6.7 Future Work in PRKAG2 Patient Population

As PET imaging is non-invasive, it can be a translational tool between the transgenic mouse model and the affected PRKAG2 patients. PET imaging would allow for the identification of metabolic dysfunction in the patients and the ability to correlate these changes to the same changes in the transgenic mouse model where biochemical assessment of tissue can be

completed. PET can therefore predict changes in cardiac disease state, monitor and guide therapeutic advancements first evaluated in mice and then translated to humans.

As stated previously, inhibition of FA oxidation for cardiac metabolic modulation has come to the forefront for HF treatment (Cera et al., 2010; Fragasso et al., 2012; Gunes et al., 2009b; Zhang et al., 2012; Zhao et al., 2012). The results of our study in the PRKAG2 transgenic mouse indicate that TMZ treatment may attenuate the disease progression. The future directions for our patient population would be the application of a clinical trial for TMZ treatment. All HF patient trials have provided TMZ for 6 months to see the effect in reducing mortality and event-free survival (Cera et al., 2010; Fragasso et al., 2012; Gunes et al., 2009b; Zhang et al., 2012; Zhao et al., 2012). The proposed project would investigate the mechanisms by which altered AMPK activity manipulates cardiac metabolism and leads to the development of the PRKAG2 glycogen storage disease. Young PRKAG2 patients (20-30 yrs of age) would be randomized to 1) treatment with TMZ with current medical therapy or 2) current medical therapy only. Patients in both groups would be monitored by echocardiography, ECG analysis and FDG/FTHA PET imaging at baseline and following one year of treatment to increase the potential to measure an effective change. We would hypothesize an increase in FTHA uptake with a decrease in FDG uptake at baseline. This would be reversed following TMZ treatment, with patients demonstrating an improvement in glucose uptake (FDG) with a reduction in FTHA uptake. We would further hypothesize that TMZ treatment would improve LV function and reduce the presence of arrythmia or conduction system disease. This novel research would establish a new non-invasive molecular imaging procedure for quantifying changes in cardiac metabolism due alterations

in the AMPK signaling axis with or without TMZ treatment. Such an approach would be innovative and provide a unique opportunity to advance the understanding of the pathophysiology of the PRKAG2 cardiac syndrome.

CHAPTER 7: REFERENCES

Abel, E.D. 2004. Glucose transport in the heart. *Front Biosci*. 9:201-15.

Abraham, A., G. Nichol, K.A. Williams, A. Guo, R.A. deKemp, L. Garrard, R.A. Davies, L. Duchesne, H. Haddad, B. Chow, J. DaSilva, and R.S. Beanlands. 2010. 18F-FDG PET imaging of myocardial viability in an experienced center with access to 18F-FDG and integration with clinical management teams: the Ottawa-FIVE substudy of the PARR 2 trial. *J Nucl Med*. 51:567-74.

Adams, J., Z.P. Chen, B.J. Van Denderen, C.J. Morton, M.W. Parker, L.A. Witters, D. Stapleton, and B.E. Kemp. 2004. Intrasteric control of AMPK via the gamma1 subunit AMP allosteric regulatory site. *Protein Sci*. 13:155-65.

Aerni-Flessner, L., M. Abi-Jaoude, A. Koenig, M. Payne, and P.W. Hruz. 2012. GLUT4, GLUT1, and GLUT8 are the dominant GLUT transcripts expressed in the murine left ventricle. *Cardiovasc Diabetol*. 11:63.

An, D., and B. Rodrigues. 2006. Role of changes in cardiac metabolism in development of diabetic cardiomyopathy. *Am J Physiol Heart Circ Physiol*. 291:H1489-506.

Aneja, A., W.H. Tang, S. Bansilal, M.J. Garcia, and M.E. Farkouh. 2008. Diabetic cardiomyopathy: insights into pathogenesis, diagnostic challenges, and therapeutic options. *Am J Med*. 121:748-57.

Anselm, D.D., A.H. Anselm, J. Renaud, H.L. Atkins, R. de Kemp, I.G. Burwash, K.A. Williams, A. Guo, C. Kelly, J. Dasilva, R.S. Beanlands, and C.A. Glover. 2011. Altered myocardial glucose utilization and the reverse mismatch pattern on rubidium-82 perfusion/F-18-FDG PET during the sub-acute phase following reperfusion of acute anterior myocardial infarction. *J Nucl Cardiol*. 18:657-67.

Antos, C.L., T.A. McKinsey, N. Frey, W. Kutschke, J. McAnally, J.M. Shelton, J.A. Richardson, J.A. Hill, and E.N. Olson. 2002. Activated glycogen synthase-3 beta suppresses cardiac hypertrophy in vivo. *Proc Natl Acad Sci U S A*. 99:907-12.

Arad, M., D.W. Benson, A.R. Perez-Atayde, W.J. McKenna, E.A. Sparks, R.J. Kanter, K. McGarry, J.G. Seidman, and C.E. Seidman. 2002. Constitutively active AMP kinase mutations cause glycogen storage disease mimicking hypertrophic cardiomyopathy. *J Clin Invest*. 109:357-62.

Arad, M., I.P. Moskowitz, V.V. Patel, F. Ahmad, A.R. Perez-Atayde, D.B. Sawyer, M. Walter, G.H. Li, P.G. Burgon, C.T. Maguire, D. Stapleton, J.P. Schmitt, X.X. Guo, A. Pizard, S. Kupershmidt, D.M. Roden, C.I. Berul, C.E. Seidman, and J.G. Seidman. 2003. Transgenic mice overexpressing mutant PRKAG2 define the cause of Wolff-Parkinson-White syndrome in glycogen storage cardiomyopathy. *Circulation*. 107:2850-6.

Arad, M., C.E. Seidman, and J.G. Seidman. 2007. AMP-activated protein kinase in the heart: role during health and disease. *Circ Res*. 100:474-88.

Atkinson, D.E. 1970. Adenine nucleotides as universal stoichiometric metabolic coupling agents. *Adv Enzyme Regul*. 9:207-19.

Bak, M.I., and J.S. Ingwall. 1998. Regulation of cardiac AMP-specific 5'-nucleotidase during ischemia mediates ATP resynthesis on reflow. *Am J Physiol*. 274:C992-1001.

Banerjee, S.K., K.R. McGaffin, X.N. Huang, and F. Ahmad. 2010a. Activation of cardiac hypertrophic signaling pathways in a transgenic mouse with the human PRKAG2 Thr400Asn mutation. *Biochim Biophys Acta*. 1802:284-91.

Banerjee, S.K., R. Ramani, S. Saba, J. Rager, R. Tian, M.A. Mathier, and F. Ahmad. 2007. A PRKAG2 mutation causes biphasic changes in myocardial AMPK activity and does not protect against ischemia. *Biochem Biophys Res Commun*. 360:381-7.

Banerjee, S.K., D.W. Wang, R. Alzamora, X.N. Huang, N.M. Pastor-Soler, K.R. Hallows, K.R. McGaffin, and F. Ahmad. 2010b. SGLT1, a novel cardiac glucose transporter, mediates increased glucose uptake in PRKAG2 cardiomyopathy. *J Mol Cell Cardiol*. 49:683-92.

Baron, S.J., J. Li, R.R. Russell, 3rd, D. Neumann, E.J. Miller, R. Tuerk, T. Wallimann, R.L. Hurley, L.A. Witters, and L.H. Young. 2005. Dual mechanisms regulating AMPK kinase action in the ischemic heart. *Circ Res*. 96:337-45.

Barre, J., P. Ledudal, B. Oosterhuis, J.P. Brakenhoff, G. Wilkens, F.A. Sollie, and D. Tran. 2003. Pharmacokinetic profile of a modified release formulation of trimetazidine (TMZ MR 35 mg) in the elderly and patients with renal failure. *Biopharm Drug Dispos*. 24:159-64.

Beanlands, R., S. Thorn, J. Dasilva, T.D. Ruddy, and J. Maddahi. 2008. Myocardial Viability. *In* Principles and Practices of PET and PET/CT. J. Wahl, editor. Lippincott Williams and Wilkins, Philidelphia. 565-588.

Beauloye, C., A.S. Marsin, L. Bertrand, J.L. Vanoverschelde, M.H. Rider, and L. Hue. 2002. The stimulation of heart glycolysis by increased workload does not require AMP-activated protein kinase but a wortmannin-sensitive mechanism. *FEBS Lett*. 531:324-8.

Bertrand, L., A. Ginion, C. Beauloye, A.D. Hebert, B. Guigas, L. Hue, and J.L. Vanoverschelde. 2006. AMPK activation restores the stimulation of glucose uptake in an in vitro model of insulin-resistant cardiomyocytes via the activation of protein kinase B. *Am J Physiol Heart Circ Physiol*. 291:H239-50.

Bertrand, L., S. Horman, C. Beauloye, and J.L. Vanoverschelde. 2008. Insulin signalling in the heart. *Cardiovasc Res*. 79:238-48.

Beyer, A., A. Kitzerow, B. Crute, B.E. Kemp, L.A. Witters, and L.M. Heilmeyer, Jr. 2000. Muscle phosphorylase kinase is not a substrate of AMP-activated protein kinase. *Biol Chem*. 381:457-61.

Birnie, D., R.A. de Kemp, A.S. Tang, T.D. Ruddy, M.H. Gollob, A. Guo, K. Williams, K. Thomson, J.N. DaSilva, and R.S. Beanlands. 2012. Reduced septal glucose metabolism predicts response to cardiac resynchronization therapy. *J Nucl Cardiol*. 19:73-83.

Blomstrand, E., and B. Saltin. 1999. Effect of muscle glycogen on glucose, lactate and amino acid metabolism during exercise and recovery in human subjects. *J Physiol*. 514 (Pt 1):293-302.

Bolli, R. 1992. Myocardial 'stunning' in man. *Circulation*. 86:1671-91.

Braunwald, E., and R.A. Kloner. 1982. The stunned myocardium: prolonged, postischemic ventricular dysfunction. *Circulation*. 66:1146-9.

Browner, M.F., K. Nakano, A.G. Bang, and R.J. Fletterick. 1989. Human muscle glycogen synthase cDNA sequence: a negatively charged protein with an asymmetric charge distribution. *Proc Natl Acad Sci U S A*. 86:1443-7.

Bulkley, B.H., and G.M. Hutchins. 1978. Pompe's disease presenting as hypertrophic myocardiopathy with Wolff-Parkinson-White syndrome. *Am Heart J*. 96:246-52.

Cao, C., Y. Chen, W. Wang, Y. Liu, and G. Liu. Ghrelin inhibits insulin resistance induced by glucotoxicity and lipotoxicity in cardiomyocyte. *Peptides*. 32:209-15.

Carling, D. 2004. The AMP-activated protein kinase cascade--a unifying system for energy control. *Trends Biochem Sci*. 29:18-24.

Carling, D. 2005. AMP-activated protein kinase: balancing the scales. *Biochimie*. 87:87-91.

Carling, D., and D.G. Hardie. 1989. The substrate and sequence specificity of the AMP-activated protein kinase. Phosphorylation of glycogen synthase and phosphorylase kinase. *Biochim Biophys Acta*. 1012:81-6.

Cera, M., A. Salerno, G. Fragasso, C. Montanaro, C. Gardini, G. Marinosci, F. Arioli, R. Spoladore, A. Facchini, C. Godino, and A. Margonato. 2010. Beneficial electrophysiological effects of trimetazidine in patients with postischemic chronic heart failure. *J Cardiovasc Pharmacol Ther*. 15:24-30.

Chen, Z., J. Heierhorst, R.J. Mann, K.I. Mitchelhill, B.J. Michell, L.A. Witters, G.S. Lynch, B.E. Kemp, and D. Stapleton. 1999. Expression of the AMP-activated protein kinase beta1 and beta2 subunits in skeletal muscle. *FEBS Lett*. 460:343-8.

Cheng, H., J. Woodgett, M. Maamari, and T. Force. 2011. Targeting GSK-3 family members in the heart: a very sharp double-edged sword. *J Mol Cell Cardiol*. 51:607-13.

Cheng, J.C., K. Shoghi, and R. Laforest. 2012. Quantitative accuracy of MAP reconstruction for dynamic PET imaging in small animals. *Med Phys*. 39:1029-41.

Cheung, P.C., I.P. Salt, S.P. Davies, D.G. Hardie, and D. Carling. 2000. Characterization of AMP-activated protein kinase gamma-subunit isoforms and their role in AMP binding. *Biochem J*. 346 Pt 3:659-69.

Chopra, I., H.F. Li, H. Wang, and K.A. Webster. 2012. Phosphorylation of the insulin receptor by AMP-activated protein kinase (AMPK) promotes ligand-independent activation of the insulin signalling pathway in rodent muscle. *Diabetologia*. 55:783-94.

Clark, H., D. Carling, and D. Saggerson. 2004. Covalent activation of heart AMP-activated protein kinase in response to physiological concentrations of long-chain fatty acids. *Eur J Biochem*. 271:2215-24.

Coakley, J.H., A.J. Wagenmakers, and R.H. Edwards. 1992. Relationship between ammonia, heart rate, and exertion in McArdle's disease. *Am J Physiol*. 262:E167-72.

Coggan, A.R., W.M. Kohrt, R.J. Spina, D.M. Bier, and J.O. Holloszy. 1990. Endurance training decreases plasma glucose turnover and oxidation during moderate-intensity exercise in men. *J Appl Physiol*. 68:990-6.

Coggan, A.R., R.J. Spina, W.M. Kohrt, and J.O. Holloszy. 1993. Effect of prolonged exercise on muscle citrate concentration before and after endurance training in men. *Am J Physiol*. 264:E215-20.

Cohen, P. 2006. The twentieth century struggle to decipher insulin signalling. *Nat Rev Mol Cell Biol*. 7:867-73.

Convert, L., G. Morin-Brassard, J. Cadorette, M. Archambault, M. Bentourkia, and R. Lecomte. 2007. A new tool for molecular imaging: the microvolumetric beta blood counter. *J Nucl Med*. 48:1197-206.

Cook, G.J., M.A. Lodge, P.K. Marsden, A. Dynes, and I. Fogelman. 1999. Non-invasive assessment of skeletal kinetics using fluorine-18 fluoride positron emission tomography: evaluation of image and population-derived arterial input functions. *Eur J Nucl Med*. 26:1424-9.

Corton, J.M., J.G. Gillespie, and D.G. Hardie. 1994. Role of the AMP-activated protein kinase in the cellular stress response. *Curr Biol*. 4:315-24.

Costford, S.R., N. Kavaslar, N. Ahituv, S.N. Chaudhry, W.S. Schackwitz, R. Dent, L.A. Pennacchio, R. McPherson, and M.E. Harper. 2007. Gain-of-function R225W mutation in human AMPKgamma(3) causing increased glycogen and decreased triglyceride in skeletal muscle. *PLoS One*. 2:e903.

Coven, D.L., X. Hu, L. Cong, R. Bergeron, G.I. Shulman, D.G. Hardie, and L.H. Young. 2003. Physiological role of AMP-activated protein kinase in the heart: graded activation during exercise. *Am J Physiol Endocrinol Metab*. 285:E629-36.

Crawford, S.A., S.R. Costford, C. Aguer, S.C. Thomas, R.A. deKemp, J.N. DaSilva, D. Lafontaine, M. Kendall, R. Dent, R.S. Beanlands, R. McPherson, and M.E. Harper. 2010. Naturally occurring R225W mutation of the gene encoding AMP-activated protein kinase (AMPK)gamma(3) results in increased oxidative capacity and glucose uptake in human primary myotubes. *Diabetologia*. 53:1986-97.

Crute, B.E., K. Seefeld, J. Gamble, B.E. Kemp, and L.A. Witters. 1998. Functional domains of the alpha1 catalytic subunit of the AMP-activated protein kinase. *J Biol Chem*. 273:35347-54.

Daniel, T., and D. Carling. 2002. Functional analysis of mutations in the gamma 2 subunit of AMP-activated protein kinase associated with cardiac hypertrophy and Wolff-Parkinson-White syndrome. *J Biol Chem*. 277:51017-24.

Danon, M.J., S.J. Oh, S. DiMauro, J.R. Manaligod, A. Eastwood, S. Naidu, and L.H. Schliselfeld. 1981. Lysosomal glycogen storage disease with normal acid maltase. *Neurology*. 31:51-7.

Davies, J.K., D.J. Wells, K. Liu, H.R. Whitrow, T.D. Daniel, R. Grignani, C.A. Lygate, J.E. Schneider, G. Noel, H. Watkins, and D. Carling. 2006. Characterization of the role of gamma2 R531G mutation in AMP-activated protein kinase in cardiac

hypertrophy and Wolff-Parkinson-White syndrome. *Am J Physiol Heart Circ Physiol*. 290:H1942-51.

Davies, S.P., N.R. Helps, P.T. Cohen, and D.G. Hardie. 1995. 5'-AMP inhibits dephosphorylation, as well as promoting phosphorylation, of the AMP-activated protein kinase. Studies using bacterially expressed human protein phosphatase-2C alpha and native bovine protein phosphatase-2AC. *FEBS Lett*. 377:421-5.

Dennis, S.C., W. Gevers, and L.H. Opie. 1991. Protons in ischemia: where do they come from; where do they go to? *J Mol Cell Cardiol*. 23:1077-86.

Depre, C., M.H. Rider, and L. Hue. 1998. Mechanisms of control of heart glycolysis. *Eur J Biochem*. 258:277-90.

Depre, C., J.L. Vanoverschelde, and H. Taegtmeyer. 1999. Glucose for the heart. *Circulation*. 99:578-88.

Di Napoli, P., P. Di Giovanni, M.A. Gaeta, G. D'Apolito, and A. Barsotti. 2007. Beneficial effects of trimetazidine treatment on exercise tolerance and B-type natriuretic peptide and troponin T plasma levels in patients with stable ischemic cardiomyopathy. *Am Heart J*. 154:602 e1-5.

Doege, H., A. Schurmann, G. Bahrenberg, A. Brauers, and H.G. Joost. 2000. GLUT8, a novel member of the sugar transport facilitator family with glucose transport activity. *J Biol Chem*. 275:16275-80.

Dolinsky, V.W., and J.R. Dyck. 2006a. The Role of AMP-activated Protein Kinase (AMPK) in the Healthy and the Diseased Heart. *Am J Physiol Heart Circ Physiol*.

Dolinsky, V.W., and J.R. Dyck. 2006b. Role of AMP-activated protein kinase in healthy and diseased hearts. *Am J Physiol Heart Circ Physiol*. 291:H2557-69.

Du, X.J. 2004. Gender modulates cardiac phenotype development in genetically modified mice. *Cardiovasc Res*. 63:510-9.

Dyck, J.R., G. Gao, J. Widmer, D. Stapleton, C.S. Fernandez, B.E. Kemp, and L.A. Witters. 1996. Regulation of 5'-AMP-activated protein kinase activity by the noncatalytic beta and gamma subunits. *J Biol Chem*. 271:17798-803.

Dyck, J.R., and G.D. Lopaschuk. 2006. AMPK alterations in cardiac physiology and pathology: enemy or ally? *J Physiol*. 574:95-112.

Embi, N., D.B. Rylatt, and P. Cohen. 1980. Glycogen synthase kinase-3 from rabbit skeletal muscle. Separation from cyclic-AMP-dependent protein kinase and phosphorylase kinase. *Eur J Biochem*. 107:519-27.

Fang, Y.H., and R.F. Muzic, Jr. 2008. Spillover and partial-volume correction for image-derived input functions for small-animal 18F-FDG PET studies. *J Nucl Med*. 49:606-14.

Felig, P., and J. Wahren. 1975. Fuel homeostasis in exercise. *N Engl J Med*. 293:1078-84.

Ferl, G.Z., X. Zhang, H.M. Wu, M.C. Kreissl, and S.C. Huang. 2007. Estimation of the 18F-FDG input function in mice by use of dynamic small-animal PET and minimal blood sample data. *J Nucl Med*. 48:2037-45.

Fessler, J.A., and L. Rogers. 1996. Spatial resolution properties of penalized-likelihood image reconstruction: space invariant tomgraphs *IEEE Trans. Imag. Processing*. 9:1346-1358.

Flores, J.E., L.M. McFarland, A. Vanderbilt, A.K. Ogasawara, and S.P. Williams. 2008. The effects of anesthetic agent and carrier gas on blood glucose and tissue uptake in mice undergoing dynamic FDG-PET imaging: sevoflurane and isoflurane compared in air and in oxygen. *Mol Imaging Biol*. 10:192-200.

Folmes, C.D., A.S. Clanachan, and G.D. Lopaschuk. 2006. Fatty acids attenuate insulin regulation of 5'-AMP-activated protein kinase and insulin cardioprotection after ischemia. *Circ Res*. 99:61-8.

Folmes, K.D., A.Y. Chan, D.P. Koonen, T.C. Pulinilkunnil, I. Baczko, B.E. Hunter, S. Thorn, M.F. Allard, R. Roberts, M.H. Gollob, P.E. Light, and J.R. Dyck. 2009. Distinct early signaling events resulting from the expression of the PRKAG2 R302Q mutant of AMPK contribute to increased myocardial glycogen. *Circ Cardiovasc Genet*. 2:457-66.

Fragasso, G., C. Montano, G. Perseghin, A. Palloshi, G. Calori, G. Lattuada, S. Oggionni, G. Bassanelli, M. Locatelli, G. Lopaschuk, and A. Margonato. 2006a. The anti-ischemic effect of trimetazidine in patients with postprandial myocardial ischemia is unrelated to meal composition. *Am Heart J*. 151:1238 e1-8.

Fragasso, G., A. Palloshi, P. Puccetti, C. Silipigni, A. Rossodivita, M. Pala, G. Calori, O. Alfieri, and A. Margonato. 2006b. A randomized clinical trial of trimetazidine, a partial free fatty acid oxidation inhibitor, in patients with heart failure. *J Am Coll Cardiol*. 48:992-8.

Fragasso, G., G. Perseghin, F. De Cobelli, A. Esposito, A. Palloshi, G. Lattuada, P. Scifo, G. Calori, A. Del Maschio, and A. Margonato. 2006c. Effects of metabolic modulation by trimetazidine on left ventricular function and phosphocreatine/adenosine triphosphate ratio in patients with heart failure. *Eur Heart J*. 27:942-8.

Fragasso, G., G. Rosano, S.H. Baek, H. Sisakian, P. Di Napoli, L. Alberti, G. Calori, S.M. Kang, L. Sahakyan, A. Sanosyan, C. Vitale, G. Marazzi, A. Margonato, and R. Belardinelli. 2012. Effect of partial fatty acid oxidation inhibition with trimetazidine on mortality and morbidity in heart failure: Results from an international multicentre retrospective cohort study. *Int J Cardiol*.

Francesconi, M., and E. Auff. 1982. Cardiac arrhythmias and the adult form of type II glycogenosis. *N Engl J Med*. 306:937-8.

Fujii, N., T. Hayashi, M.F. Hirshman, J.T. Smith, S.A. Habinowski, L. Kaijser, J. Mu, O. Ljungqvist, M.J. Birnbaum, L.A. Witters, A. Thorell, and L.J. Goodyear. 2000. Exercise induces isoform-specific increase in 5'AMP-activated protein kinase activity in human skeletal muscle. *Biochem Biophys Res Commun*. 273:1150-5.

Ganguly, P.K., R.E. Beamish, K.S. Dhalla, I.R. Innes, and N.S. Dhalla. 1987. Norepinephrine storage, distribution, and release in diabetic cardiomyopathy. *Am J Physiol*. 252:E734-9.

Ganguly, P.K., K.S. Dhalla, I.R. Innes, R.E. Beamish, and N.S. Dhalla. 1986. Altered norepinephrine turnover and metabolism in diabetic cardiomyopathy. *Circ Res*. 59:684-93.

Genissel, P., Y. Chodjania, J.L. Demolis, I. Ragueneau, and P. Jaillon. 2004. Assessment of the sustained release properties of a new oral formulation of trimetazidine in pigs and dogs and confirmation in healthy human volunteers. *Eur J Drug Metab Pharmacokinet*. 29:61-8.

Gibbs, C.L. 1978. Cardiac energetics. *Physiol Rev*. 58:174-254.

Ginion, A., J. Auquier, C.R. Benton, C. Mouton, J.L. Vanoverschelde, L. Hue, S. Horman, C. Beauloye, and L. Bertrand. 2011. Inhibition of the mTOR/p70S6K pathway is not involved in the insulin-sensitizing effect of AMPK on cardiac glucose uptake. *Am J Physiol Heart Circ Physiol*. 301:H469-77.

Gollob, M.H. 2003. Glycogen storage disease as a unifying mechanism of disease in the PRKAG2 cardiac syndrome. *Biochem Soc Trans*. 31:228-31.

Gollob, M.H. 2008. Modulating phenotypic expression of the PRKAG2 cardiac syndrome. *Circulation*. 117:134-5.

Gollob, M.H., M. Green, and J.P. Veinot. 2006. Altered AMP-activated protein kinase activity and pathologic cardiac disease. *Heart and Metabolism*. 32:28-31.

Gollob, M.H., M.S. Green, A.S. Tang, T. Gollob, A. Karibe, A.S. Ali Hassan, F. Ahmad, R. Lozado, G. Shah, L. Fananapazir, L.L. Bachinski, and R. Roberts. 2001a. Identification of a gene responsible for familial Wolff-Parkinson-White syndrome. *N Engl J Med*. 344:1823-31.

Gollob, M.H., M.S. Green, A.S. Tang, and R. Roberts. 2002. PRKAG2 cardiac syndrome: familial ventricular preexcitation, conduction system disease, and cardiac hypertrophy. *Curr Opin Cardiol*. 17:229-34.

Gollob, M.H., and R. Roberts. 2002. AMP-activated protein kinase and familial Wolff-Parkinson-White syndrome: new perspectives on heart development and arrhythmogenesis. *Eur Heart J*. 23:679-81.

Gollob, M.H., J.J. Seger, T.N. Gollob, T. Tapscott, O. Gonzales, L. Bachinski, and R. Roberts. 2001b. Novel PRKAG2 mutation responsible for the genetic syndrome of ventricular preexcitation and conduction system disease with childhood onset and absence of cardiac hypertrophy. *Circulation*. 104:3030-3.

Goodwin, G.W., C.S. Taylor, and H. Taegtmeyer. 1998. Regulation of energy metabolism of the heart during acute increase in heart work. *J Biol Chem*. 273:29530-9.

Grover-McKay, M., S.A. Walsh, and S.A. Thompson. 1999. Glucose transporter 3 (GLUT3) protein is present in human myocardium. *Biochim Biophys Acta*. 1416:145-54.

Gunes, Y., U. Guntekin, M. Tuncer, and M. Sahin. 2009a. Improved left and right ventricular functions with trimetazidine in patients with heart failure: a tissue Doppler study. *Heart Vessels*. 24:277-82.

Gunes, Y., M. Tuncer, U. Guntekin, S. Akdag, and H.A. Gumrukcuoglu. 2009b. The effects of trimetazidine on p-wave duration and dispersion in heart failure patients. *Pacing Clin Electrophysiol*. 32:239-44.

Ha, A.C., J.M. Renaud, R.A. Dekemp, S. Thorn, J. Dasilva, L. Garrard, K. Yoshinaga, A. Abraham, M.S. Green, R.S. Beanlands, and M.H. Gollob. 2009. In vivo assessment of myocardial glucose uptake by positron emission tomography in adults with the PRKAG2 cardiac syndrome. *Circ Cardiovasc Imaging*. 2:485-91.

Habets, D.D., W.A. Coumans, P.J. Voshol, M.A. den Boer, M. Febbraio, A. Bonen, J.F. Glatz, and J.J. Luiken. 2007. AMPK-mediated increase in myocardial long-chain fatty acid uptake critically depends on sarcolemmal CD36. *Biochem Biophys Res Commun*. 355:204-10.

Hallows, K.R., J.E. McCane, B.E. Kemp, L.A. Witters, and J.K. Foskett. 2003. Regulation of channel gating by AMP-activated protein kinase modulates cystic fibrosis transmembrane conductance regulator activity in lung submucosal cells. *J Biol Chem*. 278:998-1004.

Haq, S., G. Choukroun, Z.B. Kang, H. Ranu, T. Matsui, A. Rosenzweig, J.D. Molkentin, A. Alessandrini, J. Woodgett, R. Hajjar, A. Michael, and T. Force. 2000. Glycogen synthase kinase-3beta is a negative regulator of cardiomyocyte hypertrophy. *J Cell Biol*. 151:117-30.

Hardie, D.G. 1989. Regulation of fatty acid synthesis via phosphorylation of acetyl-CoA carboxylase. *Prog Lipid Res*. 28:117-46.

Hardie, D.G. 2003. Minireview: the AMP-activated protein kinase cascade: the key sensor of cellular energy status. *Endocrinology*. 144:5179-83.

Hardie, D.G. 2008. Role of AMP-activated protein kinase in the metabolic syndrome and in heart disease. *FEBS Lett*. 582:81-9.

Hardie, D.G., and K. Sakamoto. 2006. AMPK: a key sensor of fuel and energy status in skeletal muscle. *Physiology (Bethesda)*. 21:48-60.

Hargreaves, M. 2000. Skeletal muscle metabolism during exercise in humans. *Clin Exp Pharmacol Physiol*. 27:225-8.

Hargreaves, M., G. McConell, and J. Proietto. 1995. Influence of muscle glycogen on glycogenolysis and glucose uptake during exercise in humans. *J Appl Physiol*. 78:288-92.

Hawley, S.A., M. Davison, A. Woods, S.P. Davies, R.K. Beri, D. Carling, and D.G. Hardie. 1996. Characterization of the AMP-activated protein kinase kinase from rat liver and identification of threonine 172 as the major site at which it phosphorylates AMP-activated protein kinase. *J Biol Chem*. 271:27879-87.

Hawley, S.A., M.A. Selbert, E.G. Goldstein, A.M. Edelman, D. Carling, and D.G. Hardie. 1995. 5'-AMP activates the AMP-activated protein kinase cascade, and Ca2+/calmodulin activates the calmodulin-dependent protein kinase I cascade, via three independent mechanisms. *J Biol Chem*. 270:27186-91.

Henning, S.L., R.B. Wambolt, B.O. Schonekess, G.D. Lopaschuk, and M.F. Allard. 1996. Contribution of glycogen to aerobic myocardial glucose utilization. *Circulation*. 93:1549-55.

Herrero, P., C.S. Dence, T.L. Sharp, M.J. Welch, and R.J. Gropler. 2004. Impact of reversible trapping of tracer and the presence of blood metabolites on

measurements of myocardial glucose utilization performed by PET and 18F-fluorodeoxyglucose using the Patlak method. *Nucl Med Biol*. 31:883-92.

Herrero, P., L.R. Peterson, J.B. McGill, S. Matthew, D. Lesniak, C. Dence, and R.J. Gropler. 2006. Increased myocardial fatty acid metabolism in patients with type 1 diabetes mellitus. *J Am Coll Cardiol*. 47:598-604.

Herrero, P., T.L. Sharp, C. Dence, B.M. Haraden, and R.J. Gropler. 2002a. Comparison of 1-(11)C-glucose and (18)F-FDG for quantifying myocardial glucose use with PET. *J Nucl Med*. 43:1530-41.

Herrero, P., C.J. Weinheimer, C. Dence, W.F. Oellerich, and R.J. Gropler. 2002b. Quantification of myocardial glucose utilization by PET and 1-carbon-11-glucose. *J Nucl Cardiol*. 9:5-14.

Horman, S., C. Beauloye, J.L. Vanoverschelde, and L. Bertrand. 2012. AMP-activated protein kinase in the control of cardiac metabolism and remodeling. *Curr Heart Fail Rep*. 9:164-73.

Horman, S., D. Vertommen, R. Heath, D. Neumann, V. Mouton, A. Woods, U. Schlattner, T. Wallimann, D. Carling, L. Hue, and M.H. Rider. 2006. Insulin antagonizes ischemia-induced Thr172 phosphorylation of AMP-activated protein kinase alpha-subunits in heart via hierarchical phosphorylation of Ser485/491. *J Biol Chem*. 281:5335-40.

Horowitz, J.D., Y.Y. Chirkov, J.A. Kennedy, and A.L. Sverdlov. 2010. Modulation of myocardial metabolism: an emerging therapeutic principle. *Curr Opin Cardiol*. 25:329-34.

Huang, J.P., S.S. Huang, J.Y. Deng, and L.M. Hung. 2009. Impairment of insulin-stimulated Akt/GLUT4 signaling is associated with cardiac contractile dysfunction and aggravates I/R injury in STZ-diabetic rats. *J Biomed Sci*. 16:77.

Hudson, E.R., D.A. Pan, J. James, J.M. Lucocq, S.A. Hawley, K.A. Green, O. Baba, T. Terashima, and D.G. Hardie. 2003. A novel domain in AMP-activated protein kinase causes glycogen storage bodies similar to those seen in hereditary cardiac arrhythmias. *Curr Biol*. 13:861-6.

Ingelsson, E., J. Sundstrom, J. Arnlov, B. Zethelius, and L. Lind. 2005. Insulin resistance and risk of congestive heart failure. *JAMA*. 294:334-41.

Ingwall, J.S. 2001. ATP and the Heart. Kluwer, Boston.

Iseli, T.J., M. Walter, B.J. van Denderen, F. Katsis, L.A. Witters, B.E. Kemp, B.J. Michell, and D. Stapleton. 2005. AMP-activated protein kinase beta subunit tethers alpha and gamma subunits via its C-terminal sequence (186-270). *J Biol Chem*. 280:13395-400.

Johnson, L.N. 1992. Glycogen phosphorylase: control by phosphorylation and allosteric effectors. *Faseb J*. 6:2274-82.

Jorgensen, S.B., E.A. Richter, and J.F. Wojtaszewski. 2006. Role of AMPK in skeletal muscle metabolic regulation and adaptation in relation to exercise. *J Physiol*. 574:17-31.

Jorgensen, S.B., B. Viollet, F. Andreelli, C. Frosig, J.B. Birk, P. Schjerling, S. Vaulont, E.A. Richter, and J.F. Wojtaszewski. 2004. Knockout of the alpha2 but not alpha1 5'-AMP-activated protein kinase isoform abolishes 5-aminoimidazole-4-carboxamide-1-beta-4-ribofuranosidebut not contraction-induced glucose uptake in skeletal muscle. *J Biol Chem*. 279:1070-9.

Kahn, B.B., T. Alquier, D. Carling, and D.G. Hardie. 2005. AMP-activated protein kinase: ancient energy gauge provides clues to modern understanding of metabolism. *Cell Metab*. 1:15-25.

Kantor, P.F., A. Lucien, R. Kozak, and G.D. Lopaschuk. 2000. The antianginal drug trimetazidine shifts cardiac energy metabolism from fatty acid oxidation to glucose oxidation by inhibiting mitochondrial long-chain 3-ketoacyl coenzyme A thiolase. *Circ Res*. 86:580-8.

Kemp, B.E., D. Stapleton, D.J. Campbell, Z.P. Chen, S. Murthy, M. Walter, A. Gupta, J.J. Adams, F. Katsis, B. van Denderen, I.G. Jennings, T. Iseli, B.J. Michell, and L.A. Witters. 2003. AMP-activated protein kinase, super metabolic regulator. *Biochem Soc Trans*. 31:162-8.

Kim, K.H., F. Lopez-Casillas, D.H. Bai, X. Luo, and M.E. Pape. 1989. Role of reversible phosphorylation of acetyl-CoA carboxylase in long-chain fatty acid synthesis. *FASEB J*. 3:2250-6.

Kim, M., M. Shen, S. Ngoy, G. Karamanlidis, R. Liao, and R. Tian. 2012. AMPK isoform expression in the normal and failing hearts. *J Mol Cell Cardiol*. 52:1066-73.

Klein, R., J.M. Renaud, M.C. Ziadi, S.L. Thorn, A. Adler, R.S. Beanlands, and R.A. deKemp. 2010. Intra- and inter-operator repeatability of myocardial blood flow and myocardial flow reserve measurements using rubidium-82 pet and a highly automated analysis program. *J Nucl Cardiol*. 17:600-16.

Kloner, R.A., and R.B. Jennings. 2001. Consequences of brief ischemia: stunning, preconditioning, and their clinical implications: part 1. *Circulation*. 104:2981-9.

Kraegen, E.W., A.K. Saha, E. Preston, D. Wilks, A.J. Hoy, G.J. Cooney, and N.B. Ruderman. 2006. Increased malonyl-CoA and diacylglycerol content and reduced AMPK activity accompany insulin resistance induced by glucose infusion in muscle and liver of rats. *Am J Physiol Endocrinol Metab*. 290:E471-9.

Kreissl, M.C., D.B. Stout, K.P. Wong, H.M. Wu, E. Caglayan, W. Ladno, X. Zhang, J.O. Prior, C. Reiners, S.C. Huang, and H.R. Schelbert. 2011. Influence of dietary state and insulin on myocardial, skeletal muscle and brain [F]-fluorodeoxyglucose kinetics in mice. *EJNMMI Res*. 1:8.

Kudo, N., A.J. Barr, R.L. Barr, S. Desai, and G.D. Lopaschuk. 1995. High rates of fatty acid oxidation during reperfusion of ischemic hearts are associated with a decrease in malonyl-CoA levels due to an increase in 5'-AMP-activated protein kinase inhibition of acetyl-CoA carboxylase. *J Biol Chem*. 270:17513-20.

Kudo, N., J.G. Gillespie, L. Kung, L.A. Witters, R. Schulz, A.S. Clanachan, and G.D. Lopaschuk. 1996. Characterization of 5'AMP-activated protein kinase activity in

the heart and its role in inhibiting acetyl-CoA carboxylase during reperfusion following ischemia. *Biochim Biophys Acta*. 1301:67-75.

Lamoureux, M., S.L. Thorn, T. Dumouchel, R. Klein, J. Renaud, M. Lortie, R. Beanlands, J.N. DaSilva, and R. deKemp. 2012. Uniformity and reproducibility of normal resting myocardial blood flow in rats with ^{13}N-ammonia and small animal PET. *Nucl Med Commun*. 33:917-25.

Lang, T., L. Yu, Q. Tu, J. Jiang, Z. Chen, Y. Xin, G. Liu, and S. Zhao. 2000. Molecular cloning, genomic organization, and mapping of PRKAG2, a heart abundant gamma2 subunit of 5'-AMP-activated protein kinase, to human chromosome 7q36. *Genomics*. 70:258-63.

Lee, L., R. Campbell, M. Scheuermann-Freestone, R. Taylor, P. Gunaruwan, L. Williams, H. Ashrafian, J. Horowitz, A.G. Fraser, K. Clarke, and M. Frenneaux. 2005. Metabolic modulation with perhexiline in chronic heart failure: a randomized, controlled trial of short-term use of a novel treatment. *Circulation*. 112:3280-8.

Lemon, P.W. 1987. Protein and exercise: update 1987. *Med Sci Sports Exerc*. 19:S179-90.

Lewis, S.F., and R.G. Haller. 1990. Disorders of muscle glycogenolysis/glycoysis: the consequences of substrate-limited oxidative metabolism in humans. *In* Biochemistry of Exercise. A.W. Taylor, P.D. Gollnick, H.Y. Green, C.D. Ianuzzo, E.G. Noble, G. Metivier, and J.R. Sutton, editors. Human Kinetics, Champaign, IL. 211-226.

Li, J., D.L. Coven, E.J. Miller, X. Hu, M.E. Young, D. Carling, A.J. Sinusas, and L.H. Young. 2006. Activation of AMPK alpha- and gamma-isoform complexes in the intact ischemic rat heart. *Am J Physiol Heart Circ Physiol*. 291:H1927-34.

Li, Y.J., P.H. Wang, C. Chen, M.H. Zou, and D.W. Wang. 2010. Improvement of mechanical heart function by trimetazidine in db/db mice. *Acta Pharmacol Sin*. 31:560-9.

Light, P.E., C.H. Wallace, and J.R. Dyck. 2003. Constitutively active adenosine monophosphate-activated protein kinase regulates voltage-gated sodium channels in ventricular myocytes. *Circulation*. 107:1962-5.

Lionetti, V., W.C. Stanley, and F.A. Recchia. 2010. Modulating fatty acid oxidation in heart failure. *Cardiovasc Res*. 90:202-9.

Liu, B., Z. el Alaoui-Talibi, A.S. Clanachan, R. Schulz, and G.D. Lopaschuk. 1996. Uncoupling of contractile function from mitochondrial TCA cycle activity and MVO2 during reperfusion of ischemic hearts. *Am J Physiol*. 270:H72-80.

Liu, Q., J.C. Docherty, J.C. Rendell, A.S. Clanachan, and G.D. Lopaschuk. 2002. High levels of fatty acids delay the recovery of intracellular pH and cardiac efficiency in post-ischemic hearts by inhibiting glucose oxidation. *J Am Coll Cardiol*. 39:718-25.

Liu, X., Y. Gai, F. Liu, W. Gao, Y. Zhang, M. Xu, and Z. Li. 2010. Trimetazidine inhibits pressure overload-induced cardiac fibrosis through NADPH oxidase-ROS-CTGF pathway. *Cardiovasc Res*.

Lo, S., J.C. Russell, and A.W. Taylor. 1970. Determination of glycogen in small tissue samples. *J Appl Physiol*. 28:234-6.

Locke, L.W., S.S. Berr, and B.K. Kundu. 2011. Image-derived input function from cardiac gated maximum a posteriori reconstructed PET images in mice. *Mol Imaging Biol*. 13:342-7.

Longnus, S.L., C. Segalen, J. Giudicelli, M.P. Sajan, R.V. Farese, and E. Van Obberghen. 2005. Insulin signalling downstream of protein kinase B is potentiated by 5'AMP-activated protein kinase in rat hearts in vivo. *Diabetologia*. 48:2591-601.

Longnus, S.L., R.B. Wambolt, H.L. Parsons, R.W. Brownsey, and M.F. Allard. 2003. 5-Aminoimidazole-4-carboxamide 1-beta -D-ribofuranoside (AICAR) stimulates myocardial glycogenolysis by allosteric mechanisms. *Am J Physiol Regul Integr Comp Physiol*. 284:R936-44.

Lopaschuk, G.D. 1997. Alterations in fatty acid oxidation during reperfusion of the heart after myocardial ischemia. *Am J Cardiol*. 80:11A-16A.

Lopaschuk, G.D., R. Barr, P.D. Thomas, and J.R. Dyck. 2003. Beneficial effects of trimetazidine in ex vivo working ischemic hearts are due to a stimulation of glucose oxidation secondary to inhibition of long-chain 3-ketoacyl coenzyme a thiolase. *Circ Res*. 93:e33-7.

Lopaschuk, G.D., S.R. Wall, P.M. Olley, and N.J. Davies. 1988. Etomoxir, a carnitine palmitoyltransferase I inhibitor, protects hearts from fatty acid-induced ischemic injury independent of changes in long chain acylcarnitine. *Circ Res*. 63:1036-43.

Lopaschuk, G.D., R.B. Wambolt, and R.L. Barr. 1993. An imbalance between glycolysis and glucose oxidation is a possible explanation for the detrimental effects of high levels of fatty acids during aerobic reperfusion of ischemic hearts. *J Pharmacol Exp Ther*. 264:135-44.

Luiken, J.J., S.L. Coort, J. Willems, W.A. Coumans, A. Bonen, G.J. van der Vusse, and J.F. Glatz. 2003. Contraction-induced fatty acid translocase/CD36 translocation in rat cardiac myocytes is mediated through AMP-activated protein kinase signaling. *Diabetes*. 52:1627-34.

Marsin, A.S., L. Bertrand, M.H. Rider, J. Deprez, C. Beauloye, M.F. Vincent, G. Van den Berghe, D. Carling, and L. Hue. 2000. Phosphorylation and activation of heart PFK-2 by AMPK has a role in the stimulation of glycolysis during ischaemia. *Curr Biol*. 10:1247-55.

McFalls, E.O., B. Murad, J.S. Liow, M.C. Gannon, H.C. Haspel, A. Lange, D. Marx, J. Sikora, and H.B. Ward. 2002. Glucose uptake and glycogen levels are increased in pig heart after repetitive ischemia. *Am J Physiol Heart Circ Physiol*. 282:H205-11.

Menard, S.L., X. Ci, F. Frisch, F. Normand-Lauziere, J. Cadorette, R. Ouellet, J.E. Van Lier, F. Benard, M. Bentourkia, R. Lecomte, and A.C. Carpentier. 2009. Mechanism of reduced myocardial glucose utilization during acute hypertriglyceridemia in rats. *Mol Imaging Biol*. 11:6-14.

Menard, S.L., E. Croteau, O. Sarrhini, R. Gelinas, P. Brassard, R. Ouellet, M. Bentourkia, J.E. van Lier, C. Des Rosiers, R. Lecomte, and A.C. Carpentier. 2010. Abnormal in vivo myocardial energy substrate uptake in diet-induced type 2 diabetic cardiomyopathy in rats. *Am J Physiol Endocrinol Metab*. 298:E1049-57.

Merrill, G.F., E.J. Kurth, D.G. Hardie, and W.W. Winder. 1997. AICA riboside increases AMP-activated protein kinase, fatty acid oxidation, and glucose uptake in rat muscle. *Am J Physiol*. 273:E1107-12.

Mielniczuk, L.M., D. Birnie, M.C. Ziadi, R.A. deKemp, J.N. DaSilva, I. Burwash, A.T. Tang, R.A. Davies, H. Haddad, A. Guo, M. Aung, K. Williams, H. Ukkonen, and R.S. Beanlands. 2011. Relation between right ventricular function and increased right ventricular [18F]fluorodeoxyglucose accumulation in patients with heart failure. *Circ Cardiovasc Imaging*. 4:59-66.

Milan, D., J.T. Jeon, C. Looft, V. Amarger, A. Robic, M. Thelander, C. Rogel-Gaillard, S. Paul, N. Iannuccelli, L. Rask, H. Ronne, K. Lundstrom, N. Reinsch, J. Gellin, E. Kalm, P.L. Roy, P. Chardon, and L. Andersson. 2000. A mutation in PRKAG3 associated with excess glycogen content in pig skeletal muscle. *Science*. 288:1248-51.

Minokoshi, Y., Y.B. Kim, O.D. Peroni, L.G. Fryer, C. Muller, D. Carling, and B.B. Kahn. 2002. Leptin stimulates fatty-acid oxidation by activating AMP-activated protein kinase. *Nature*. 415:339-43.

Mody, F.V., B.N. Singh, I.H. Mohiuddin, K.B. Coyle, D.B. Buxton, H.W. Hansen, R. Sumida, and H.R. Schelbert. 1998. Trimetazidine-induced enhancement of myocardial glucose utilization in normal and ischemic myocardial tissue: an evaluation by positron emission tomography. *Am J Cardiol*. 82:42K-49K.

Molkentin, J.D., J.R. Lu, C.L. Antos, B. Markham, J. Richardson, J. Robbins, S.R. Grant, and E.N. Olson. 1998. A calcineurin-dependent transcriptional pathway for cardiac hypertrophy. *Cell*. 93:215-28.

Montessuit, C., and R. Lerch. 2012. Regulation and dysregulation of glucose transport in cardiomyocytes. *Biochim Biophys Acta*.

Musi, N., and L.J. Goodyear. 2003. AMP-activated protein kinase and muscle glucose uptake. *Acta Physiol Scand*. 178:337-45.

Musi, N., M.F. Hirshman, M. Arad, Y. Xing, N. Fujii, J. Pomerleau, F. Ahmad, C.I. Berul, J.G. Seidman, R. Tian, and L.J. Goodyear. 2005. Functional role of AMP-activated protein kinase in the heart during exercise. *FEBS Lett*. 579:2045-50.

Nagendran, J., T.J. Waller, and J.R. Dyck. 2012. AMPK signalling and the control of substrate use in the heart. *Mol Cell Endocrinol*. 366:180-193.

Navaratnam, V. 1987. Heart Muscle: Ultrastructural Studies. Cambridge University Press, New York.

Neely, J.R., and H.E. Morgan. 1974. Relationship between carbohydrate and lipid metabolism and the energy balance of heart muscle. *Annu Rev Physiol*. 36:413-59.

Nielsen, J.N., J.F. Wojtaszewski, R.G. Haller, D.G. Hardie, B.E. Kemp, E.A. Richter, and J. Vissing. 2002. Role of 5'AMP-activated protein kinase in glycogen synthase

activity and glucose utilization: insights from patients with McArdle's disease. *J Physiol*. 541:979-89.

Nishimura, H., F.V. Pallardo, G.A. Seidner, S. Vannucci, I.A. Simpson, and M.J. Birnbaum. 1993. Kinetics of GLUT1 and GLUT4 glucose transporters expressed in Xenopus oocytes. *J Biol Chem*. 268:8514-20.

Nuttall, F.Q., M.C. Gannon, G. Bai, and E.Y. Lee. 1994. Primary structure of human liver glycogen synthase deduced by cDNA cloning. *Arch Biochem Biophys*. 311:443-9.

Oakhill, J.S., R. Steel, Z.P. Chen, J.W. Scott, N. Ling, S. Tam, and B.E. Kemp. 2011. AMPK is a direct adenylate charge-regulated protein kinase. *Science*. 332:1433-5.

Oliveira, S.M., J. Ehtisham, C.S. Redwood, I. Ostman-Smith, E.M. Blair, and H. Watkins. 2003. Mutation analysis of AMP-activated protein kinase subunits in inherited cardiomyopathies: implications for kinase function and disease pathogenesis. *J Mol Cell Cardiol*. 35:1251-5.

Oliver, M.F., and L.H. Opie. 1994. Effects of glucose and fatty acids on myocardial ischaemia and arrhythmias. *Lancet*. 343:155-8.

Onay-Besikci, A., and S.A. Ozkan. 2008. Trimetazidine revisited: a comprehensive review of the pharmacological effects and analytical techniques for the determination of trimetazidine. *Cardiovasc Ther*. 26:147-65.

Opie, L.H. 1990. Myocardial ischemia--metabolic pathways and implications of increased glycolysis. *Cardiovasc Drugs Ther*. 4 Suppl 4:777-90.

Opie, L.H. 1991. The Heart: Physiology and Metabolism. Raven, New York.

Ottensmeyer, F.P., D.R. Beniac, R.Z. Luo, and C.C. Yip. 2000. Mechanism of transmembrane signaling: insulin binding and the insulin receptor. *Biochemistry*. 39:12103-12.

Owen, M.R., E. Doran, and A.P. Halestrap. 2000. Evidence that metformin exerts its anti-diabetic effects through inhibition of complex 1 of the mitochondrial respiratory chain. *Biochem J*. 348 Pt 3:607-14.

Palfreyman, R.W., A.E. Clark, R.M. Denton, G.D. Holman, and I.J. Kozka. 1992. Kinetic resolution of the separate GLUT1 and GLUT4 glucose transport activities in 3T3-L1 cells. *Biochem J*. 284 (Pt 1):275-82.

Patlak, C., and R. Blasberg. 1985. Graphical evaluation of bloo-to-brain transfer constants from multiple-time uptake data. Generalizations. *J Cer Blood Flow Met*. 5:584-90.

Patlak, C.S., R.G. Blasberg, and J.D. Fenstermacher. 1983. Graphical evaluation of blood-to-brain transfer constants from multiple-time uptake data. *J Cereb Blood Flow Metab*. 3:1-7.

Pederson, B.A., H. Chen, J.M. Schroeder, W. Shou, A.A. DePaoli-Roach, and P.J. Roach. 2004. Abnormal cardiac development in the absence of heart glycogen. *Mol Cell Biol*. 24:7179-87.

Polekhina, G., A. Gupta, B.J. Michell, B. van Denderen, S. Murthy, S.C. Feil, I.G. Jennings, D.J. Campbell, L.A. Witters, M.W. Parker, B.E. Kemp, and D. Stapleton. 2003.

AMPK beta subunit targets metabolic stress sensing to glycogen. *Curr Biol*. 13:867-71.

Ponticos, M., Q.L. Lu, J.E. Morgan, D.G. Hardie, T.A. Partridge, and D. Carling. 1998. Dual regulation of the AMP-activated protein kinase provides a novel mechanism for the control of creatine kinase in skeletal muscle. *Embo J*. 17:1688-99.

Pulinilkunnil, T., P. Puthanveetil, M.S. Kim, F. Wang, V. Schmitt, and B. Rodrigues. 2010. Ischemia-reperfusion alters cardiac lipoprotein lipase. *Biochim Biophys Acta*. 1801:171-5.

Rabbani, N., L. Godfrey, M. Xue, F. Shaheen, M. Geoffrion, R. Milne, and P.J. Thornalley. 2011. Glycation of LDL by methylglyoxal increases arterial atherogenicity: a possible contributor to increased risk of cardiovascular disease in diabetes. *Diabetes*. 60:1973-80.

Raben, N., C. Schreiner, R. Baum, S. Takikita, S. Xu, T. Xie, R. Myerowitz, M. Komatsu, J.H. Van der Meulen, K. Nagaraju, E. Ralston, and P.H. Plotz. 2010. Suppression of autophagy permits successful enzyme replacement therapy in a lysosomal storage disorder--murine Pompe disease. *Autophagy*. 6:1078-89.

Raher, M.J., H.B. Thibault, E.S. Buys, D. Kuruppu, N. Shimizu, A.L. Brownell, S.L. Blake, J. Rieusset, M. Kaneki, G. Derumeaux, M.H. Picard, K.D. Bloch, and M. Scherrer-Crosbie. 2008. A short duration of high-fat diet induces insulin resistance and predisposes to adverse left ventricular remodeling after pressure overload. *Am J Physiol Heart Circ Physiol*. 295:H2495-502.

Reaven, G.M., H. Chang, and B.B. Hoffman. 1988. Additive hypoglycemic effects of drugs that modify free-fatty acid metabolism by different mechanisms in rats with streptozocin-induced diabetes. *Diabetes*. 37:28-32.

Richter, E.A., and H. Galbo. 1986. High glycogen levels enhance glycogen breakdown in isolated contracting skeletal muscle. *J Appl Physiol*. 61:827-31.

Richter, E.A., N.B. Ruderman, H. Gavras, E.R. Belur, and H. Galbo. 1982. Muscle glycogenolysis during exercise: dual control by epinephrine and contractions. *Am J Physiol*. 242:E25-32.

Roach, P.J., A.A. Depaoli-Roach, T.D. Hurley, and V.S. Tagliabracci. 2012. Glycogen and its metabolism: some new developments and old themes. *Biochem J*. 441:763-87.

Robergs, R.A., F. Ghiasvand, and D. Parker. 2004. Biochemistry of exercise-induced metabolic acidosis. *Am J Physiol Regul Integr Comp Physiol*. 287:R502-16.

Rosenblatt-Velin, N., C. Montessuit, I. Papageorgiou, J. Terrand, and R. Lerch. 2001. Postinfarction heart failure in rats is associated with upregulation of GLUT-1 and downregulation of genes of fatty acid metabolism. *Cardiovasc Res*. 52:407-16.

Ruderman, N., and M. Prentki. 2004. AMP kinase and malonyl-CoA: targets for therapy of the metabolic syndrome. *Nat Rev Drug Discov*. 3:340-51.

Russell, R.R., 3rd, R. Bergeron, G.I. Shulman, and L.H. Young. 1999. Translocation of myocardial GLUT-4 and increased glucose uptake through activation of AMPK by AICAR. *Am J Physiol*. 277:H643-9.

Saddik, M., and G.D. Lopaschuk. 1994. Triacylglycerol turnover in isolated working hearts of acutely diabetic rats. *Can J Physiol Pharmacol*. 72:1110-9.

Saha, A.K., X.J. Xu, T.W. Balon, A. Brandon, E.W. Kraegen, and N.B. Ruderman. 2010. Insulin resistance due to nutrient excess: is it a consequence of AMPK downregulation? *Cell Cycle*. 10:3447-51.

Sahlin, K., N.H. Areskog, R.G. Haller, K.G. Henriksson, L. Jorfeldt, and S.F. Lewis. 1990. Impaired oxidative metabolism increases adenine nucleotide breakdown in McArdle's disease. *J Appl Physiol*. 69:1231-5.

Sakamoto, K., E. Zarrinpashneh, G.R. Budas, A.C. Pouleur, A. Dutta, A.R. Prescott, J.L. Vanoverschelde, A. Ashworth, A. Jovanovic, D.R. Alessi, and L. Bertrand. 2006. Deficiency of LKB1 in heart prevents ischemia-mediated activation of AMPKalpha2 but not AMPKalpha1. *Am J Physiol Endocrinol Metab*. 290:E780-8.

Salt, I., J.W. Celler, S.A. Hawley, A. Prescott, A. Woods, D. Carling, and D.G. Hardie. 1998. AMP-activated protein kinase: greater AMP dependence, and preferential nuclear localization, of complexes containing the alpha2 isoform. *Biochem J*. 334 (Pt 1):177-87.

Schelbert, H.R., E. Henze, H. Sochor, R.G. Grossman, S.C. Huang, J.R. Barrio, M. Schwaiger, and M.E. Phelps. 1986. Effects of substrate availability on myocardial C-11 palmitate kinetics by positron emission tomography in normal subjects and patients with ventricular dysfunction. *Am Heart J*. 111:1055-64.

Scott, J.W., S.A. Hawley, K.A. Green, M. Anis, G. Stewart, G.A. Scullion, D.G. Norman, and D.G. Hardie. 2004. CBS domains form energy-sensing modules whose binding of adenosine ligands is disrupted by disease mutations. *J Clin Invest*. 113:274-84.

Sellier, P., and J.P. Broustet. 2003. Assessment of anti-ischemic and antianginal effect at trough plasma concentration and safety of trimetazidine MR 35 mg in patients with stable angina pectoris: a multicenter, double-blind, placebo-controlled study. *Am J Cardiovasc Drugs*. 3:361-9.

Shearer, J., I. Marchand, M.A. Tarnopolsky, D.J. Dyck, and T.E. Graham. 2001. Pro- and macroglycogenolysis during repeated exercise: roles of glycogen content and phosphorylase activation. *J Appl Physiol*. 90:880-8.

Shin, Y.S. 2006. Glycogen storage disease: clinical, biochemical, and molecular heterogeneity. *Semin Pediatr Neurol*. 13:115-20.

Shoghi, K.I., B.N. Finck, K.B. Schechtman, T. Sharp, P. Herrero, R.J. Gropler, and M.J. Welch. 2009. In vivo metabolic phenotyping of myocardial substrate metabolism in rodents: differential efficacy of metformin and rosiglitazone monotherapy. *Circ Cardiovasc Imaging*. 2:373-81.

Shoghi, K.I., R.J. Gropler, T. Sharp, P. Herrero, N. Fettig, Y. Su, M.S. Mitra, A. Kovacs, B.N. Finck, and M.J. Welch. 2008. Time course of alterations in myocardial glucose utilization in the Zucker diabetic fatty rat with correlation to gene expression of glucose transporters: a small-animal PET investigation. *J Nucl Med*. 49:1320-7.

Shukla, T., G. Nichol, G. Wells, R.A. deKemp, R.A. Davies, H. Haddad, L. Duchesne, M. Freeman, K. Gulenchyn, N. Racine, D. Humen, F. Benard, T.D. Ruddy, B.J. Chow, J.

DaSilva, L. Garrard, A. Guo, L. Chen, and R.S. Beanlands. 2012. Does FDG PET-assisted management of patients with left ventricular dysfunction improve quality of life? A substudy of the PARR-2 trial. *Can J Cardiol*. 28:54-61.

Sidhu, J.S., Y.S. Rajawat, T.G. Rami, M.H. Gollob, Z. Wang, R. Yuan, A.J. Marian, F.J. DeMayo, D. Weilbacher, G.E. Taffet, J.K. Davies, D. Carling, D.S. Khoury, and R. Roberts. 2005. Transgenic mouse model of ventricular preexcitation and atrioventricular reentrant tachycardia induced by an AMP-activated protein kinase loss-of-function mutation responsible for Wolff-Parkinson-White syndrome. *Circulation*. 111:21-9.

Simoes, M.V., S. Egert, S. Ziegler, M. Miyagawa, S. Reder, T. Lehner, N. Nguyen, M.J. Charron, and M. Schwaiger. 2004. Delayed response of insulin-stimulated fluorine-18 deoxyglucose uptake in glucose transporter-4-null mice hearts. *J Am Coll Cardiol*. 43:1690-7.

Smoak, I.W., and S. Branch. 2000. Glut-1 expression and its response to hypoglycemia in the embryonic mouse heart. *Anat Embryol (Berl)*. 201:327-33.

Spriet, L.L., K. Soderlund, M. Bergstrom, and E. Hultman. 1987. Anaerobic energy release in skeletal muscle during electrical stimulation in men. *J Appl Physiol*. 62:611-5.

Spriet, L.L., and M.J. Watt. 2003. Regulatory mechanisms in the interaction between carbohydrate and lipid oxidation during exercise. *Acta Physiol Scand*. 178:443-52.

Stanley, W.C. 2004. Myocardial energy metabolism during ischemia and the mechanisms of metabolic therapies. *J Cardiovasc Pharmacol Ther*. 9 Suppl 1:S31-45.

Stanley, W.C., F.A. Recchia, and G.D. Lopaschuk. 2005. Myocardial substrate metabolism in the normal and failing heart. *Physiol Rev*. 85:1093-129.

Stapleton, D., K.I. Mitchelhill, G. Gao, J. Widmer, B.J. Michell, T. Teh, C.M. House, C.S. Fernandez, T. Cox, L.A. Witters, and B.E. Kemp. 1996. Mammalian AMP-activated protein kinase subfamily. *J Biol Chem*. 271:611-4.

Stein, S.C., A. Woods, N.A. Jones, M.D. Davison, and D. Carling. 2000. The regulation of AMP-activated protein kinase by phosphorylation. *Biochem J*. 345 Pt 3:437-43.

Suga, H. 1990. Ventricular energetics. *Physiol Rev*. 70:247-77.

Szkilnik, R., J. Konecki, P. Nowak, G. Szwzerbak, T. Zagzil, M. Swoboda, and R. Brus. 2005. Effect of trimetazidine on the [3H]glucose uptake in the brain and peripheral tissues of rats. *Acta Biochim Pol*. 52:116.

Szkudelski, T. 2001. The mechanism of alloxan and streptozotocin action in B cells of the rat pancreas. *Physiol Res*. 50:537-46.

Taegtmeyer, H. 2004. Glycogen in the heart--an expanded view. *J Mol Cell Cardiol*. 37:7-10.

Taegtmeyer, H., S. Sen, and D. Vela. 2010. Return to the fetal gene program: a suggested metabolic link to gene expression in the heart. *Ann N Y Acad Sci*. 1188:191-8.

Tantawy, M.N., and T.E. Peterson. 2010. Simplified [18F]FDG image-derived input function using the left ventricle, liver, and one venous blood sample. *Mol Imaging*. 9:76-86.

Tardy-Cantalupi, I., C. Montessuit, I. Papageorgiou, A. Remondino-Muller, F. Assimacopoulos-Jeannet, D.R. Morel, and R. Lerch. 1999. Effect of transient ischemia on the expression of glucose transporters GLUT-1 and GLUT-4 in rat myocardium. *J Mol Cell Cardiol*. 31:1143-55.

Tarnopolsky, M.A. 2006. What can metabolic myopathies teach us about exercise physiology? *Appl Physiol Nutr Metab*. 31:21-30.

Tesch, G.H., and T.J. Allen. 2007. Rodent models of streptozotocin-induced diabetic nephropathy. *Nephrology (Carlton)*. 12:261-6.

Thomas, A.J., J.N. DaSilva, M. Lortie, J.M. Renaud, M. Kenk, R.S. Beanlands, and R.A. deKemp. 2011. PET of (R)-11C-rolipram binding to phosphodiesterase-4 is reproducible and sensitive to increased norepinephrine in the rat heart. *J Nucl Med*. 52:263-9.

Thorens, B., and M. Mueckler. Glucose transporters in the 21st Century. *Am J Physiol Endocrinol Metab*. 298:E141-5.

Thorn, S., R. deKemp, T. Dumouchel, R. Klein, J. Renaud, G. Wells, M. Gollob, R. Beanlands, and J. Dasilva. 2012 (accepted, pending revisions). Repeatable Non-Invasive Imaging of FDG PET in the Mouse Myocardium: Evaluation of Tracer Kinetics in a Type 1 Diabetes Model. *Journal of Nuclear Medicine*.

Thorn, S., R. deKemp, T. Dumouchel, R. Klein, J. Renaud, G. Wells, M. Gollob, R. Beanlands, and J. Dasilva. 2013 (in press). Repeatable Non-Invasive Imaging of FDG PET in the Mouse Myocardium: Evaluation of Tracer Kinetics in a Type 1 Diabetes Model. *J Nucl Med*.

Thornton, C., M.A. Snowden, and D. Carling. 1998. Identification of a novel AMP-activated protein kinase beta subunit isoform that is highly expressed in skeletal muscle. *J Biol Chem*. 273:12443-50.

Tian, R., N. Musi, J. D'Agostino, M.F. Hirshman, and L.J. Goodyear. 2001. Increased adenosine monophosphate-activated protein kinase activity in rat hearts with pressure-overload hypertrophy. *Circulation*. 104:1664-9.

Tirone, T.A., and F.C. Brunicardi. 2001. Overview of glucose regulation. *World J Surg*. 25:461-7.

Towler, M.C., and D.G. Hardie. 2007. AMP-activated protein kinase in metabolic control and insulin signaling. *Circ Res*. 100:328-41.

Treebak, J.T., S. Glund, A. Deshmukh, D.K. Klein, Y.C. Long, T.E. Jensen, S.B. Jorgensen, B. Viollet, L. Andersson, D. Neumann, T. Wallimann, E.A. Richter, A.V. Chibalin, J.R. Zierath, and J.F. Wojtaszewski. 2006. AMPK-mediated AS160 phosphorylation in skeletal muscle is dependent on AMPK catalytic and regulatory subunits. *Diabetes*. 55:2051-8.

Turdi, S., X. Fan, J. Li, J. Zhao, A.F. Huff, M. Du, and J. Ren. 2010. AMP-activated protein kinase deficiency exacerbates aging-induced myocardial contractile dysfunction. *Aging Cell*. 9:592-606.

Tuunanen, H., E. Engblom, A. Naum, K. Nagren, M. Scheinin, B. Hesse, K.E. Juhani Airaksinen, P. Nuutila, P. Iozzo, H. Ukkonen, L.H. Opie, and J. Knuuti. 2008. Trimetazidine, a metabolic modulator, has cardiac and extracardiac benefits in idiopathic dilated cardiomyopathy. *Circulation*. 118:1250-8.

Unal, O.F., S.M. Ghoreishi, A. Atas, N. Akyurek, G. Akyol, and B. Gursel. 2005. Prevention of gentamicin induced ototoxicity by trimetazidine in animal model. *Int J Pediatr Otorhinolaryngol*. 69:193-9.

Verloes, A., M. Massin, J. Lombet, B. Grattagliano, D. Soyeur, J. Rigo, L. Koulischer, and F. Van Hoof. 1997. Nosology of lysosomal glycogen storage diseases without in vitro acid maltase deficiency. Delineation of a neonatal form. *Am J Med Genet*. 72:135-42.

Viollet, B., F. Andreelli, S.B. Jorgensen, C. Perrin, D. Flamez, J. Mu, J.F. Wojtaszewski, F.C. Schuit, M. Birnbaum, E. Richter, R. Burcelin, and S. Vaulont. 2003a. Physiological role of AMP-activated protein kinase (AMPK): insights from knockout mouse models. *Biochem Soc Trans*. 31:216-9.

Viollet, B., F. Andreelli, S.B. Jorgensen, C. Perrin, A. Geloen, D. Flamez, J. Mu, C. Lenzner, O. Baud, M. Bennoun, E. Gomas, G. Nicolas, J.F. Wojtaszewski, A. Kahn, D. Carling, F.C. Schuit, M.J. Birnbaum, E.A. Richter, R. Burcelin, and S. Vaulont. 2003b. The AMP-activated protein kinase alpha2 catalytic subunit controls whole-body insulin sensitivity. *J Clin Invest*. 111:91-8.

vom Dahl, J., W.H. Herman, R.J. Hicks, F.J. Oritz-Alonzo, K.S. Lee, K.C. Allman, E.R. Wolfe, V. Kalff, and M. Schwaiger. 1993. Myocardial glucose uptake in patients with insulin-dependent diabetes mellitus assessed quantitatively by dynamic positron emission tomography. *Circulation*. 88:395-404.

Wahl, R.L. 2002. Principles and practice of positron emission tomography. Lippincott Williams and Wilkins, Philadelphia.

Wang, W., and G.D. Lopaschuk. 2007. Metabolic therapy for the treatment of ischemic heart disease: reality and expectations. *Expert Rev Cardiovasc Ther*. 5:1123-34.

Watt, M.J., G.R. Steinberg, Z.P. Chen, B.E. Kemp, and M.A. Febbraio. 2006. Fatty acids stimulate AMP-activated protein kinase and enhance fatty acid oxidation in L6 myotubes. *J Physiol*. 574:139-47.

Winder, W.W., and D.G. Hardie. 1996. Inactivation of acetyl-CoA carboxylase and activation of AMP-activated protein kinase in muscle during exercise. *Am J Physiol*. 270:E299-304.

Wojtaszewski, J.F., S.B. Jorgensen, Y. Hellsten, D.G. Hardie, and E.A. Richter. 2002. Glycogen-dependent effects of 5-aminoimidazole-4-carboxamide (AICA)-riboside on AMP-activated protein kinase and glycogen synthase activities in rat skeletal muscle. *Diabetes*. 51:284-92.

Wojtaszewski, J.F., C. MacDonald, J.N. Nielsen, Y. Hellsten, D.G. Hardie, B.E. Kemp, B. Kiens, and E.A. Richter. 2003. Regulation of 5'AMP-activated protein kinase activity and substrate utilization in exercising human skeletal muscle. *Am J Physiol Endocrinol Metab*. 284:E813-22.

Wolf, C.M., M. Arad, F. Ahmad, A. Sanbe, S.A. Bernstein, O. Toka, T. Konno, G. Morley, J. Robbins, J.G. Seidman, C.E. Seidman, and C.I. Berul. 2008. Reversibility of PRKAG2 glycogen-storage cardiomyopathy and electrophysiological manifestations. *Circulation*. 117:144-54.

Wong, K.P., W. Sha, X. Zhang, and S.C. Huang. 2011. Effects of administration route, dietary condition, and blood glucose level on kinetics and uptake of 18F-FDG in mice. *J Nucl Med*. 52:800-7.

Wood, I.S., and P. Trayhurn. 2003. Glucose transporters (GLUT and SGLT): expanded families of sugar transport proteins. *Br J Nutr*. 89:3-9.

Woods, A., D. Azzout-Marniche, M. Foretz, S.C. Stein, P. Lemarchand, P. Ferre, F. Foufelle, and D. Carling. 2000. Characterization of the role of AMP-activated protein kinase in the regulation of glucose-activated gene expression using constitutively active and dominant negative forms of the kinase. *Mol Cell Biol*. 20:6704-11.

Woods, A., D. Vertommen, D. Neumann, R. Turk, J. Bayliss, U. Schlattner, T. Wallimann, D. Carling, and M.H. Rider. 2003. Identification of phosphorylation sites in AMP-activated protein kinase (AMPK) for upstream AMPK kinases and study of their roles by site-directed mutagenesis. *J Biol Chem*. 278:28434-42.

Xiao, B., M.J. Sanders, E. Underwood, R. Heath, F.V. Mayer, D. Carmena, C. Jing, P.A. Walker, J.F. Eccleston, L.F. Haire, P. Saiu, S.A. Howell, R. Aasland, S.R. Martin, D. Carling, and S.J. Gamblin. 2011. Structure of mammalian AMPK and its regulation by ADP. *Nature*. 472:230-3.

Yamauchi, T., J. Kamon, Y. Minokoshi, Y. Ito, H. Waki, S. Uchida, S. Yamashita, M. Noda, S. Kita, K. Ueki, K. Eto, Y. Akanuma, P. Froguel, F. Foufelle, P. Ferre, D. Carling, S. Kimura, R. Nagai, B.B. Kahn, and T. Kadowaki. 2002. Adiponectin stimulates glucose utilization and fatty-acid oxidation by activating AMP-activated protein kinase. *Nat Med*. 8:1288-95.

Yang, J., and G.D. Holman. 2006. Long-term metformin treatment stimulates cardiomyocyte glucose transport through an AMP-activated protein kinase-dependent reduction in GLUT4 endocytosis. *Endocrinology*. 147:2728-36.

Yoshinaga, K., B.J. Chow, R. deKemp, S. Thorn, T. Ruddy , R.A. Davies, J. DaSilva, and R. Beanlands. 2005. Application of cardiac molecular imaging using positron emission tomography in evaluation of drug and therapeutics for cardiovascular disorders. *Curr. Pharm. Des.* 11:903-32.

Young, L.H., J. Li, S.J. Baron, and R.R. Russell. 2005. AMP-activated protein kinase: a key stress signaling pathway in the heart. *Trends Cardiovasc Med*. 15:110-8.

Yu, H., N. Fujii, M.F. Hirshman, J.M. Pomerleau, and L.J. Goodyear. 2004. Cloning and characterization of mouse 5'-AMP-activated protein kinase gamma3 subunit. *Am J Physiol Cell Physiol*. 286:C283-92.

Yu, H., M.F. Hirshman, N. Fujii, J.M. Pomerleau, L.E. Peter, and L.J. Goodyear. 2006. Muscle-specific overexpression of wild type and R225Q mutant AMP-activated protein kinase gamma3-subunit differentially regulates glycogen accumulation. *Am J Physiol Endocrinol Metab*. 291:E557-65.

Zaha, V.G., and L.H. Young. 2012. AMP-Activated Protein Kinase Regulation and Biological Actions in the Heart. *Circ Res*. 111:800-14.

Zhang, L., Y. Lu, H. Jiang, A. Sun, Y. Zou, and J. Ge. 2012. Additional use of trimetazidine in patients with chronic heart failure: a meta-analysis. *J Am Coll Cardiol*. 59:913-22.

Zhao, P., J. Zhang, X.G. Yin, P. Maharaj, S. Narraindoo, L.Q. Cui, and Y.S. Tang. 2012. The effect of trimetazidine on cardiac function in diabetic patients with idiopathic dilated cardiomyopathy. *Life Sci*.

Zhou, H., T. Zhang, M. Bogdani, E. Oseid, S. Parazzoli, M.C. Vantyghem, J. Harmon, M. Slucca, and R.P. Robertson. 2008. Intrahepatic glucose flux as a mechanism for defective intrahepatic islet alpha-cell response to hypoglycemia. *Diabetes*. 57:1567-74.